EXPERIMENTAL PERFORMANCE OF CONCRETE MASONRY SHEAR WALLS UNDER IN-PLANE LOADING

By

CHRISTINA MARIE KAPOI

A thesis submitted in partial fulfillment of
the requirements for the degree of

MASTER OF SCIENCE IN CIVIL ENGINEERING

WASHINGTON STATE UNIVERSITY
Department of Civil and Environmental Engineering

MAY 2012

To the Faculty of Washington State University:

The members of the Committee appointed to examine the thesis of CHRISTINA MARIE KAPOI find it satisfactory and recommend that it be accepted.

_____

David I. McLean, Ph.D., P.E. Chair

_____

J. Daniel Dolan, Ph.D., P.E.

_____

William Cofer, Ph.D., P.E.

ACKNOWLEDGEMENTS

I would like to acknowledge the financial support I received from the National Institute of Science and Technology (NIST). I would also like to acknowledge The Eastern Washington Masonry Promotion Group for their financial support and Mutual Materials and Central Pre-Mix for the materials they donated.

I want to express my deepest gratitude to Dr. David McLean for selecting me to work on this project and for all of the guidance, support and knowledge he has passed on throughout my master's program. I would also like to thank Dr. Dan Dolan and Dr. Bill Cofer for serving as my committee members. I value the assistance and knowledge I received from Dr. Benson Shing, Dr. Richard Klingner, Farhad Ahmadi and the other project members during the design and analysis of my walls.

I sincerely thank everyone at the Composite Materials and Engineering Center, especially Bob Duncan and Scott Lewis, for all of their guidance and assistance during the construction and testing of my walls. I also thank my fellow WSU students, Jake Sherman and Will Cyrier, for all of the time and hard work they contributed to the successful completion of my project, and the other students who lent a hand at various stages. In addition, I want to acknowledge Vicki Ruddick and Lola Gillespie in the Department of Civil and Environmental Engineering for all of their help.

I would especially like to thank my parents for all of their support, guidance and help throughout my education. I can't begin to express how much love, encouragement, patience and time my husband Drew gave me; I could not have done it without him by my side.

EXPERIMENTAL PERFORMANCE OF CONCRETE MASONRY SHEAR WALLS

UNDER IN-PLANE LOADING

Abstract

By Christina Marie Kapoi, M.S.
Washington State University
May 2012

Committee Chair: David I. McLean

This study was conducted as part of a joint effort between the University of California at San Diego, the University of Texas at Austin, and Washington State University. The objective of the overall project is to develop improved performance-based design methodologies and provisions for reinforced masonry shear walls under seismic loading. The primary objective of the research reported in this thesis was to investigate the behavior of reinforced masonry shear walls subjected to in-plane lateral loading while varying wall aspect ratio, level of applied axial stress and reinforcement ratio. The secondary objective was to examine the effects of concentrated reinforcement at the ends of the walls (jambs) compared with evenly distributed reinforcement on shear wall performance.

Eight, fully grouted, concrete masonry shear walls were designed according to the 2011 MSJC Code. Walls were tested to failure under cyclic in-plane lateral loading. The walls had three height-to-length aspect ratios (0.78, 1.0 and 2.0), two magnitudes of axial compressive stresses (0 and 158 psi), and two vertical reinforcement ratios (0.0033 and 0.0072). In addition, two of the walls compared the effects of jamb reinforcement vs. evenly distributed reinforcement.

Wall performance was evaluated by comparison of failure modes, predicted vs. actual load capacity, drift capacity, displacement ductility, height of plasticity, equivalent plastic hinge

length, amount of energy dissipation, and equivalent hysteretic damping. The walls exhibited either a flexural failure or a complex flexure/shear/crushing failure which depended upon the aspect ratio and amount of vertical reinforcement. Results showed that the amount of drift at failure was highly dependent upon the aspect ratio but was not influenced by the amount of axial compressive stress or the vertical reinforcement ratio. The displacement ductility was sensitive to the amount of vertical reinforcement but not the amount of axial compressive stress. There were no apparent correlations between the plastic hinge length and any of the design parameters. The performance of walls with jamb reinforcement was similar to that of walls with evenly distributed reinforcement. Large-diameter vertical reinforcement bars with lap splices at the base of the wall should be avoided because of their propensity towards abrupt failure.

TABLE OF CONTENTS

Page

ACKNOWLEDGEMENTS iii

ABSTRACT iv

LIST OF TABLES ix

LIST OF FIGURES xii

1. CHAPTER 1: INTRODUCTION 1

1.1 Background 1

1.2 Scope and Objective 3

2. CHAPTER 2: LITERATURE REVIEW 4

2.1 Introduction 4

2.2 Failure Modes of Masonry Shear Walls 4

2.3 Ductility 6

2.4 MSJC Code Provisions 7

2.5 Shing et al 9

2.6 Ibrahim and Suter 10

2.7 Eikanas 11

2.8 Voon and Ingham 13

2.9 Shedid et al 14

2.10 Sherman 15

2.11 Summary 16

3. CHAPTER 3: EXPERIMENTAL PROGRAM 17

3.1 Introduction 17

3.2 Footing Description 17
3.3 Wall Specimen Description 18
3.4 Load Beam Description 21
3.5 Material Properties 22
3.6 Construction of Wall Specimens 23
3.7 Test Setup 24
3.8 Instrumentation 26
3.9 System Control & Data Acquisition 28
3.10 Test Procedures 28
3.11 Summary 29
4. CHAPTER 4: RESULTS OF WALL TESTS 31
4.1 Introduction 31
4.2 Wall Specimen C1 31
4.3 Wall Specimen C2 48
4.4 Wall Specimen C3 57
4.5 Wall Specimen C4 65
4.6 Wall Specimen C5 75
4.7 Wall Specimen C6 84
4.8 Wall Specimen C7 93
4.9 Wall Specimen C8 102
4.10 Summary 111
5. CHAPTER 5: ANALYSIS OF TEST RESULTS 112
5.1 Introduction 112

5.2 Failure Modes 112
5.3 Wall Capacity 119
5.4 Drift 120
5.5 Displacement Ductility 122
5.6 Height of Plasticity and Plastic Hinge Length 123
5.7 Energy Dissipation 124
5.8 Equivalent Hysteretic Damping 125
5.9 Effects of Design Parameters on Wall Behavior 125
5.9.1 Aspect Ratio 126
5.9.2 Axial Compressive Stress 128
5.9.3 Vertical Reinforcement Ratio 130
5.9.4 Jamb Reinforcement 133
5.10 Summary and Conclusions 137
6. CHAPTER 6: SUMMARY, CONCLUSIONS AND FUTURE RESEARCH 139
6.1 Summary 139
6.2 Conclusions 140
6.3 Future Research 143
REFERENCES 144
APPENDIX A 146

LIST OF TABLES

Page

Table 3.1 Details of Wall Specimens 20

Table 3.2 Average Material Compressive Strengths, psi 23

Table 3.3 Vertical Reinforcement Yield Strengths, ksi 23

Table 4.1 Wall C1: Test Observations 34

Table 4.2 Wall C1: Components of Total Drift 38

Table 4.3 Wall C1: Displacement Ductility 43

Table 4.4 Wall C1: Curvature Ductility 44

Table 4.5 Wall C1: Height of Plasticity 45

Table 4.6 Wall C1: Equivalent Plastic Hinge Length 45

Table 4.7 Wall C2: Test Observations 50

Table 4.8 Wall C2: Components of Total Drift 53

Table 4.9 Wall C2: Displacement Ductility 56

Table 4.10 Wall C2: Curvature Ductility 56

Table 4.11 Wall C2: Height of Plasticity & Equivalent Plastic Hinge Length 56

Table 4.12 Wall C3: Test Observations 59

Table 4.13 Wall C3: Components of Total Drift 61

Table 4.14 Wall C3: Displacement Ductility 64

Table 4.15 Wall C3: Curvature Ductility 64

Table 4.16 Wall C3: Height of Plasticity & Equivalent Plastic Hinge Length 65

Table 4.17 Wall C4: Test Observations 68

Table 4.18 Wall C4: Components of Total Drift 70

Table 4.19 Wall C4: Displacement Ductility 73
Table 4.20 Wall C4: Curvature Ductility 74
Table 4.21 Wall C4: Height of Plasticity & Equivalent Plastic Hinge Length 74
Table 4.22 Wall C5: Test Observations 77
Table 4.23 Wall C5: Components of Total Drift 81
Table 4.24 Wall C5: Displacement Ductility 82
Table 4.25 Wall C5: Curvature Ductility 83
Table 4.26 Wall C5: Height of Plasticity & Equivalent Plastic Hinge Length 84
Table 4.27 Wall C6: Test Observations 85
Table 4.28 Wall C6: Components of Total Drift 89
Table 4.29 Wall C6: Displacement Ductility 92
Table 4.30 Wall C6: Curvature Ductility 92
Table 4.31 Wall C6: Height of Plasticity & Equivalent Plastic Hinge Length 93
Table 4.32 Wall C7: Test Observations 94
Table 4.33 Wall C7: Components of Total Drift 99
Table 4.34 Wall C7: Displacement Ductility 100
Table 4.35 Wall C7: Curvature Ductility 100
Table 4.36 Wall C7: Height of Plasticity & Equivalent Plastic Hinge Length 101
Table 4.37 Wall C8: Test Observations 104
Table 4.38 Wall C8: Components of Total Drift 108
Table 4.39 Wall C8: Displacement Ductility 109
Table 4.40 Wall C8: Curvature Ductility 110
Table 4.41 Wall C8: Height of Plasticity & Equivalent Plastic Hinge Length 111

Table 5.1 Evaluation of Failure Modes 112
Table 5.2 Comparison of Expected and Experimental Wall Capacities 119
Table 5.3 Total Wall Drift at Three Limit-States 120
Table 5.4 Components of Total Drift at 20% Load Degradation 122
Table 5.5 Average Yield & Ultimate Displacements and Displacement Ductility 123
Table 5.6 Ratios of Height of Plasticity and Plastic Hinge Length over Wall Height 124
Table 5.7 Total Energy Dissipation 124
Table 5.8 Equivalent Hysteretic Damping 125
Table 5.9 Evaluation of Aspect Ratio 126
Table 5.10 Evaluation of Axial Compressive Stress 128
Table 5.11 Evaluation of Reinforcement Ratio 131
Table 5.12 Evaluation of Jamb Reinforcement 133

LIST OF FIGURES

Page

Figure 2.1 Masonry Shear Wall Failure Modes (adapted from Eikanas, 2003) 5

Figure 2.2 Yield and Ultimate Displacement Definitions (from Priestley et al., 2007) 7

Figure 2.3 Prescribed Strain Distribution (MSJC, 2011) 9

Figure 3.1 Typical Footing Design 18

Figure 3.2 Evenly Distributed Vertical Reinforcement 19

Figure 3.3 Jamb Reinforcement 19

Figure 3.4 Typical Wall Specimen 20

Figure 3.5 Jamb Reinforcement Wall Specimen 21

Figure 3.6 Typical Load Beam Design 22

Figure 3.7 Typical Wall Specimen Test Setup 26

Figure 3.8 Displacement Potentiometer (Left) and Strain Gage (Right) Locations 27

Figure 3.9 System Control & Data Acquisition Flow Chart
(adapted from Sherman, 2011) 28

Figure 3.10 Preliminary Loading Protocol 30

Figure 3.11 Primary Loading Protocol 30

Figure 4.1 Wall C1: Wall at Test Completion 33

Figure 4.2 Wall C1: South Toe (Left) and North Toe (Right) at Test Completion 33

Figure 4.3 Wall C1: Load-Displacement Hysteresis Curves 35

Figure 4.4 Flexural and Shear Deformations (Massone and Wallace, 2004) 37

Figure 4.5 Wall C1: Total Lateral Displacement and its Components 39

Figure 4.6 Typical Strain Profile (adapted from Sherman, 2011) 40

Figure 4.7 Wall C1: Curvature vs. Wall Height 41
Figure 4.8 Elastoplastic Approximation 42
Figure 4.9 Illustration of Total Energy Equation (adapted from Snook, 2005) 46
Figure 4.10 Hysteretic Area for Damping Calculation (from Priestley et al., 2007) 48
Figure 4.11 Wall C2: Entire Wall at Test Completion 49
Figure 4.12 Wall C2: South Toe (Left) and North Toe (Right) at Test Completion 50
Figure 4.13 Wall C2: Load-Displacement Hysteresis Curves 52
Figure 4.14 Wall C2: South Toe (Left) and North Toe (Right) at Onset of Toe Damage ... 52
Figure 4.15 Wall C2: Total Lateral Displacement and its Components 54
Figure 4.16 Wall C2: Curvature vs. Wall Height 55
Figure 4.17 Wall C3: Entire Wall at Test Completion 58
Figure 4.18 Wall C3: South Toe (Left) and North Toe (Right) at Test Completion 59
Figure 4.19 Wall C3: Load-Displacement Hysteresis Curves 60
Figure 4.20 Wall C3: South Toe (Left) and North Toe (Right) at Onset of Toe Damage ... 61
Figure 4.21 Wall C3: Total Lateral Displacement and its Components 62
Figure 4.22 Wall C3: Curvature vs. Wall Height 63
Figure 4.23 Wall C4: Entire Wall at Test Completion 67
Figure 4.24 Wall C4: South Toe (Left) and North Toe (Right) at Test Completion 67
Figure 4.25 Wall C4: Load-Displacement Hysteresis Curves 69
Figure 4.26 Wall C4: South Toe (Left) and North Toe (Right) at Onset of Toe Damage ... 69
Figure 4.27 Wall C4: Total Lateral Displacement and its Components 71
Figure 4.28 Wall C4: Curvature vs. Wall Height 73
Figure 4.29 Wall C5: Entire Wall at Test Completion 76

Figure 4.30 Wall C5: South Toe (Left) and North Toe (Right) at Test Completion 77
Figure 4.31 Wall C5: Load-Displacement Hysteresis Curves 78
Figure 4.32 Wall C5: South Toe (Left) and North Toe (Right) at Onset of Toe Damage... 79
Figure 4.33 Wall C5: Total Lateral Displacement and its Components 80
Figure 4.34 Wall C5: Curvature vs. Wall Height 82
Figure 4.35 Wall C6: Entire Wall at Test Completion 86
Figure 4.36 Wall C6: South Toe (Left) and North Toe (Right) at Test Completion 86
Figure 4.37 Wall C6: Load-Displacement Hysteresis Curves 88
Figure 4.38 Wall C6: South Toe (Left) and North Toe (Right) at Onset of Toe Damage... 88
Figure 4.39 Wall C6: Total Lateral Displacement and its Components 90
Figure 4.40 Wall C6: Curvature vs. Wall Height 91
Figure 4.41 Wall C7: Entire Wall at Test Completion 95
Figure 4.42 Wall C7: South Toe (Left) and North Toe (Right) at Test Completion 95
Figure 4.43 Wall C7: Load-Displacement Hysteresis Curves 97
Figure 4.44 Wall C7: South Toe (Left) and North Toe (Right) at Onset of Toe Damage... 97
Figure 4.45 Wall C7: Total Lateral Displacement and its Components 98
Figure 4.46 Wall C7: Curvature vs. Wall Height 99
Figure 4.47 Wall C8: Entire Wall at Test Completion 103
Figure 4.48 Wall C8: South Toe (Left) and North Toe (Right) at Test Completion 103
Figure 4.49 Wall C8: Load-Displacement Hysteresis Curves 105
Figure 4.50 Wall C8: South Toe (Left) and North Toe (Right) at Onset of Toe Damage. 106
Figure 4.51 Wall C8: Total Lateral Displacement and its Components 107
Figure 4.52 Wall C8: Curvature vs. Wall Height 109

Figure 5.1 Wall C2: Development of Flexural Cracks 113

Figure 5.2 Wall C2: Further Development of Flexural Cracks Along with Some Shear Cracks 114

Figure 5.3 Wall C2: Toe Damage Typical of Flexural Failure 114

Figure 5.4 Wall C3: Development of Flexural, Shear and Splitting Cracks 115

Figure 5.5 Wall C3: Opening of Shear Cracks 116

Figure 5.6 Wall C3: Crushing and Spalling of Face Shells 116

Figure 5.7 Propagation of Shear Cracks 117

Figure 5.8 Crushing of Face Shells 117

Figure 5.9 Spalling of Face Shells 118

Figure 5.10 Load-Displacement Envelopes for Aspect Ratio Comparison 127

Figure 5.11 Load-Displacement Envelopes for Axial Compressive Stress Comparison .. 129

Figure 5.12 Load-Displacement Envelopes for Reinforcement Ratio Comparison 132

Figure 5.13 Wall C6: Progression of Failure (3ΔY Cycle 1) 134

Figure 5.14 Wall C7: Progression of Failure (3ΔY Cycle 1) 134

Figure 5.15 Wall C6: Progression of Failure (6ΔY Cycle 1) 135

Figure 5.16 Wall C7: Progression of Failure (6ΔY Cycle 1) 135

Figure 5.17 Load-Displacement Envelopes for Jamb Reinforcement Comparison 136

CHAPTER 1:

INTRODUCTION

1.1 Background

Masonry has been a popular construction material for millennia. It has been used to build notable historical structures such as the Egyptian pyramids, the Roman coliseum, medieval castles and many more. The prevalence of masonry construction throughout the world can be attributed to its relative versatility, its durability and ability to withstand the natural elements, its cost effectiveness, and its ease of construction. Although masonry had been used for thousands of years, the concept of reinforced masonry has been around for only about one hundred years. We continue to learn about the performance of masonry structures under certain loading conditions, especially seismic loading.

Reinforced masonry shear walls in seismic regions serve to simultaneously resist vertical (gravity) and lateral (seismic) loads. This load combination can cause different failure mechanisms to occur: flexure, shear or a combination of the two. Flexural behavior is typically characterized by tensile yielding of the vertical reinforcement, formation of plastic hinges in the flexural regions of the wall, and eventual crushing of the masonry. Shear behavior is typically characterized by diagonal tensile cracking of the masonry. Flexural failures are preferred because they generally are more ductile and dissipate more energy, while shear failures are undesirable because they generally exhibit more brittle behavior. The wall parameters that influence which of these failure mechanisms arise include the height-to-length aspect ratio of the walls, the level of axial load, and the amount and distribution of horizontal and vertical reinforcement. Understanding how the performance and failure of masonry shear walls are altered, given different combinations of these parameters, is crucial when designing a structure.

Over the past 40 years, major changes regarding seismic design procedures have occurred. Historically, seismic design procedures were based primarily on forces and the strength necessary to resist them largely because that is what dead and live loads are traditionally designed for. It was believed that the strength of a structure was synonymous with the performance of a structure (Priestley, 2000). Research conducted during the 1970's and 1980's focused on determining the ductility of structural systems and incorporating this into the design requirements, but the overall design methods were still based on resisting forces. In the 1990's, a new design method based on desired levels of displacements, instead of forces, was introduced and has been the focus of research since then (Priestley et al., 2007).

The new design method, referred to as performance-based design, was developed to overcome shortcomings in the previous force-based design methodology. One of the problems with force-based design arises from having to assume member size and thus stiffness in the initial design. This is used to calculate the period and distribution of forces within the structure. During the design process, if member sizes are modified then the distribution of forces must also be recalculated, although they rarely are. Force-based design also incorrectly assumes that different structural elements all yield at the same time. Lastly, the assumption that unique force-reduction factors can be applied to specific types of structures and materials is invalid (Priestley et al., 2007).

Force-based design methods are based on the elastic behavior of shear walls while performance-based design methods recognize that the inelastic behavior of shear walls is a more accurate representation of their performance. This is incorporated into the design method by taking the stiffness of a shear wall as the secant stiffness obtained at maximum displacement. Performance-based design also recognizes that the amount of damping in a structure is

dependent upon the material. Using this information, the effective period at maximum displacement is found (Priestley, 2000). An iterative design approach is not required. Performance-based design provides a more consistent and realistic prediction of shear wall behavior and may also result in more economical designs than the force-based design method.

1.2 Scope and Objective

This project was funded by the National Institute of Standards and Technology (NIST). It was conducted as part of a joint effort between researchers at the University of California at San Diego, the University of Texas at Austin, and Washington State University. The objective of the overall project is to develop improved performance-based design methodologies and provisions for reinforced concrete masonry shear walls under seismic loading.

The primary objective of the research reported in this thesis was to investigate the behavior of reinforced concrete masonry shear walls subjected to in-plane lateral loading while varying the wall aspect ratio, level of applied axial stress, and reinforcement ratio. The secondary objective was to examine the effects of concentrated reinforcement at the ends of the walls (jambs) compared with evenly distributed reinforcement on shear wall performance. The influence of each parameter on wall behavior was evaluated based on failure modes as well as measured values of strength, drift, ductility, plastic hinge lengths, energy dissipation, and equivalent hysteretic damping.

CHAPTER 2:

LITERATURE REVIEW

2.1 Introduction

Numerous experimental studies on the seismic behavior of concrete masonry shear walls have been conducted since the 1970's. The knowledge gained from these studies has helped develop new design methodologies and requirements. This chapter provides a review of masonry shear wall behavior under cyclic in-plane lateral loading, including information on the different failure modes, drift capacity, displacement ductility and plastic hinge length. Also included is a review of the applicable seismic design provisions of the 2011 MSJC Building Code Requirements for Masonry Structures.

2.2 Failure Modes of Masonry Shear Walls

Reinforced concrete masonry shear walls located in high seismic regions need to simultaneously resist in-plane and out-of-plane lateral loads as well as vertical loads. Various loading conditions may cause four distinct failure mechanisms, or a combination thereof, to arise. These failure mechanisms, depicted in Figure 2.1, include rocking, sliding, flexure and shear. Rocking and sliding can be prevented with adequate anchorage, leaving flexure and shear as the dominant failure mechanisms. Wall behavior is dependent upon the height-to-length aspect ratio of the wall, the magnitude of the applied axial load, and the amount and distribution of horizontal and vertical reinforcement.

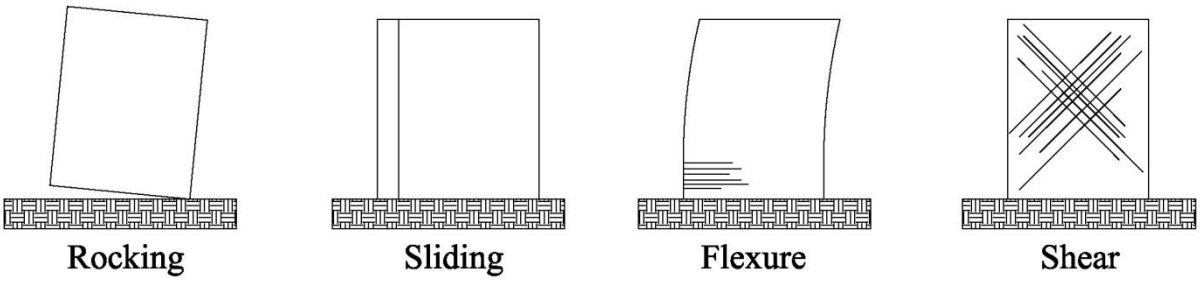

Figure 2.1 Masonry Shear Wall Failure Modes (adapted from Eikanas, 2003)

Flexure is the preferred method of failure because of its ductile nature and effectiveness at dissipating energy. It is typically characterized by tensile yielding of the vertical reinforcement, the formation of a plastic hinge zone and crushing of masonry at critical wall sections (Shedid et al., 2008; Shing et al., 1989). Crushing of the masonry is often accompanied by vertical splitting of the masonry in the toe regions. At increased displacements, face shell spalling and eventual crushing of the grout also occur in the toe regions (Shedid et al, 2008). Flexural wall behavior is negatively affected by high vertical reinforcement ratios which correspond to decreased levels of drift and ductility and can result in more brittle failures (Eikanas, 2003; Sherman, 2011). The flexural strength increases as the magnitude of applied axial stress increases (Shing et al., 1989). Walls with height-to-length aspect ratios greater than 1.5 exhibit more flexure-dominated behavior than shear-dominated behavior. Masonry shear walls are typically designed to fail in flexure to ensure a ductile response.

Shear failures are undesirable because they exhibit more brittle behavior and "rapid strength degradation soon after the maximum strength is reached" (Voon and Ingham, 2006). They are characterized by diagonal tensile cracking that often starts as horizontal flexural cracks that develop into wide-open diagonal cracks and extend throughout the masonry. Walls with height-to-length aspect ratios less than 1.0 are often dominated by shear behavior. The shear resistance of a masonry shear wall comes from the "tension of shear reinforcement, dowel-action

of vertical reinforcement, applied axial stress and aggregate interlocking" (Shing et. al., 1989). Shear strength can be increased by evenly distributing the horizontal reinforcement up the height of the wall which helps distribute the stresses (Voon and Ingham, 2006). This can also change the wall's behavior from a brittle failure to a more ductile failure. Larger amounts of vertical reinforcement reduce the size and amount of crack openings which enhances the aggregate-interlock system (Shing et. al., 1989). Lastly, larger magnitudes of applied axial load increase the shear strength by delaying the initiation of cracking and enhancing the aggregate-interlock system (Ibrahim and Suter, 1999; Voon and Ingham, 2006).

2.3 Ductility

Ductility is a measure of inelastic deformations such as displacement, curvature and strain. It is defined as the ratio of "maximum to effective yield deformations" (Priestley et al., 2007). The difficulty in determining ductility arises when trying to define when yield and ultimate deformations occur. The point of initial yielding has been defined as: (1) the intersection of the line through the origin with initial stiffness, and the nominal strength; (2) the displacement at first yield; (3) and the intersection of the line through the origin with secant stiffness through first yield, and the nominal strength. The ultimate deformation has been defined as: (4) displacement at peak strength; (5) displacement corresponding to 20% or 50% degradation from peak strength; (6) and displacement at initial fracture of the transverse reinforcement (Priestley et al., 2007). Figure 2.2 contains a force-displacement curve with points corresponding to the above definitions for yield and maximum displacement. The value for the ductility factor is highly dependent upon which points are chosen for the yield and ultimate deformations. This can lead to considerably different ductility capacities being reported for the

same structure. Priestley et al. (2007) define the yield displacement at point 3 and the ultimate displacement at point 5.

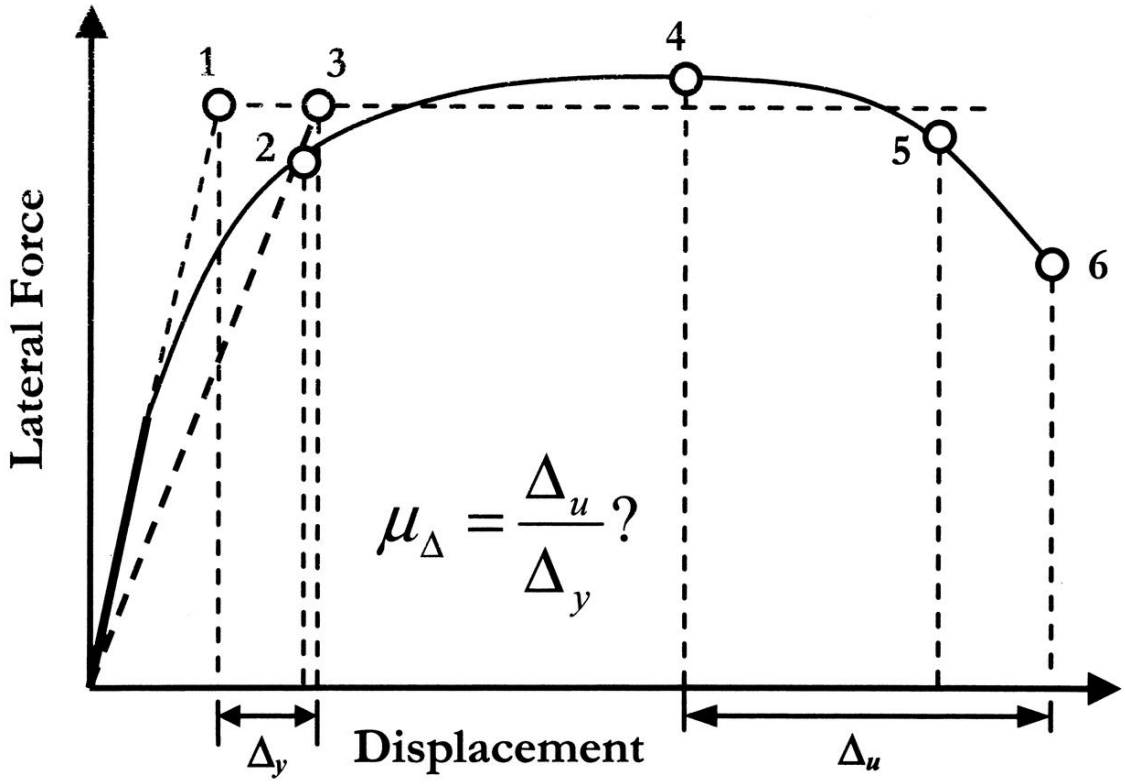

Figure 2.2 Yield and Ultimate Displacement Definitions (from Priestley et al., 2007)

2.4 MSJC Code Provisions

Seismic design requirements for reinforced concrete masonry shear walls are given in Section 1.18 of the 2011 *Building Code Requirements and Specification for Masonry Structures* reported by the Masonry Standards Joint Committee (MSJC). The MSJC establishes three classifications of reinforced concrete masonry shear walls: ordinary, intermediate and special.

The discussion here will focus solely on the provisions for special reinforced masonry shear walls. Reinforcement detailing is found in Section 1.18.3.2.6 of the MSJC Code. Provisions state that the minimum area of vertical and horizontal reinforcement shall not be less

than 0.2 in^2 or 0.0007 multiplied by the gross cross-sectional area of the wall. The vertical reinforcement must also be greater than one-third of the required shear reinforcement. The sum of the vertical and horizontal reinforcement must be greater than 0.002 multiplied by the gross cross-sectional area of the wall. The maximum spacing of vertical and horizontal reinforcement shall be the smallest of one-third the length of the wall, one-third the height of the wall or 48 in.

The MSJC Code provisions require a shear design capacity check that is given in Section 1.18.3.2.6.1.1. This check decreases the probability that shear failures will occur prior to flexural failures. For walls being designed according to strength design requirements, the design shear strength shall exceed the shear corresponding to the development of 1.25 times the nominal flexural strength. However, the nominal shear strength, computed in accordance with Section 3.3.4.1.2 of the MSJC Code, need not exceed 2.5 times the required shear strength.

Strength design requirements for reinforced concrete masonry shear walls are given in Section 3.3 of the MSJC Code. The maximum size of reinforcement shall not be greater than a No. 9 bar. In addition, the nominal bar diameter shall not exceed one-eighth of the nominal member thickness, one-quarter of the least clear dimension of the cell or four percent of the cell area. Specific provisions for the maximum area of flexural tensile reinforcement are given in Section 3.3.3.5 and are described in detail in the commentary section. The limitations of the provisions ensure that the tensile reinforcement yields prior to crushing of the masonry in the compression zone. This is accomplished by creating a strain distribution, shown in Figure 2.3, where the tensile strain (ε_y) is equal to a factor ($\alpha = 4$ for special reinforced masonry shear walls) multiplied by the reinforcement yield strain, and the masonry compressive strain (ε_{mu}) is equal to 0.0025. The corresponding stresses and forces are then determined and used to find the maximum vertical reinforcement ratio which is given in Equation 2.1.

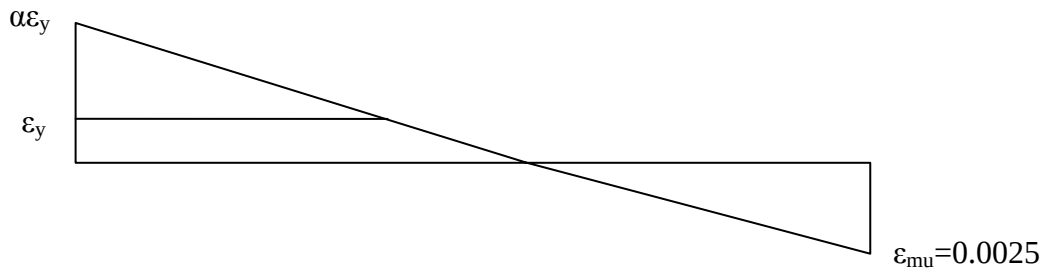

Figure 2.3 Prescribed Strain Distribution (MSJC, 2011)

$$\rho_{max} = \frac{0.64 f_m^{'}\left(\frac{\varepsilon_{mu}}{\varepsilon_{mu}+\alpha\varepsilon_y}\right)-\sigma}{f_y\left(\frac{\alpha\varepsilon_y-\varepsilon_{mu}}{\varepsilon_{mu}+\alpha\varepsilon_y}\right)} \qquad \text{Equation 2.1}$$

Where:

f'_m = masonry compressive strength (ksi)

f_y = reinforcement yield strength (ksi)

2.5 Shing et al.

Shing et al. (1989) tested and evaluated 22 masonry shear walls to investigate the effects the amount of horizontal and vertical reinforcement and the applied axial stress had on the inelastic behavior of masonry shear walls. The analysis focused on the influence these design parameters had on the flexural and shear strengths, ductility and energy dissipation capacities of masonry shear walls. Sixteen of the 22 walls were constructed with concrete masonry blocks and are the focus of the remaining discussion. The walls were nominally 72 in. tall, 72 in. long, 6 in. thick, and were fully grouted. The horizontal and vertical reinforcement were uniformly distributed every 16 in. The walls were subjected to various magnitudes of constant axial stress and a prescribed in-plane lateral displacement sequence.

The flexural strength of each wall specimen was evaluated using moment-curvature analysis developed by the computer program UNCOLA and compared to the experimental results. The analytical and experimental results showed good correlation for walls with a vertical

reinforcement ratio of 0.38%; their failure mechanism was primarily flexural or a combination of flexural and shear. Walls with higher vertical reinforcement ratios, 0.54% and 0.74%, showed less correlation between the analytical and experimental results; their failure mechanism was dominated by shear. The moment-curvature analysis was based on the assumption that plane-sections remain plane. This assumption is not valid when shear provides a significant contribution to the deformations and explains the poor correlation between the analytical predictions and experimental results for walls with higher reinforcement ratios.

Test results showed that larger amounts of vertical reinforcement increased the flexural and shear strengths of the walls. Increasing the amount of horizontal reinforcement had little influence on shear strength but it was observed to change the failure mode from shear-dominated to flexure-dominated. Increasing the magnitude of the applied axial load tended to change the behavior of the wall from a more ductile flexural/shear mode to a brittle shear mode. The authors concluded that the axial load had a more significant influence on the flexural strength than on the shear strength of a wall. Results showed that walls failing in flexure were more ductile and had higher levels of energy dissipation than walls failing in shear. Among the walls failing in shear, those with larger amounts of vertical and horizontal reinforcement were more ductile and capable of dissipating more energy.

2.6 Ibrahim and Suter

Ibrahim and Suter (1999) tested and evaluated five concrete masonry shear walls to investigate the effects the applied axial stress, the amount of vertical reinforcement, and the height-to-length aspect ratio had on the behavior of masonry shear walls. The analysis focused on the influence these design parameters had on the shear strength and ductility of masonry shear

walls. The walls had three height-to-length aspect ratios (0.467, 0.636 and 1.0) and two vertical reinforcement ratios (0.004 and 0.006). The horizontal reinforcement ratio was 0.002 for all the walls. Walls were subjected to two magnitudes of constant axial stress and a prescribed in-plane lateral displacement sequence.

The failure mode for one of the walls was governed by a mixture of flexure/shear behavior, and the remaining four walls were governed by a brittle shear-dominated failure. The authors note that despite failing in shear, these walls still exhibited considerable ductility capacity. This was likely due to the vertical reinforcement increasing the masonry confinement and the axial stress enhancing the aggregate interlock forces. Test results showed that as the magnitude of the applied axial stress was increased, the shear strength and displacement ductility increased while the drift decreased. It was also evident that the shear strength, drift and displacement ductility increased with larger amounts of vertical reinforcement. Lastly as the height-to-length aspect ratio increased the level of drift and the displacement ductility increased while the shear strength decreased.

2.7 Eikanas

Eikanas (2003) tested and analyzed seven fully grouted concrete masonry shear walls to investigate the effects the amount of vertical reinforcement and the height-to-length aspect ratio had on the inelastic behavior of masonry shear walls under in-plane lateral loading. The analysis focused on the influence these design parameters had on the definition of failure, the rate of load degradation after toe crushing and drift, and the plastic hinge length. The walls had four height-to-length aspect ratios (0.72, 0.93, 1.5 and 2.1) and two vertical reinforcement ratios (approximately ρ_{max} and approximately $2\rho_{max}$). Enough horizontal reinforcement was provided

to ensure a flexural failure mode. The walls were subjected to a constant axial stress and a prescribed in-plane lateral displacement sequence.

The experimental results were compared to the provisions set forth by the 2000 IBC (ICC, 2000). The code requirements limit the maximum vertical reinforcement ratio to produce a 1% wall drift and attain a specified tensile reinforcement strain before reaching a critical masonry strain of 0.0025, which the 2000 IBC defines as toe crushing/failure. However, test results showed that critical masonry strain was reached significantly before 1% drift, toe crushing and 20% load degradation were achieved. Drift increased by at least 210% from the point of reaching critical masonry strain to the onset of toe crushing and an additional 20% prior to failure. It was concluded that much greater drift capacities are attainable prior to failure than is implied by the 2000 IBC.

Test results indicated that an increase in the height-to-length aspect ratio corresponded to larger drift capacities at failure. It was observed that the aspect ratio also influenced wall behavior; smaller aspect ratios led to increased shear behavior along with decreased drift capacities. Increasing the aspect ratio corresponded to a decrease in the plastic hinge length. The results of the wall tests showed that larger vertical reinforcement ratios resulted in smaller drift capacities at failure. The wall behavior was also influenced by the vertical reinforcement ratio; walls with lower ratios experienced more sliding while walls with higher ratios tended to increase the amount of shear contribution in squat walls. It was observed that larger reinforcement ratios corresponded to a decrease in the plastic hinge length. The 2000 IBC does not associate the aspect ratio with wall behavior and uses the same requirements for determining the vertical reinforcement ratio in all types of walls. It was concluded that the aspect ratio should

be considered when determining the vertical reinforcement ratio because both parameters greatly influence wall behavior.

2.8 Voon and Ingham

Voon and Ingham (2006) tested and evaluated ten masonry shear walls to investigate the effects the amount and distribution of horizontal reinforcement, the applied axial stress, and the height-to-length aspect ratio had on the shear strength of masonry shear walls. Eight of the walls were nominally 72 in. long and 72 in. tall (height-to-length aspect ratio 1.0), while the other two walls provided height-to-length aspect ratios of 2.0 and 0.6. Eight of the walls were fully grouted while the remaining walls were partially grouted. The vertical reinforcement in each wall was consistent in amount and distribution. The horizontal reinforcement varied in amount and distribution. The walls were subjected to various magnitudes of constant axial stress and a prescribed in-plane lateral displacement sequence.

The shear strength of each wall was predicted using the design requirements specified in the National Earthquake Hazards Reduction Program (NEHRP, 1997) and compared to the experimental results. The predicted shear strength values were reasonably accurate for walls with a height-to-length aspect ratio less than or equal to 1.0 and were overestimated for walls with a height-to-length aspect ratio equal to 2.0.

Eight of the walls exhibited characteristics of a shear-dominated failure while two exhibited a mixture of flexure/shear. Results showed that increasing the amount of shear reinforcement directly influenced the shear capacity by improving the post-cracking performance of the walls. Distributing the reinforcement up the height of the wall using smaller diameter bars was advantageous when compared to concentrating the reinforcement in a few larger diameter

bars. By distributing the bars, the shear stresses were more evenly distributed throughout the wall which prevented the initial diagonal cracks from widening and caused new diagonal cracks to form which resulted in a more ductile behavior and higher energy dissipation capabilities. Results showed that increasing the magnitude of the applied axial stress delayed the initiation of cracking and increased the shear strength of the wall. The authors also found that the shear strength increased as the height-to-length aspect ratio of the walls decreased.

2.9 Shedid et al.

Shedid et al. (2008) tested and analyzed six masonry shear walls to investigate the effects the amount and distribution of vertical reinforcement and the applied axial stress had on the inelastic behavior of masonry shear walls. The walls were nominally 72 in. long, 144 in. tall, 8 in. thick and were fully grouted. The vertical reinforcement was uniformly distributed every 8 in. or 16 in. Enough horizontal reinforcement was provided to ensure a flexural failure mode. The walls were subjected to various magnitudes of constant axial stress and a prescribed in-plane lateral displacement sequence.

The yield strength and ultimate flexural strength of each wall specimen were predicted and compared to the experimental results. The predicted strength values were calculated using the design requirements specified in the 2004 Canadian Standards Association S304.1 (CSA) and the 2005 Masonry Standards Joint Committee (MSJC). The strength predictions were calculated twice for each standard: once neglecting the influence of compression reinforcement, and once including the influence of compression reinforcement. The experimental values for the yield and ultimate strengths were very similar to those found using the CSA and MSJC design requirements. It was found that neglecting the effects from compression reinforcement resulted

in predicted values slightly less than experimental values while including the effects from compression reinforcement resulted in predicted values slightly greater than experimental values. The authors concluded that flexural strength predictions using beam theory are accurate for walls with low magnitudes of axial load.

All of the walls exhibited characteristics typical of a flexural failure. Results showed that the lateral load capacity increased as the vertical reinforcement ratio increased and the axial stress was held constant. It was also found that the lateral load capacity slightly increased as the axial stress increased and the vertical reinforcement ratio was held constant. Results showed that the yield displacement increased with larger amounts of vertical reinforcement and axial stress. It was found that the displacement ductility decreased significantly with increasing amounts of vertical reinforcement and only slightly decreased with increasing amounts of axial stress. It was concluded that all of the walls behaved in a ductile manner.

2.10 Sherman

Sherman (2011) tested and evaluated eight fully grouted concrete masonry shear walls to investigate the effects the height-to-length aspect ratio, the applied axial stress, the amount of vertical reinforcement, and the presence of lap splices had on the inelastic behavior of masonry shear walls. The walls had three height-to-length aspect ratios (0.78, 1.0 and 2.0) and two vertical reinforcement ratios (0.0033 and 0.0072). Enough horizontal reinforcement was provided to ensure a flexure-dominated failure. The walls were subjected to various magnitudes of constant axial stress and a prescribed in-plane lateral displacement sequence.

Connections between the test parameters and the effects they had on wall performance were evaluated. All eight walls exhibited behaviors typical of a flexure-dominated failure. The

experimental results indicated that on average, the total drift at failure decreased with an increase in aspect ratio. For the specimens with larger aspect ratios, larger yield displacements and smaller average ultimate displacements correlated to a reduction in displacement ductility. The aspect ratio did not have a significant effect on the height of plasticity or the plastic hinge length. Results showed that when the magnitude of applied axial stress decreased the height of plasticity and the plastic hinge length increased. The magnitude of applied axial stress did not have a significant effect on the displacement ductility, average drift or total energy dissipation. Walls with larger vertical reinforcement ratios had smaller values for average drift, displacement ductility, height of plasticity and plastic hinge length. The vertical reinforcement ratio did not have a significant effect on the total energy dissipated. Lastly, the presence of lap splices in a wall was associated with decreased values for drift, displacement ductility, height of plasticity, plastic hinge length and energy dissipation. It was concluded that greater drift capacities can be achieved prior to failure than is implied by the 2008 MSJC and that walls with lap splices perform poorly and should be avoided in high seismic regions.

2.11 Summary

This chapter provided a review of the two main failure mechanisms for shear walls under in-plane loading: flexure and shear. It also included a discussion on ductility and the current seismic design provisions regarding the minimum and maximum amount of reinforcement given in the 2011 MSJC Building Code Requirements for Masonry Structures (MSJC, 2011). Several experimental studies that examined the behavior of reinforced concrete masonry shear walls under cyclic in-plane lateral loading were also reviewed.

CHAPTER 3:

EXPERIMENTAL PROGRAM

3.1 Introduction

Eight concrete masonry shear walls were constructed in this study to investigate the effects of varying wall design parameters on the seismic performance of the wall. This chapter provides a detailed description of each wall specimen, how they were constructed, testing methods, instrumentation and data acquisition systems used during testing.

3.2 Footing Description

The wall specimens were all built on heavily reinforced concrete footings. There were three sizes of footings. The footings were all 24 in. wide, 18 in. deep and had lengths of 68 in., 86 in. and 104 in. for wall lengths of 40 in., 56 in. and 72 in., respectively. Reinforcement in all of the footings consisted of No. 4 shear stirrups at 8 in. on center. The footings also included longitudinal bars consisting of either nine No. 5 bars for wall lengths of 40 in., nine No. 7 bars for wall lengths of 72 in. or twelve No. 7 bars for wall lengths of 56 in., all evenly spaced within the footing. The flexural (vertical) reinforcement was anchored in the footings with 90 degree hooks and extended above the footing either the required lap splice length or the total height of the wall. Wall Specimens C7 and C8 had additional shear stirrups and hoops, spaced every 3 in. vertically, within the footing that encompassed each of the four vertical reinforcing bars located in the end cells of the walls.

The footings were designed to act as a rigid support for the wall specimens. This was achieved by anchoring the footings to a reaction floor through eight or twelve bolt tubes cast into the footing for wall lengths of 40 in. or wall lengths of 56 in. and 72 in., respectively. Bent No. 4

bars were placed in each of the four corners as a lifting hook to move the specimens with an overhead crane. Figure 3.1 depicts a typical footing design without the extra reinforcement added to Wall Specimens C7 and C8.

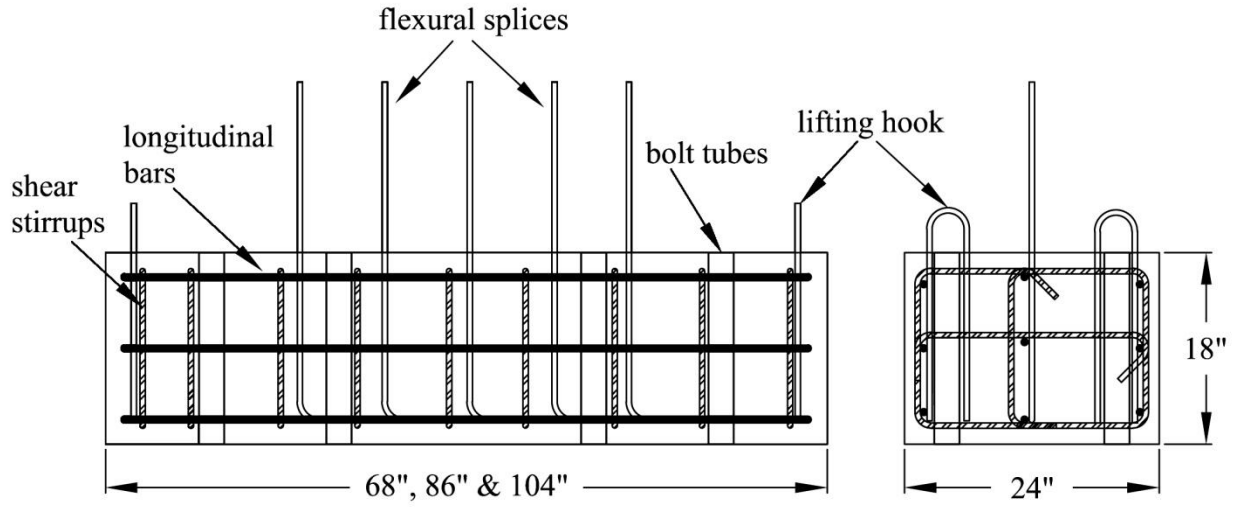

Figure 3.1 Typical Footing Design

3.3 Wall Specimen Description

The wall specimens were constructed of fully-grouted concrete masonry units laid in running bond. All the walls had a nominal thickness of 8 in. while the length and height varied to provide aspect ratios of 0.78, 1.0 and 2.0. The bar size and spacing of the vertical reinforcement varied among the wall specimens. Wall Specimens C1 through C6 had evenly distributed vertical reinforcement while Wall Specimens C7 and C8 had concentrated vertical reinforcement at the ends of the walls (jambs). Figures 3.2 and 3.3 depict how the evenly distributed vertical reinforcement and the jamb reinforcement are arranged within the masonry cells, respectively. For Walls C1 through C7, the provided vertical reinforcement ratio (ρ_{v_prov}) was less than the maximum vertical reinforcement ratio (ρ_{v_max}) determined from the provisions

in Section 3.3.3.5 of the 2011 MSJC Code. For Wall C8, the provided vertical reinforcement ratio was greater than the maximum vertical reinforcement ratio permitted. Wall Specimens C1 and C2 and C3 through C5 had lap splices at the base of the wall that were 16 in. and 46 in. long, respectively. The length of each lap splice was determined from the provisions in Section 3.3.3.3 of the 2011 MSJC Code. Wall Specimens C6 through C8 did not have lap splices.

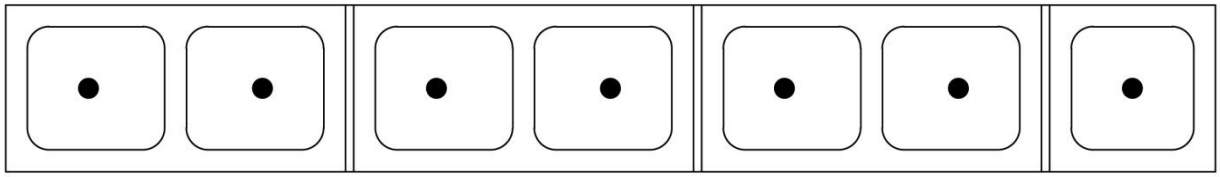

Figure 3.2 Evenly Distributed Vertical Reinforcement

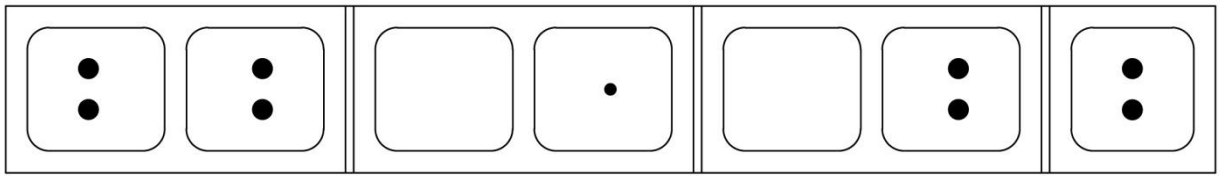

Figure 3.3 Jamb Reinforcement

Shear (horizontal) reinforcement varied among the wall specimens. It was provided to ensure that the nominal shear strength was greater than the nominal flexural strength predicted with moment-curvature analysis. The horizontal reinforcement consisted of one No. 4 bar in every course for Wall Specimens C1 through C3 and C6, two No. 4 bars in every course for Wall Specimens C4 and C5, and two No. 3 bars in every course for Wall Specimens C7 and C8. The horizontal reinforcement was anchored around the outermost vertical reinforcement bars with 180 degree hooks. The details previously discussed are listed in Table 3.1 for each wall specimen. Figures 3.4 and 3.5 show a typical wall specimen with evenly distributed vertical reinforcement and a wall specimen with jamb reinforcement, respectively.

Table 3.1 Details of Wall Specimens

Wall	Nominal Length, L in.	Nominal Height, H in.	Aspect Ratio	P/ ($f'_m A_g$)	Vertical Reinf. (ρ_v)	ρ_{v_prov}	ρ_{v_max}	Horizontal Reinf. (ρ_h)	Splice Length, in.
C1	40	80	2.0	0	#4 @ 8 in.	0.0033	0.0115	#4 @ 8 in.	16
C2	40	80	2.0	0.0625	#4 @ 8 in.	0.0033	0.0067	#4 @ 8 in.	16
C3	40	80	2.0	0.0625	#7 @ 16 in.	0.0059	0.0067	#4 @ 8 in.	46
C4	72	56	0.78	0.0625	#7 @ 16 in.	0.0055	0.0067	2 #4 @ 8 in.	46
C5	72	72	1.0	0.0625	#7 @ 16 in.	0.0055	0.0067	2 #4 @ 8 in.	46
C6	56	112	2.0	0	#6 @ 8 in.	0.0072	0.0115	#4 @ 16 in.	NA
C7	56	112	2.0	0	8 #6	0.0087	0.0115	2 #3 @ 8 in.	NA
C8	56	112	2.0	0.0625	8 #6	0.0087	0.0067	2 #3 @ 8 in.	NA

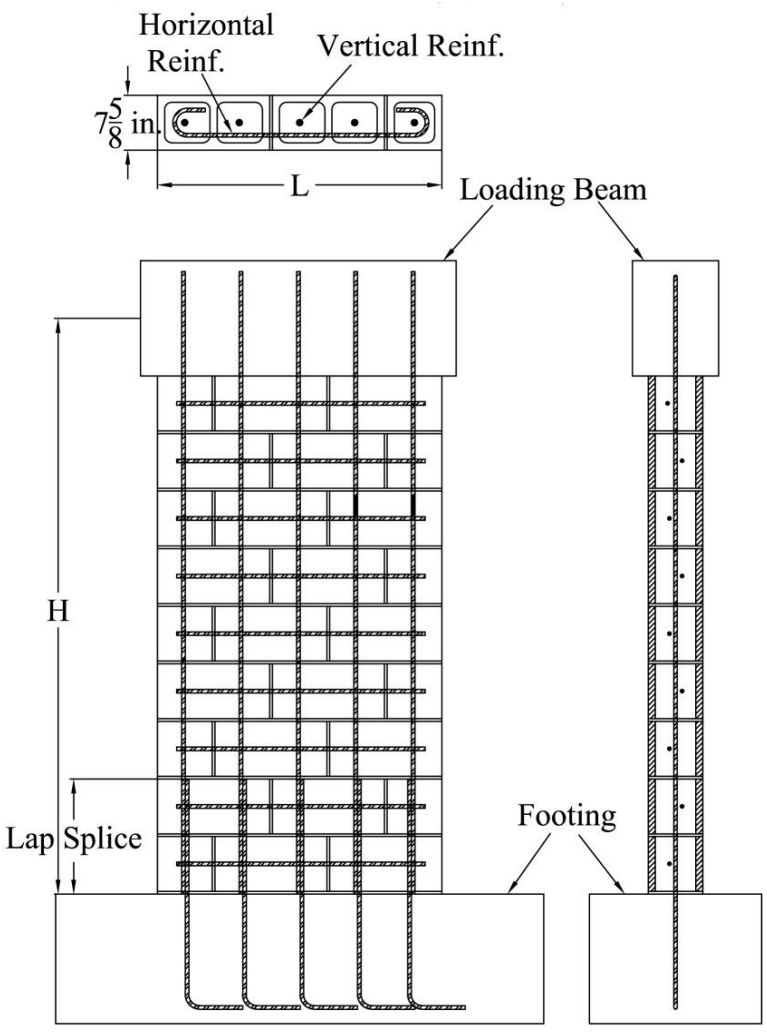

Figure 3.4 Typical Wall Specimen

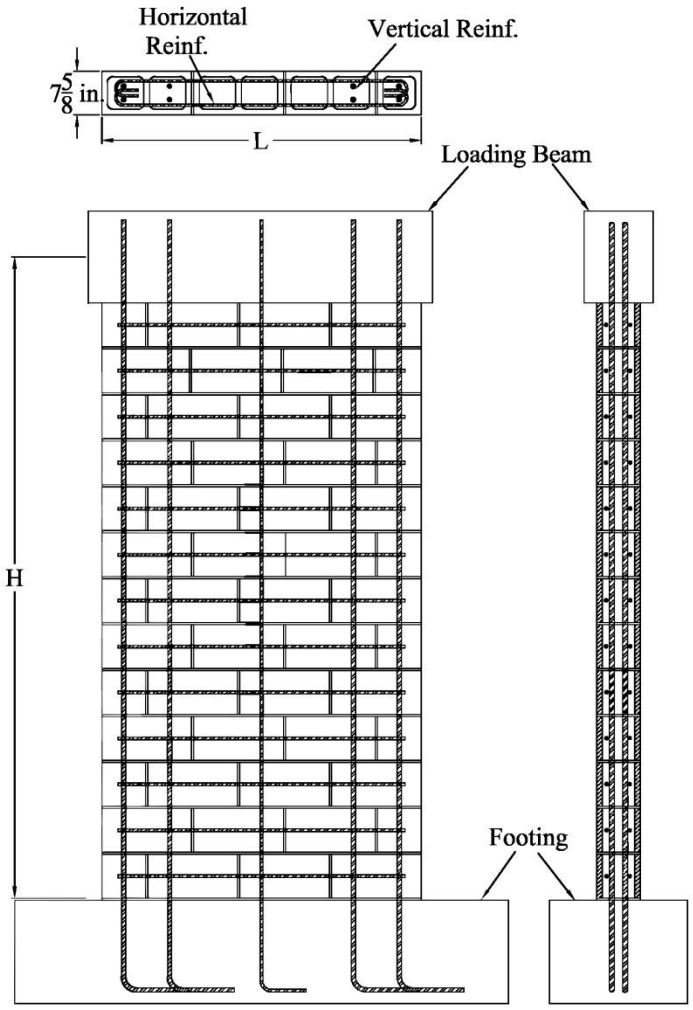

Figure 3.5 Jamb Reinforcement Wall Specimen

3.4 Load Beam Description

Concrete beams were built on top of the wall specimens as a means to apply the in-plane lateral load to the walls. There were three sizes of load beams. They were all 12 in. wide, 16 in. deep, and had lengths of 44 in., 60 in. and 76 in. for wall lengths of 40 in., 56 in. and 72 in., respectively. Reinforcement in all of the load beams consisted of No. 4 shear stirrups at 8 in. on center and six No. 5 longitudinal bars that were evenly spaced around the perimeter of the beam.

The flexural reinforcement extended 14.5 in. into the load beam. Figure 3.4 depicts a typical load beam design.

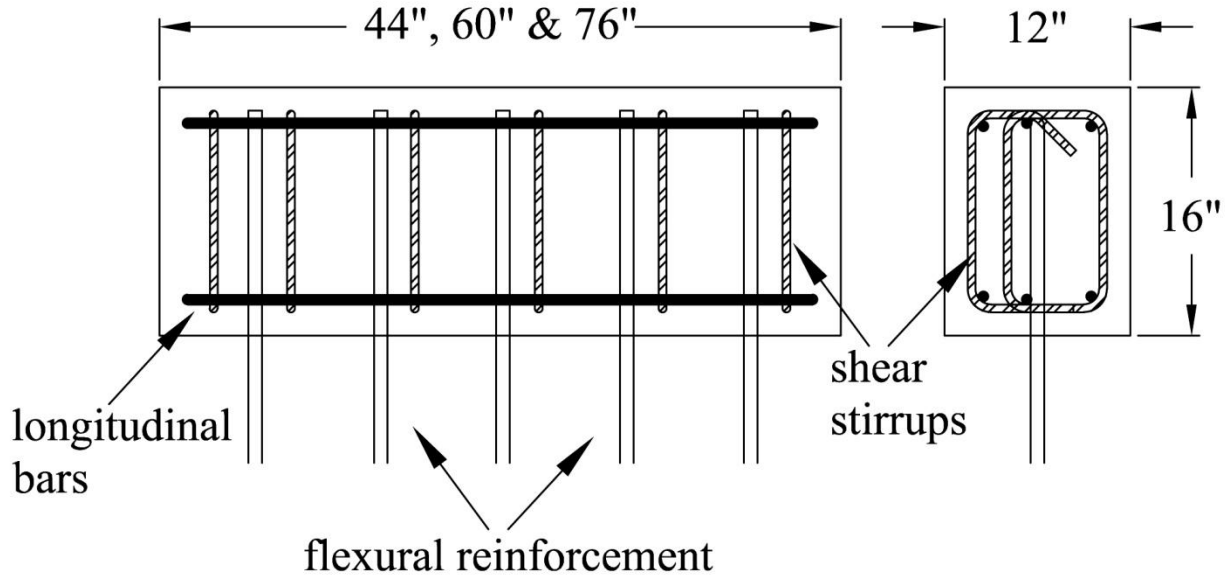

Figure 3.6 Typical Load Beam Design

3.5 Material Properties

The masonry blocks used in this project were nominal 8x8x16-in. standard hollow concrete masonry units and nominal 8x8x8-in. hollow concrete masonry half blocks. Bond beams were used to accommodate placement of the horizontal shear reinforcement. Three standard blocks were set aside for testing, later capped with gypsum cement, and then tested according to ASTM C140-11. Type S mortar was mixed on-site and used to construct the wall specimens. Three mortar test cylinders were made during construction and later tested according to ASTM C780-11. Eight-sack, fine aggregate grout, complying with ASTM C476-10, was used in all the wall specimens. Three grout prisms were made during construction, later capped with gypsum cement, and then tested according to ASTM C1019-11. Three two-block prisms conforming to ASTM C1314 were also made during construction and capped with gypsum

cement for later testing. The average compressive strength for each material is given in Table 3.2.

Table 3.2 Average Material Compressive Strengths, psi

	Masonry Units	**Mortar**	**Grout**	**Masonry Prisms**
Walls C1-C2	3,465	3,220	5,528	3,038
Walls C3-C8		3,330	4,770	2,279

The reinforcement used in all of the wall specimens was Grade 60. The vertical reinforcement consisted of No. 4, No. 6 and No. 7 bars. The horizontal reinforcement consisted of No. 4 and No. 3 bars. The yield strengths for each size of vertical reinforcement bar were obtained from the mill reports provided by the manufacturer and are listed in Table 3.3.

Table 3.3 Vertical Reinforcement Yield Strengths, ksi

	No. 4	**No. 6**	**No. 7**
Walls C1	65.3	---	---
Wall C2	66.0	---	---
Walls C3-C5	---	---	66.0
Wall C6-C8	---	67.5	---

3.6 Construction of Wall Specimens

All eight wall specimens were constructed at the Composite Materials and Engineering Center at Washington State University. The walls were constructed in two groups. The procedures for constructing the footings, walls and load beams were the same for each group of walls. The footing reinforcement cages were tied and placed inside wooden forms along with the vertical reinforcement and bolt tubes. Concrete was ordered from a local ready-mix supplier and as it was cast into the forms it was consolidated with a vibrator. The surface was smoothed with a trowel and then slightly roughened within the expected footprint of the wall by scoring the

surface with the trowel. Care was taken to minimize damage to the strain gages within the footing and those attached to the starter-bars while the concrete was being poured. The next day, the forms were removed from the footing and the vertical reinforcement was tied to the starter-bars when applicable.

All eight wall specimens were constructed by professional masons using running bond with face shell and web bedding. The horizontal reinforcement was placed in the bond beams at their respective courses. The wall specimens were constructed over two days. Six to eight courses were laid on the first day. The remaining courses were laid on the second day and then grout was pumped into the cells and consolidated with a vibrator. Wall Specimens C1 through C5 were grouted in one lift and Wall Specimens C6 through C8 were grouted in two lifts.

The formwork for the load beams was assembled on top of the wall specimens and was supported by small stud walls. The reinforcement cages for the load beams were tied and placed within the forms. Concrete was ordered from a local ready-mix supplier and placed into the formwork for the load beam. The concrete was consolidated with a vibrator and then the surface was smoothed with a trowel.

3.7 Test Setup

The wall specimens were designed with a fixed base to represent a cantilever shear wall. The footings were anchored to a reaction floor with 1.25-in. diameter steel bolts. Footing anchors were secured to the reaction floor at each end of the footing, and steel plates were used to distribute the force between the footing anchors and the footing. This setup prevented the footing from sliding on the reaction floor during testing.

Three identical hydraulic jacks provided the axial (vertical) load for the wall specimens. Each jack has a rated capacity of 10,000 psi, which corresponds to 120 kips of applied force per jack. The jacks were connected in parallel thus maintaining equal pressure to each jack. The pressure that was applied to each wall specimen was determined according to Equation 3.1.

$$Pressure\ Gauge\ reading = \frac{Specified\ Axial\ Load\ (kip)}{360\ kip} * 10{,}000psi \qquad \text{(Equation 3.1)}$$

The pressure from the hydraulic power supply system was maintained at a constant level, and therefore the specified axial load remained constant as the three actuators extended and retracted with the vertical deflection of the wall. The upward pressure from the actuators was resisted by a box beam attached to a sliding trolley system. The trolley slid on the main reaction frame through a set of 12 low-friction bearings that rode against a stainless steel plate attached to the cross-beam in the reaction frame setup. This arrangement enabled the jacks to move with the wall while maintaining a constant vertical load. This effectively created a "free" boundary condition.

A 220-kip capacity hydraulic actuator provided the in-plane load for the wall specimens. The actuator was operated under displacement control. The actuator was connected to the main reaction frame and to a steel end-plate. The load was applied to the wall through two steel end-plates that were affixed to the North and South ends of the load beam and attached to each other by threaded rods. The test setup is shown in Figure 3.7 (North direction on the left).

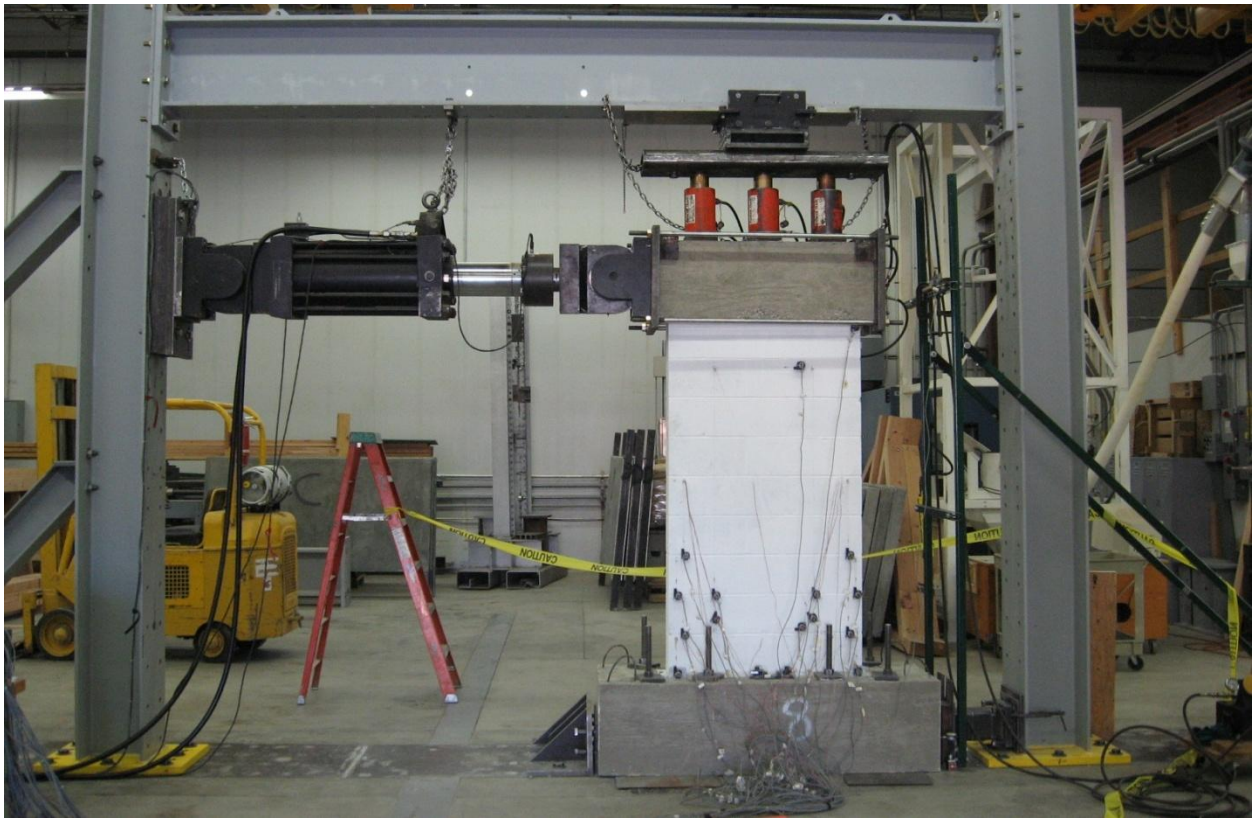

Figure 3.7 Typical Wall Specimen Test Setup

3.8 Instrumentation

Strain gages, displacement potentiometers, a load cell and a dial gauge were used to monitor and acquire data while the wall specimens were tested. The locations of the strain gages are shown on the right side of Figure 3.8. Two strain gages were placed within the footing on the outermost vertical reinforcement bars. Strain gages were also placed on each vertical bar just above the footing. The outermost vertical reinforcement had additional strain gages placed at the top of the first, second and third courses. Lastly, strain gages were placed on the horizontal reinforcement in the first and fifth courses.

The locations of the displacement potentiometers, numbered 3 through 20, are shown on the left side of Figure 3.8. The locations of some of the displacement potentiometers varied

when the aspect ratio of the walls changed. The displacement potentiometers were used to measure the vertical displacements, sliding displacements and shear displacements at several locations on each wall specimen. A displacement potentiometer was used to measure the global wall displacement in the direction of loading. It was placed on a rigid frame that was separate from the main reaction frame setup and then connected to the loading beam at the height of the load application. Another displacement potentiometer was attached to the hydraulic actuator to measure the actuator piston displacement. A load cell was attached to the hydraulic actuator to measure the applied in-plane lateral load. A dial gauge was placed against the footing to measure any sliding that occurred between the footing and the reaction floor.

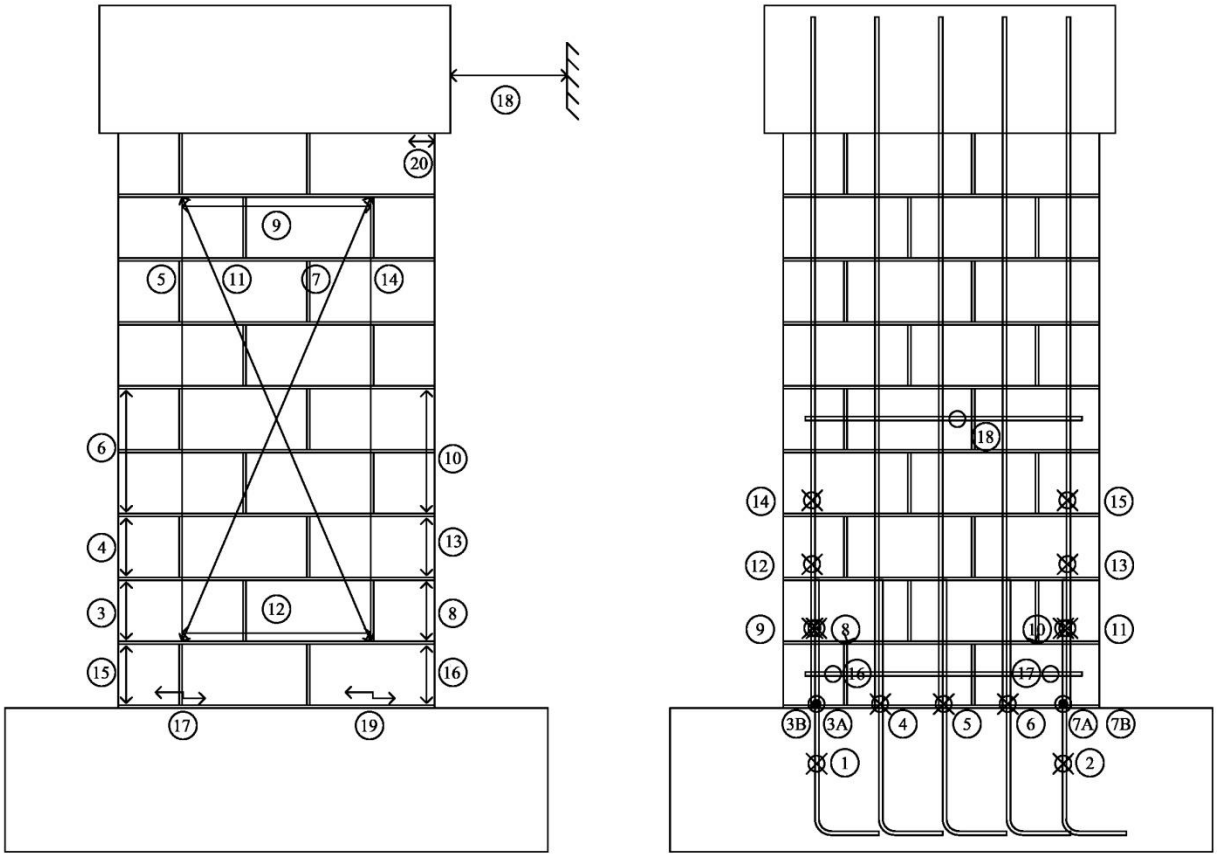

Figure 3.8 Displacement Potentiometer (Left) and Strain Gage (Right) Locations

3.9 System Control & Data Acquisition

The system control and data acquisition was obtained using two computers. One computer controlled the lateral load application by sending a specified load or displacement pattern to the hydraulic controller. The second computer controlled the data acquisition software; it collected one scan signal per second from the load and displacement cells, the displacement potentiometers, and the strain gages. Figure 3.7 illustrates how the signals from the computer were transmitted and how the data was processed and sent back to the computer.

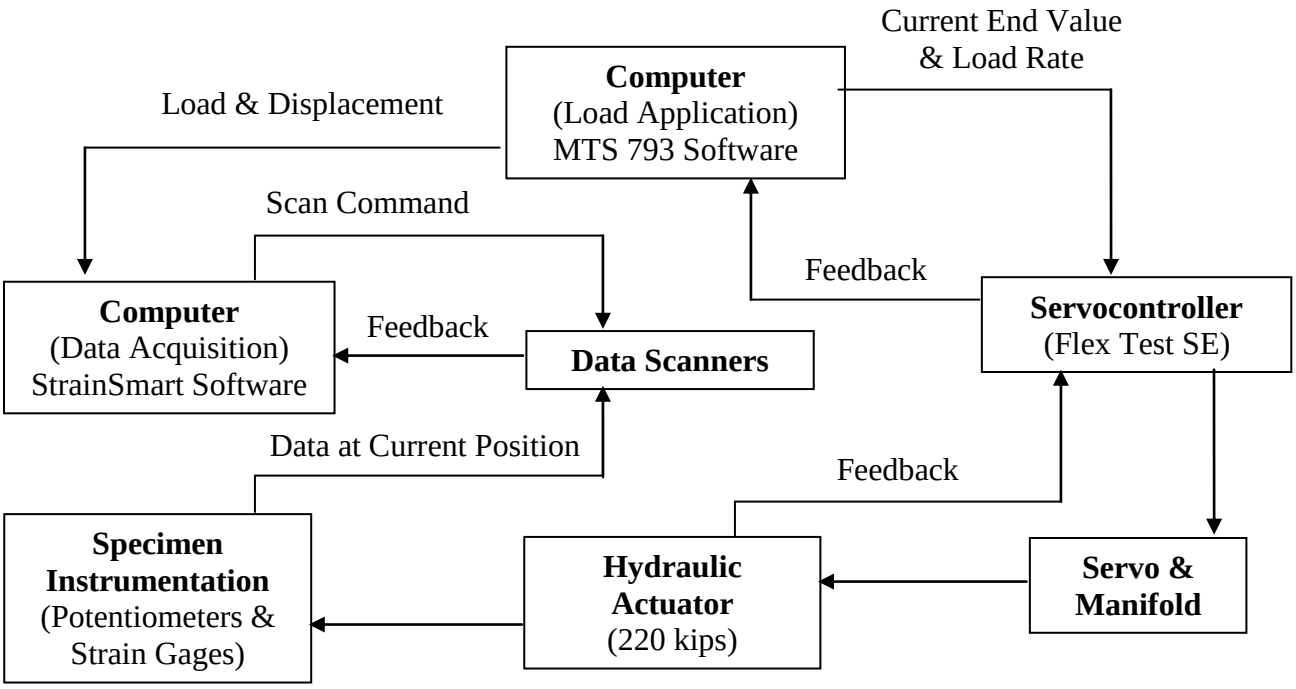

Figure 3.9 System Control & Data Acquisition Flow Chart (adapted from Sherman 2011)

3.10 Test Procedures

All of the wall specimens were tested under displacement control. The cross-sectional analysis program XTRACT was used to obtain the moment-curvature relationship for each wall specimen based on a monotonic pushover test. The maximum moment obtained from XTRACT

was divided by the height of the wall (H) to obtain the expected peak load. This peak load was equivalent to the applied lateral load needed to cause failure in each wall.

The preliminary test protocol consisted of two complete cycles of the actuator (both negative and positive directions) at loads corresponding to 25%, 50% and 75% of the expected peak load, as determined by XTRACT. The preliminary cyclic loading protocol is shown in Figure 3.10. The displacements at 75% of peak load (in the negative and positive directions for both cycles) were extracted from the preliminary data set. These displacements were multiplied by 4/3 and averaged to obtain a value for delta-Y (ΔY), where ΔY is the predicted displacement at peak load. The primary test protocol consisted of two complete cycles (both negative and positive directions) of displacements at increasing multiples of ΔY. Figure 3.11 shows cyclic patterns of displacement for the primary test. Displacement levels (ΔY) were sequentially increased until the resultant in-plane lateral load was reduced to 50% of the maximum in-plane lateral load that was recorded during earlier displacement levels or until loss of structural integrity (failure) of the wall specimen, whichever occurred first. The displacement rate used for all of the wall specimens during the preliminary and primary tests was 0.3 in./min.

3.11 Summary

This chapter provided a detailed description of the wall specimens and how they were constructed. It also described the test set-up and test protocol that was used for the wall specimens. Lastly, an account of the instrumentation and data acquisition systems were given.

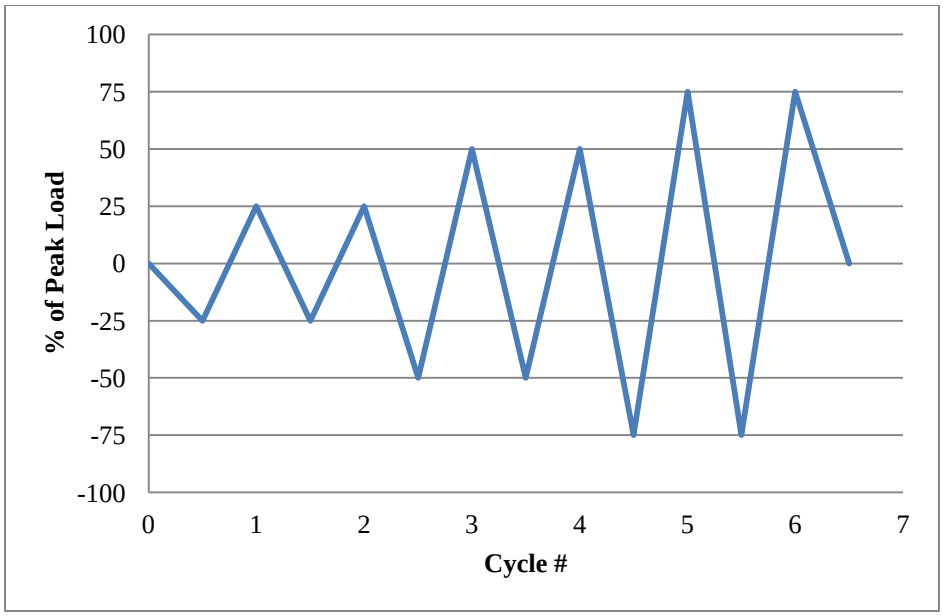

Figure 3.10 Preliminary Loading Protocol

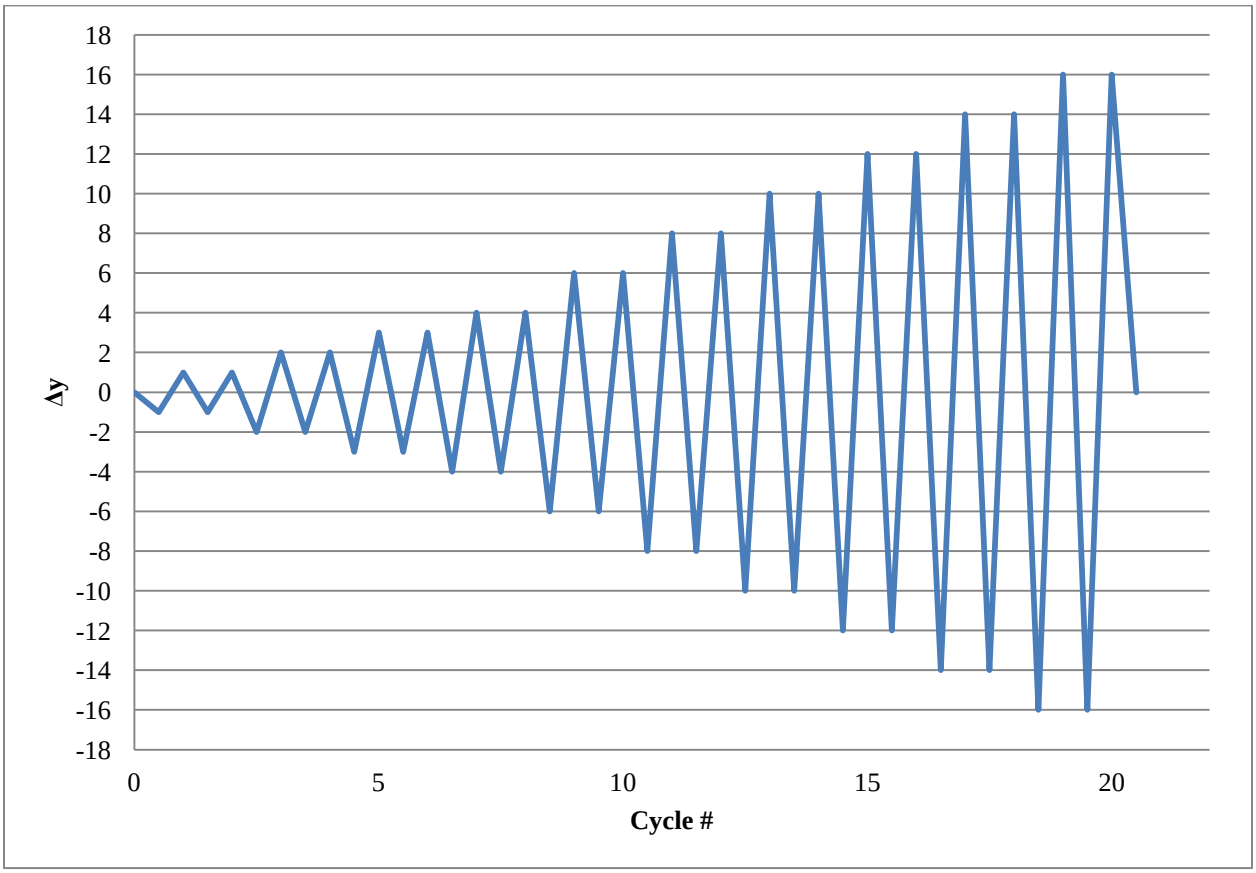

Figure 3.11 Primary Loading Protocol

CHAPTER 4:

RESULTS OF WALL TESTS

4.1 Introduction

Results for the eight concrete masonry shear walls tested in this study are presented in this chapter. Included are: test observations, load-displacement hysteresis curves, displacement and drift components, curvature measurements, displacement and curvature ductilities, height of plasticity, equivalent plastic hinge lengths, energy dissipation, and equivalent hysteretic damping. The analysis procedures and equations used for determining the lateral load capacity, displacement and drift components, wall curvatures, displacement and curvature ductility, height of plasticity, equivalent plastic hinge length, energy dissipation, and equivalent hysteretic damping are also presented. These procedures are the same as those used by Sherman (2011).

4.2 Wall Specimen C1

Wall Specimen C1 had a height-to-length aspect ratio of 2.0, No. 4 vertical reinforcement spaced 8-in. on center with a splice at the base of the wall, No. 4 horizontal reinforcement spaced 8-in. on center, and zero axial load. The length of the lap splice was 16 in. and was determined from the provisions in Section 3.3.3.3 of the 2011 MSJC Code. The maximum lateral load capacity was predicted using two methods. The first method was based on Section 3.3 of the 2011 MSJC Code. Material and strength reduction factors were neglected while calculating the load capacity. The compressive resistance of the vertical reinforcement was considered in calculating the load capacity although Section 3.3.2(e) of the code states to neglect this contribution unless it is adequately tied (MSJC, 2011). The second method was based on a moment-curvature analysis performed using the software program XTRACT. The predicted

maximum lateral load capacity of Wall Specimen C1 was 13 kips and 16.5 kips using the MSJC and EXTRACT analysis methods, respectively. Strains were measured on the horizontal reinforcement located in the first and fifth courses and on the extreme vertical reinforcement located at mid-height of the footing to determine if yielding occurred. The horizontal reinforcement did not yield in either course. The extreme vertical reinforcement yielded in the footing of Wall Specimen C1.

Test Observations:

The preliminary test for Wall Specimen C1 produced a yield displacement (ΔY) of 0.38 in. In the primary test, this specimen was loaded to displacements of ±1, 2, 3, 4 and 6 times the yield displacement. During testing, the wall behavior was dominated by flexural cracking that initiated at $1\Delta Y$ and continued to propagate and open at increasing displacement levels. Separation of the mortar joints occurred from the base of the wall to the third course above the footing. Testing was briefly stopped at $3\Delta Y$ due to noticeable out-of-plane rotation of the wall. Bracing was erected which prevented out-of-plane rotation from happening during the remainder of the test. Vertical splitting in the South toe was observed near failure. At test completion, damaged masonry face shells and grout were removed from the base of the wall. At this point, it was observed that necking of the extreme vertical reinforcement had occurred in the North toe. The entire wall specimen and the North and South toe regions of the wall at test completion are shown in Figures 4.1 and 4.2, respectively. Test observations and their corresponding lateral displacements and loads are presented in Table 4.1.

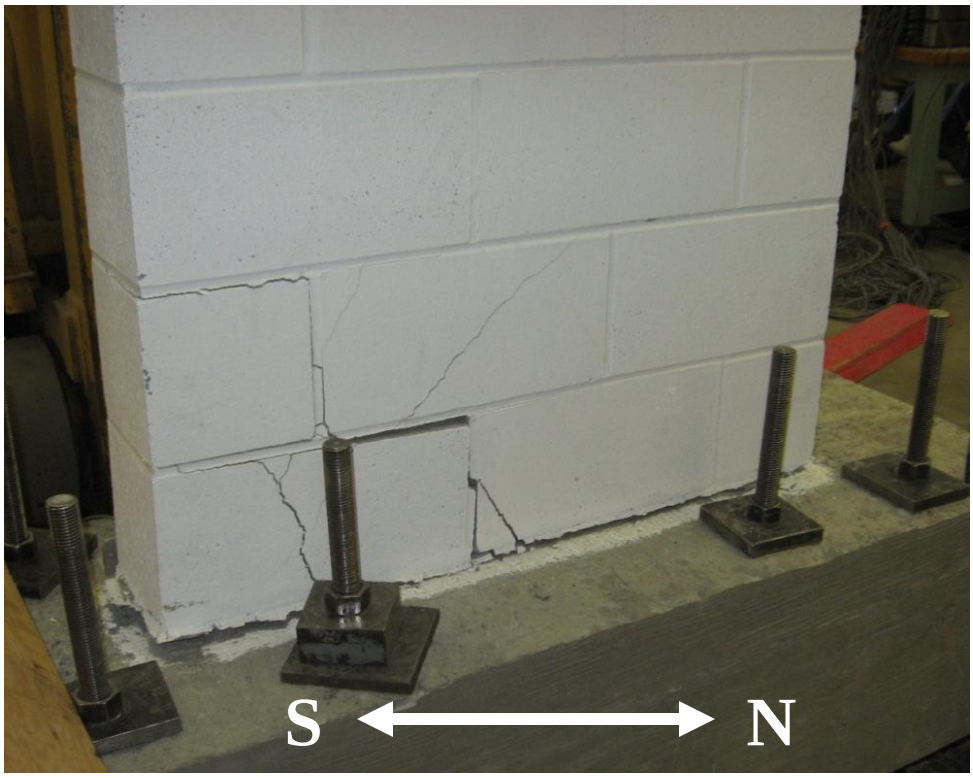

Figure 4.1 Wall C1: Wall at Test Completion

Figure 4.2 Wall C1: South Toe (Left) and North Toe (Right) at Test Completion

Table 4.1 Wall C1: Test Observations

Load (kips)	Disp. (in.)	Test Observation
-8.09	-0.15	1st Yield of extreme vertical reinforcement bar in south toe (push)
6.10	0.16	Critical masonry strain in north toe (pull)
9.72	0.17	1st Yield of extreme vertical reinforcement bar in north toe (pull)
-4.33	-0.17	Critical masonry strain in south toe (push)
-13.51	-0.38	Flexural cracking in north toe (push)*
15.27	0.41	Flexural cracking in south toe (pull)*
-14.16	-0.79	1% Drift in push to south
14.28	0.79	1% Drift in pull to north
17.74	1.16	Maximum load resistance in pull to north
-14.81	-1.53	Onset of toe crushing in south toe (push)*
10.06	1.24	20% load degradation from maximum load resistance in pull to north
-13.68	-2.20	20% load degradation from maximum load resistance in push to south
-17.66	-2.31	Maximum load resistance in push to south

*Visual Observation

Load Displacement:

The load-displacement hysteresis curves for the preliminary and primary tests for Wall Specimen C1 are presented in Figure 4.3. A legend, located in the upper left hand corner, contains six important limit-state events that occurred during testing. Each event is marked on the hysteresis curves in the push (negative load and displacement) and pull (positive load and displacement) directions. The limit-state events include the onset of yielding of the extreme tensile reinforcement (ε_y = 0.00228), reaching critical masonry strain (ε_{mu} = 0.0025), attaining maximum lateral load, reaching 1% drift, the onset of toe crushing, and failure which is defined in this thesis as 20% load degradation of the maximum load attained. The onset of yielding of the extreme tensile reinforcement was measured using strain gages attached to the vertical reinforcement. The critical masonry strain was calculated using displacement potentiometers located in the first eight in. of the wall height. The data obtained from the displacement potentiometers was averaged over a given gage length and assigned at the mid-height of the gage

length. The maximum lateral load attained was determined from the load cell measurements. Reaching 1% drift was determined by dividing the in-plane lateral displacements by the height of the wall (H). The onset of toe crushing was established based on visual observations. Failure was defined as the point in a given displacement level, after the maximum lateral load was attained, where the lateral load dropped to less than 80% of the maximum lateral load. These six major events are presented in Table 4.1 along with the lateral displacement and load at the time of their occurrence.

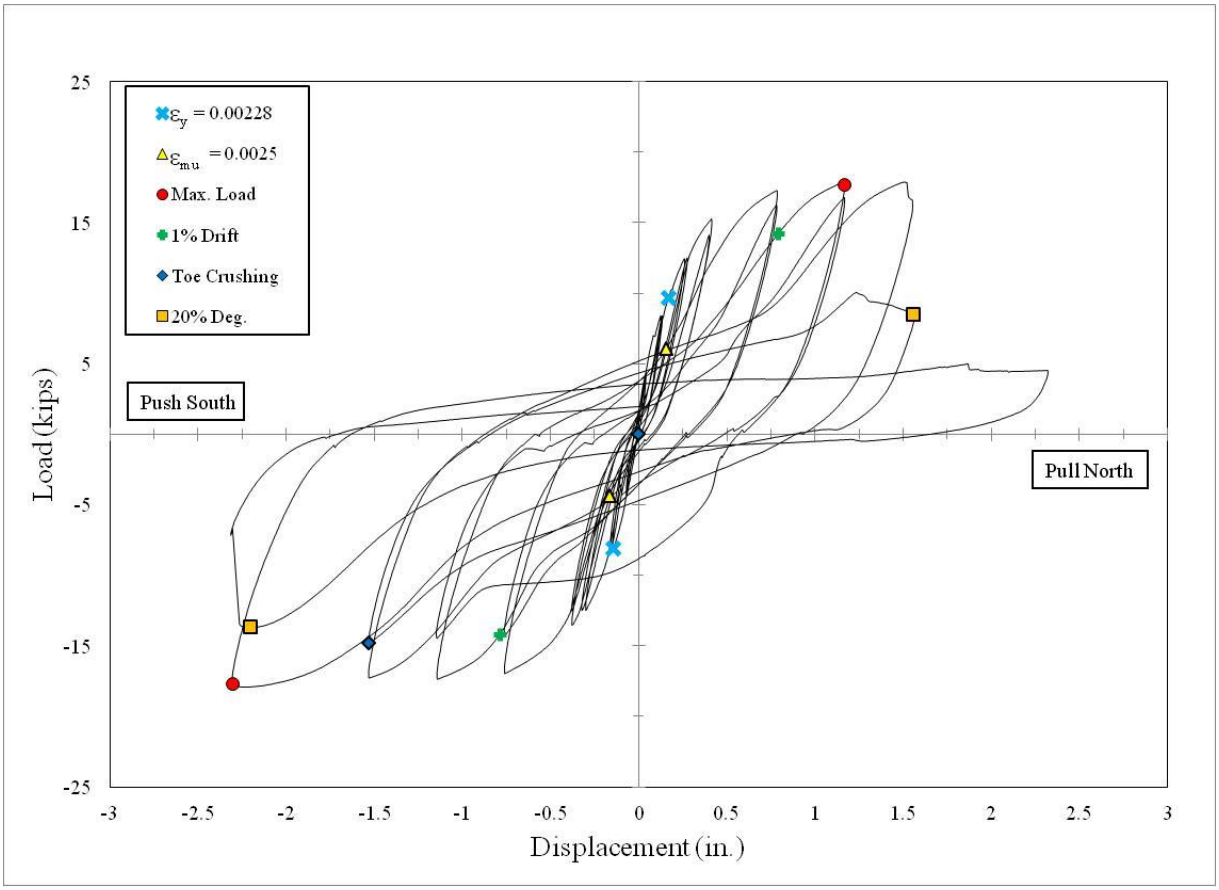

Figure 4.3 Wall C1: Load-Displacement Hysteresis Curves

Wall Specimen C1 reached critical masonry strain during the preliminary test. The onset of yielding of the extreme tensile reinforcement occurred near the end of the preliminary test. The specimen reached 1% drift in the second cycle of 2ΔY and the first cycle of 3ΔY in the push

and pull directions, respectively. Maximum lateral load in the pull direction was also attained in the first cycle of 3ΔY. 20% load degradation in the pull direction occurred in the second cycle of 4ΔY. The maximum lateral load and 20% load degradation in the push direction occurred in the first and second cycles of 6ΔY, respectively. Toe crushing did not occur in the pull direction. Wall Specimen C1 exhibited fairly symmetrical load-displacement relationships in the two loading directions before maximum load was reached. Following this event, the specimen experienced rapid strength degradation in the pull direction and a gradual decrease in strength in the push direction.

Displacement and Drift Components:

The total in-plane lateral displacements are comprised of three components: flexure, sliding and shear. The total lateral displacement was measured with a displacement potentiometer attached to an external reference frame and extended to the load beam at the height of load application. The flexural displacement was found by subtracting the sliding and shear displacements from the total displacements. Two displacement potentiometers that extended in opposite directions from the centerline of the wall measured the sliding displacements at the interface between the base of the wall and the footing. Another displacement potentiometer measured the sliding displacement at the interface between the top of the wall and the load beam; the displacements at this location were very small and were neglected for all the wall specimens. The shear displacement was calculated based on a method used in a previous study by Massone and Wallace (2004). This study used two diagonal and two vertical displacement potentiometers to determine the shear displacement based off of the contributions from both flexural and shear deformations as seen in Figure 4.4. The undeformed

wall is shown with the dashed lines, the shear deformation is represented by the shaded rhomboid, and the combined shear and flexural deformations are depicted by the solid lines.

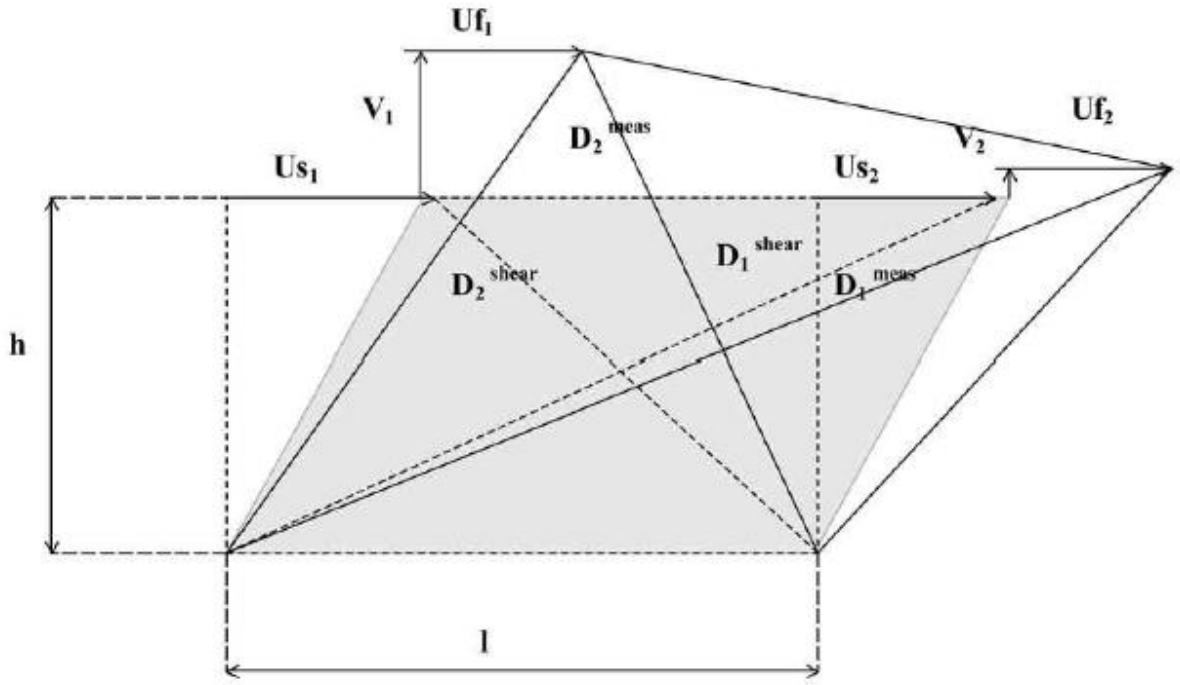

Figure 4.4 Flexural and Shear Deformations (Massone and Wallace, 2004)

The average shear displacement was derived from Figure 4.4 and is defined in Equation 4.1. The first term in this equation represents the shear displacements from shear deformations, and the second term represents the shear displacements from flexural deformations. Massone and Wallace (2004) determined the value for α based on the assumption that the center of rotation occurred at 1/3 of the wall height; this assumption was also used in this study.

$$\Delta_{shear} = \frac{\sqrt{(D_1^{meas})^2 - h^2} - \sqrt{(D_2^{meas})^2 - h^2}}{2} + \left(\frac{1}{2} - \alpha\right)\left(\frac{V_1 - V_2}{l}\right)h \quad \text{Equation 4.1}$$

Where:

Δ_{shear} = average shear displacement;

D_1 & D_2 = diagonal lengths of the deformed displacement potentiometers forming an X across the wall specimen;

V_1 & V_2 = vertical displacements at the top of the wall specimen;

h = height of diagonal pattern (in.);

l = length of diagonal pattern (in.); and

α = distance from the top of the wall to the center of the rotation; assumed to be 0.67.

Load-displacement hysteresis curves that show the total lateral displacement and the three components of displacement are given in Figure 4.5.

Drift was defined as the in-plane lateral displacement divided by the height of the wall. The average total drift and average drift contributions from flexure, sliding and shear deformations are presented in Table 4.2 at three important limit-states: critical masonry strain, peak lateral load and failure. Wall Specimen C1 was dominated by flexural deformations with small levels of shear and sliding deformations occurring near failure.

Table 4.2 Wall C1: Components of Total Drift

Limit-State	Total Drift (%)	Flexure (% Total)	Sliding (% Total)	Shear (% Total)
ε_{mu}	0.2	98.4	1.6	0.0
Peak Load	2.2	91.1	5.8	3.1
Failure	2.4	91.3	6.0	2.7

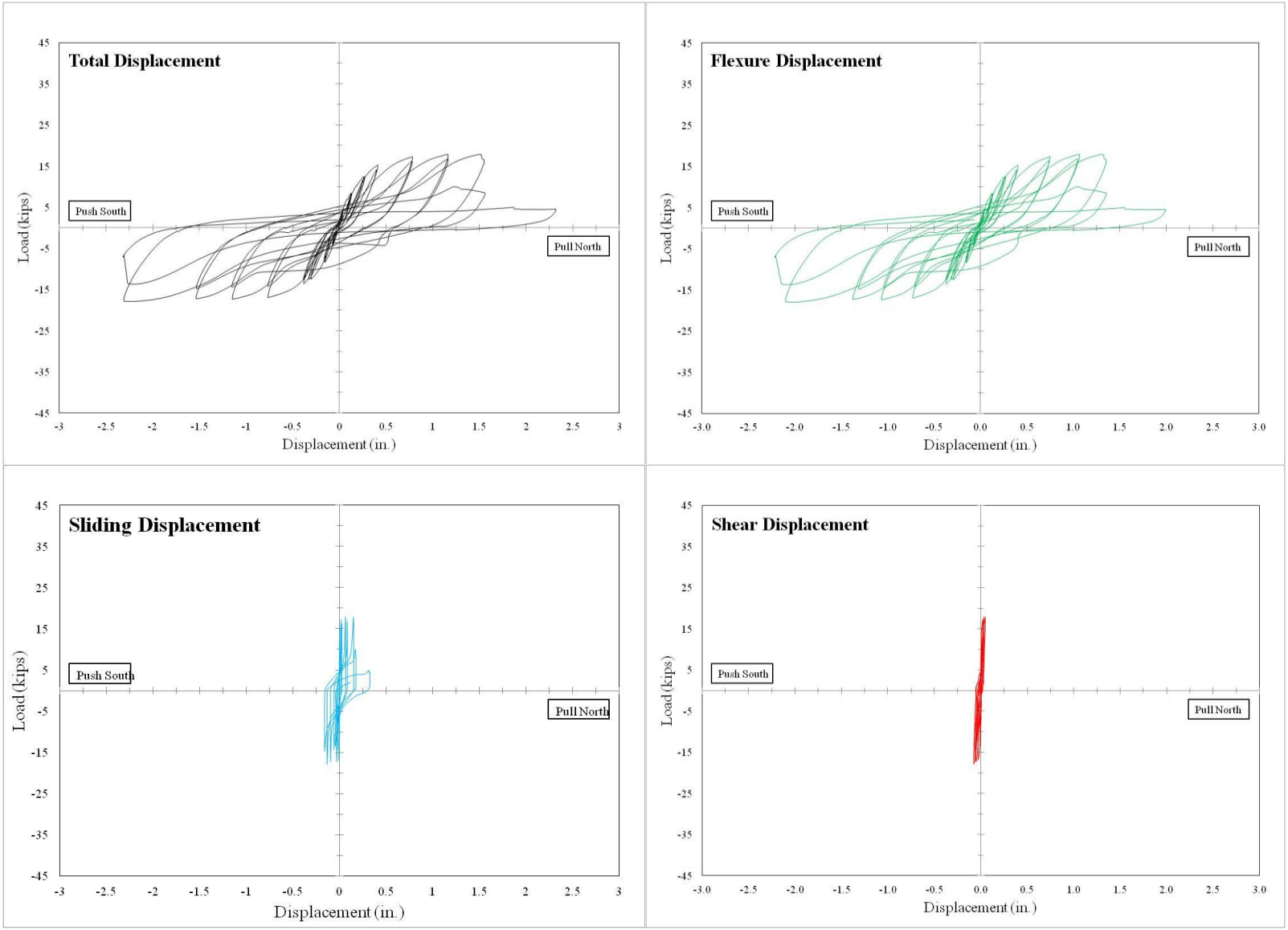

Figure 4.5 Wall C1: Total Lateral-Displacement and its Components

Wall Curvatures:

The curvatures over the wall height were determined based on strain profiles found using the displacements measured from four displacement potentiometers located along the inside edge of opposite sides of the wall. The curvatures were determined in the primary test only and were taken from the first cycle at each displacement level. The strain calculations were averaged over a given gage length and were represented at mid-height of the gage length. For a number of walls, strains and curvatures were unavailable at larger displacement levels due to face shell spalling and resulting damage to the attachment points for the displacement potentiometers. The strain profile at a typical cross-section is shown in Figure 4.6.

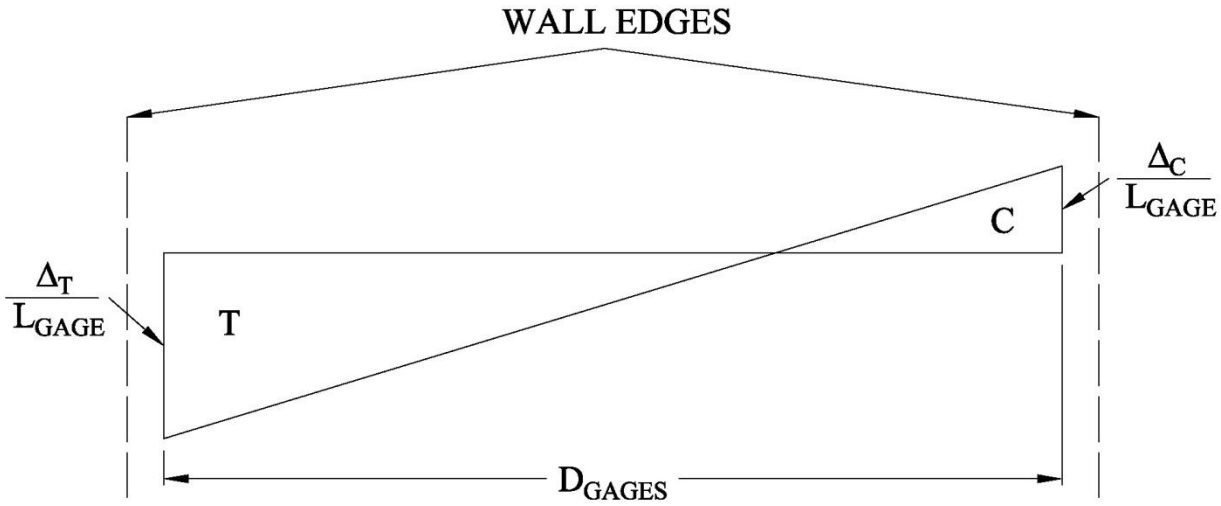

Figure 4.6 Typical Strain Profile (adapted from Sherman, 2011)

The average curvature for a given cross-section was derived from Figure 4.6 and is defined in Equation 4.2.

$$\phi = \frac{\left|\frac{\Delta_T}{l_{gage}}\right| + \left|\frac{\Delta_C}{l_{gage}}\right|}{d_{gages}} \qquad \text{Equation 4.2}$$

Where:

ϕ = curvature at a given cross-section (1/in.);

Δ_T & Δ_C = measured tensile and compressive displacements (in.);

l_{gage} = applicable gage length (in.); and

d_{gage} = in-plane distance between gages (in.).

A plot of curvatures over the height of Wall Specimen C1 is given in Figure 4.7. Curvatures over the wall height were symmetric about the wall center line through 6ΔY. The ultimate curvature was defined at 20% load degradation of the maximum load attained for both loading directions.

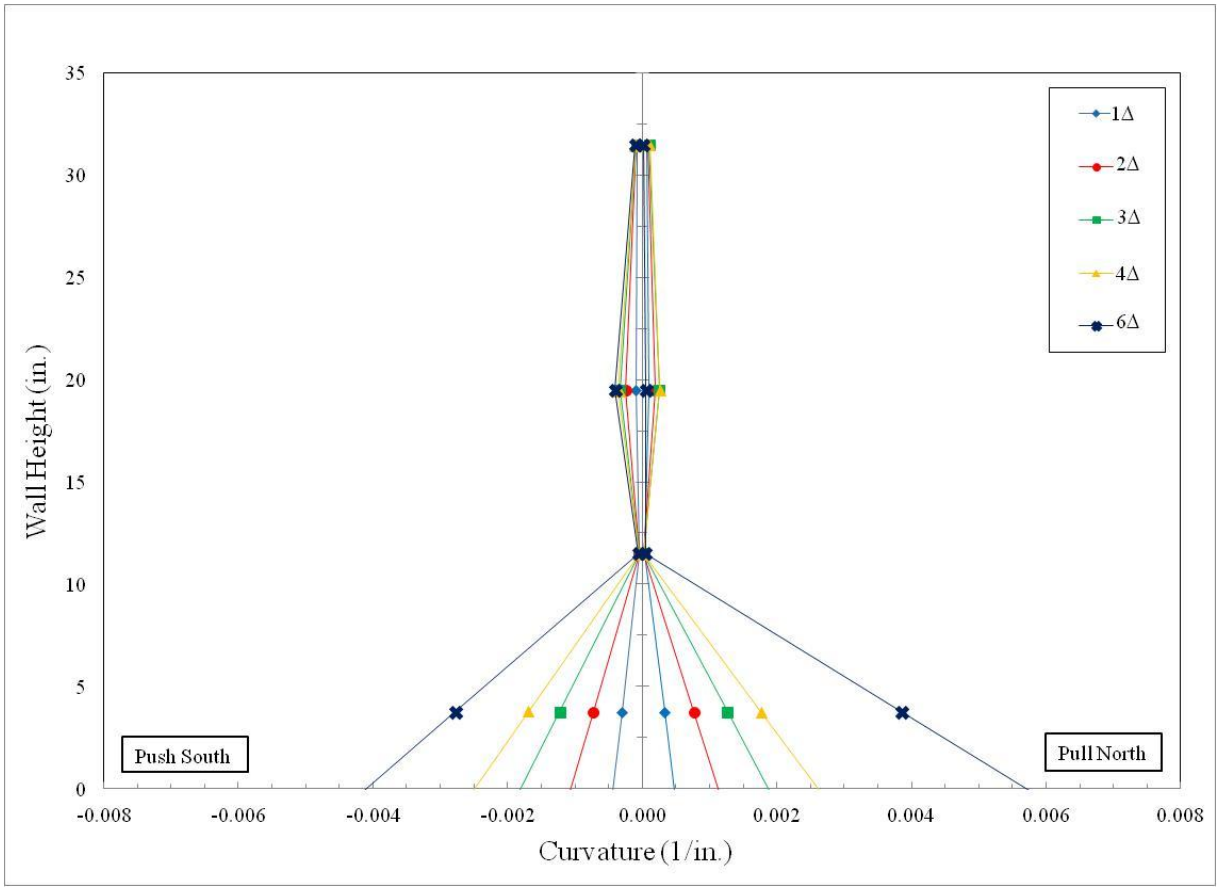

Figure 4.7 Wall C1: Curvature vs. Wall Height

Displacement and Curvature Ductility:

The displacement ductility was found based on an elastoplastic approximation, using the Trapezoid Rule, such that the area under the elastoplastic approximation was set equal to the actual area under the load-displacement envelope as shown in Figure 4.8. The load-displacement envelope was developed using the peak loads in the preliminary and primary tests that were taken from the first cycle at each load or displacement level, respectively. The load-displacement envelope ended when 20% load degradation of the maximum load was reached.

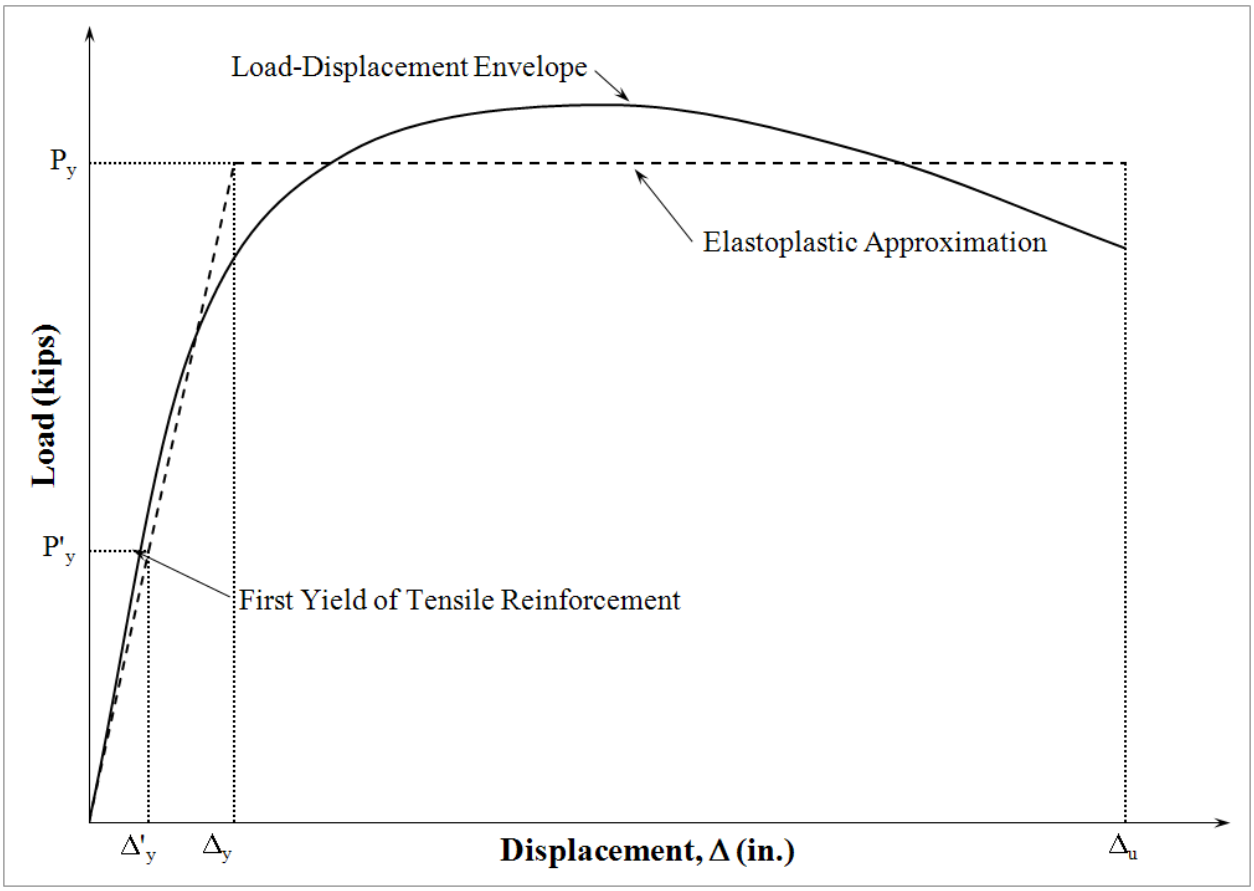

Figure 4.8 Elastoplastic Approximation

The displacement ductility is defined in Equation 4.3.

$$\mu_\Delta = \frac{\Delta_u}{\Delta_y} \qquad \text{Equation 4.3}$$

Where:

μ_Δ = displacement ductility;

Δ_u = ultimate displacement at 20% load degradation (in.); and

Δ_y = yield displacement of elastoplastic approximation (in.).

The yield displacement was defined as the secant stiffness through the initial measured yielding of the extreme tensile reinforcement to the yield force of the elastoplastic approximation. The yield force of the elastoplastic approximation is defined in Equation 4.4.

$$P_y = \left(\frac{P'_y}{\Delta'_y} \right) \Delta_y \qquad \text{Equation 4.4}$$

Where:

P_y = yield force of elastoplastic approximation (kips);

P'_y = yield force at first yield of tensile reinforcement (kips);

Δ'_y = yield displacement at first yield of tensile reinforcement (in.); and

Δ_y = yield displacement of elastoplastic approximation (in.).

The displacement ductilities for the positive and negative loading directions along with the average value are presented in Table 4.3 for Wall Specimen C1. The total drift reached at 20% load degradation was 2.4%.

Table 4.3 Wall C1: Displacement Ductility

Direction of Load	**Displacement**					
	P'_y (kips)	Δ'_y (in.)	Δ_u (in.)	P_y (kips)	Δ_y (in.)	μ_Δ
Push South	-8.1	-0.15	-2.20	-15.9	-0.29	7.7
Pull North	9.7	0.17	1.56	16.7	0.29	5.4
Average	8.9	0.16	1.88	16.3	0.29	6.6

The curvature ductility was found using a process similar to the displacement ductility. The elastoplastic approximation was based on the actual area under the moment-curvature envelope. The moment-curvature envelope ended when 20% load degradation of the maximum load was reached or when valid readings from the displacement potentiometers where no longer available. The curvature ductility is defined in Equation 4.5.

$$\mu_\phi = \frac{\phi_u}{\phi_y} \qquad \text{Equation 4.5}$$

Where:

μ_ϕ = curvature ductility;

ϕ_u = ultimate curvature at 20% load degradation (1/in.); and

ϕ_y = yield curvature of elastoplastic approximation (1/in.).

The curvature ductilities for the positive and negative loading directions along with the average value are presented in Table 4.4 for Wall Specimen C1.

Table 4.4 Wall C1: Curvature Ductility

Direction of Load	**Curvature**					
	M'_y (kip-in.)	ϕ'_y (in.$^{-1}$)	ϕ_u (in.$^{-1}$)	M_y (kip-in.)	ϕ_y (in.$^{-1}$)	μ_ϕ
Push South	-641	-0.00013	-0.0032	-1131	-0.00022	14.1
Pull North	770	0.00011	0.0020	1196	0.00018	11.6
Average	706	0.00012	0.0026	1164	0.00020	12.8

Height of Plasticity and Equivalent Plastic Hinge Length:

The height of the plasticity zone (L_p) was defined as the height above the base of the wall where the average curvatures at failure were higher than the average curvature at the initial yield of the extreme tensile reinforcement. Final curvature values were established at the point of failure, defined as 20% load degradation of the maximum load, or when valid readings from the

displacement potentiometers were no longer available. The height of plasticity, given in the positive and negative loading directions along with the average value, is presented in Table 4.5 for Wall Specimen C1. The ratio of the average height of plasticity zone to the wall length is also provided in the table.

Table 4.5 Wall C1: Height of Plasticity

Direction of Load	**Height of Plasticity Zone (in.)**
Push South	26.6
Pull North	11.1
Average	18.9
L_p/L_w	47.6%

The equivalent plastic hinge length (l_p) was found by rearranging Equation 4.6 which represents the ultimate displacement of the wall at 20% load degradation (Paulay and Priestley 1992). The first term in this equation represents the yield displacement (Δ_y), and the second term represents the plastic displacement for the idealized curvature profile over the wall height. The equivalent plastic hinge length, given in the positive and negative loading directions along with the average value, is presented in Table 4.6 for Wall Specimen C1. The ratio of the average equivalent plastic hinge length to the wall length is also provided in the table.

$$\Delta_u = \frac{\phi_y H^2}{3} + \left(\phi_u - \phi_y\right)\left(l_p\right)\left(H - \frac{l_p}{2}\right) \qquad \text{Equation 4.6}$$

Table 4.6 Wall C1: Equivalent Plastic Hinge Length

Direction of Load	**Plastic Hinge Length (in.)**
Push South	8.7
Pull North	9.2
Average	8.9
l_p/L	22.6%

Energy Dissipation:

The total energy dissipated by each wall specimen was calculated at the end of the displacement level in which failure occurred for the positive and negative loading directions. The total energy was found by calculating the area under the hysteresis loops, using the Trapezoid Rule, as shown in Figure 4.9.

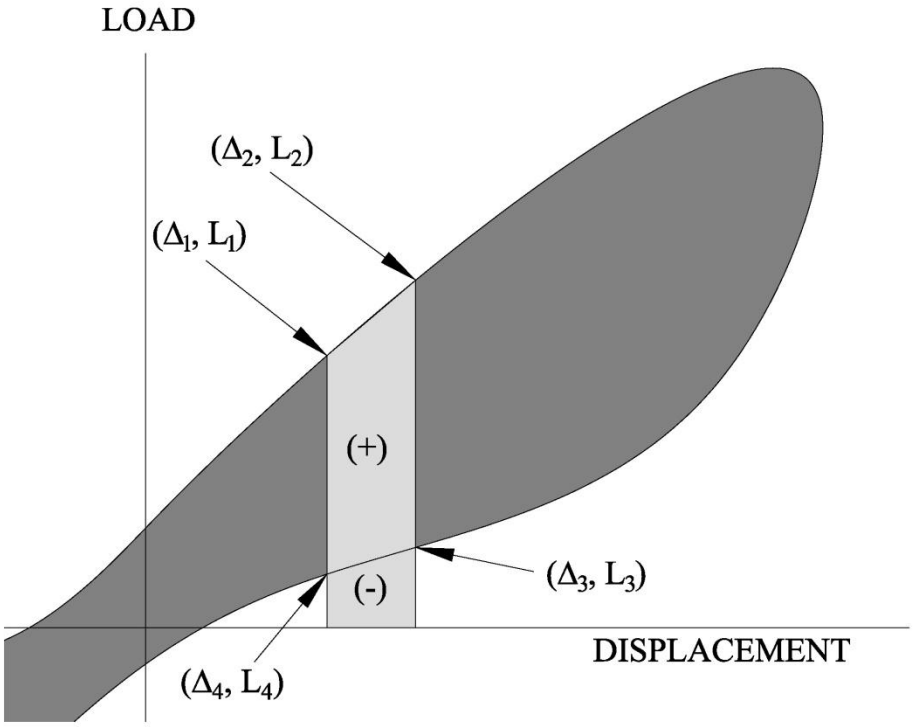

Figure 4.9 Illustration of Total Energy Equation (adapted from Snook, 2005)

The total energy dissipated is defined in Equation 4.7. The equation assumes a straight line between the two data points and calculates the area between the hysteresis loops by adding the area under data points (Δ_1, L_1) and (Δ_2, L_2) and subtracting the area under data points (Δ_3, L_3) and (Δ_4, L_4). The equation is applicable in all four load-displacement quadrants.

$$E = \frac{1}{2}(\Delta_2 - \Delta_1)(L_2 + L_1) \qquad \text{Equation 4.7}$$

Where:

E = energy between data points (kip-in.);

Δ_1 & Δ_2 = displacement at data points (in.); and

L_1 & L_2 = load at data points (kip).

The total energy dissipated in Wall Specimen C1 through the end of the displacement level in which failure occurred for the positive and negative loading directions was 168 kip-in.

Equivalent Hysteretic Damping:

The equivalent hysteretic damping for each wall specimen was calculated at the first cycle of the displacement level corresponding to approximately 0.6% and 1.5% drift. These values of drift were selected to roughly correspond to displacements producing moderate and significant levels of damage in the wall specimens, respectively. The equivalent hysteretic damping is defined in Equation 4.8 and illustrated in Figure 4.10.

$$\xi_{hyst} = \frac{A_h}{2\pi F_m \Delta_m} \quad \text{Equation 4.8}$$

Where:

A_h = area within first cycle of the target displacement level (kip-in.);

F_m = maximum force at the target displacement level (kip); and

Δ_m = maximum displacement at the target displacement level (in.).

The area within the first cycle of the displacement level was calculated using the same method described above for calculating the total energy dissipated by each wall specimen.

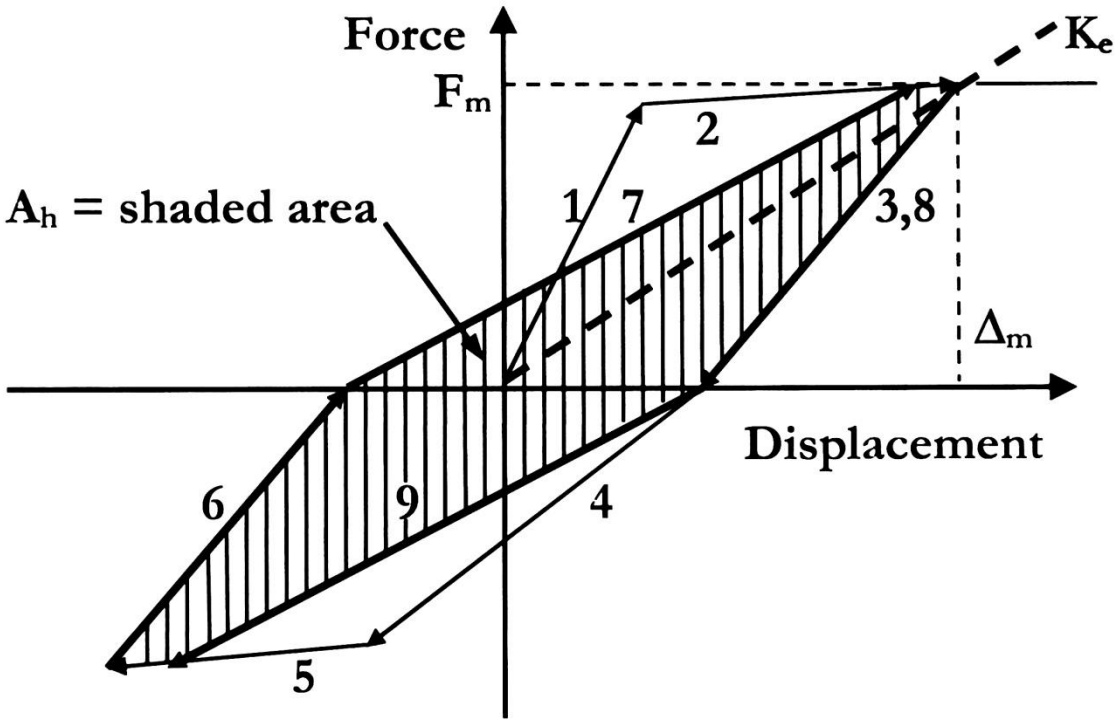

Figure 4.10 Hysteretic Area for Damping Calculation (from Priestley et al., 2007)

The equivalent hysteretic damping for Wall Specimen C1 at approximately 0.6% and 1.5% drift was 6.5% and 17.1%, respectively.

4.3 Wall Specimen C2

Wall Specimen C2 had a height-to-length aspect ratio of 2.0, No. 4 vertical reinforcement spaced 8-in. on center with a splice length of 16 in. at the base of the wall, No. 4 horizontal reinforcement spaced 8-in. on center, and an axial load of 48 kips. The predicted maximum lateral load capacity of Wall Specimen C2 was 23 kips and 24.6 kips using the MSJC and XTRACT analysis methods, respectively. The instrumented horizontal reinforcement in the wall did not yield. The extreme vertical reinforcement yielded in the footing of Wall Specimen C2.

Test Observations:

The preliminary test for Wall Specimen C2 produced a yield displacement (ΔY) of 0.23 in. In the primary test, the specimen was loaded to displacements of ±1, 2, 3, 4, 6, 8, 10 and 12 times the yield displacement. During testing, the wall behavior was dominated by flexural cracking that initiated at 4ΔY with minimal shear cracking. Separation of the mortar joints started at the base of the wall and continued along the height of the wall. Vertical splitting in both toes was observed near failure. Spalling up to the second course occurred in both toes at the last displacement level. The entire wall specimen and the North and South toe regions of the wall at test completion are shown in Figures 4.11 and 4.12, respectively. Test observations and their corresponding lateral displacements and loads are presented in Table 4.7.

Figure 4.11 Wall C2: Entire Wall at Test Completion

Figure 4.12 Wall C2: South Toe (Left) and North Toe (Right) at Test Completion

Table 4.7 Wall C2: Test Observations

Load (kips)	Disp. (in.)	Test Observation
19.1	0.16	1st Yield of extreme vertical reinforcement bar in north toe (pull)
-18.0	-0.18	1st Yield of extreme vertical reinforcement bar in south toe (push)
-24.7	-0.39	Critical masonry strain in south toe (push)
-24.8	-0.47	Flexural cracking in north toe (push)*
27.1	0.48	Flexural cracking in south toe (pull)*
28.1	0.61	Critical masonry strain in north toe (pull)
-28.2	-0.79	1% Drift in push to south
29.1	0.79	1% Drift in pull to north
-29.8	-1.40	Onset of toe crushing in south toe (push)*
32.5	1.41	Maximum load resistance in pull to north
-29.9	-1.87	Maximum load resistance in push to south
25.9	1.87	Onset of toe crushing in north toe (pull)*
25.9	1.87	20% load degradation from maximum load resistance in pull to north
-22.9	-1.87	20% load degradation from maximum load resistance in push to south

*Visual Observation

Load Displacement:

The load-displacement hysteresis curves for the preliminary and primary tests for Wall Specimen C2 are presented in Figure 4.13. The six important limit-state events are marked on

the load-displacement curves and are presented in Table 4.7 along with the lateral displacement and load at the time of their occurrence. The initial yielding of the extreme tensile reinforcement (ε_y = 0.00228) occurred near the end of the preliminary test and in the first cycle of 1ΔY in the push and pull directions, respectively. Critical masonry strain was reached in the first cycle of 2ΔY and 3ΔY in the push and pull directions, respectively. The specimen reached 1% drift in the first cycle of 4ΔY for both loading directions. The maximum lateral load in the pull direction and the onset of toe crushing in the South toe occurred in the first cycle of 6ΔY. The specimen attained maximum lateral load (push), onset of toe crushing (North toe) and 20% load degradation (pull) in the first cycle of 8ΔY. The onset of toe damage in both toe regions is presented in Figure 4.14. Twenty percent load degradation occurred in the second cycle of 8ΔY in the push direction. Wall Specimen C2 exhibited symmetrical load-displacement relationships in the two loading directions throughout the entire test. Following the maximum load, the specimen experienced a gradual decrease in strength in the both directions.

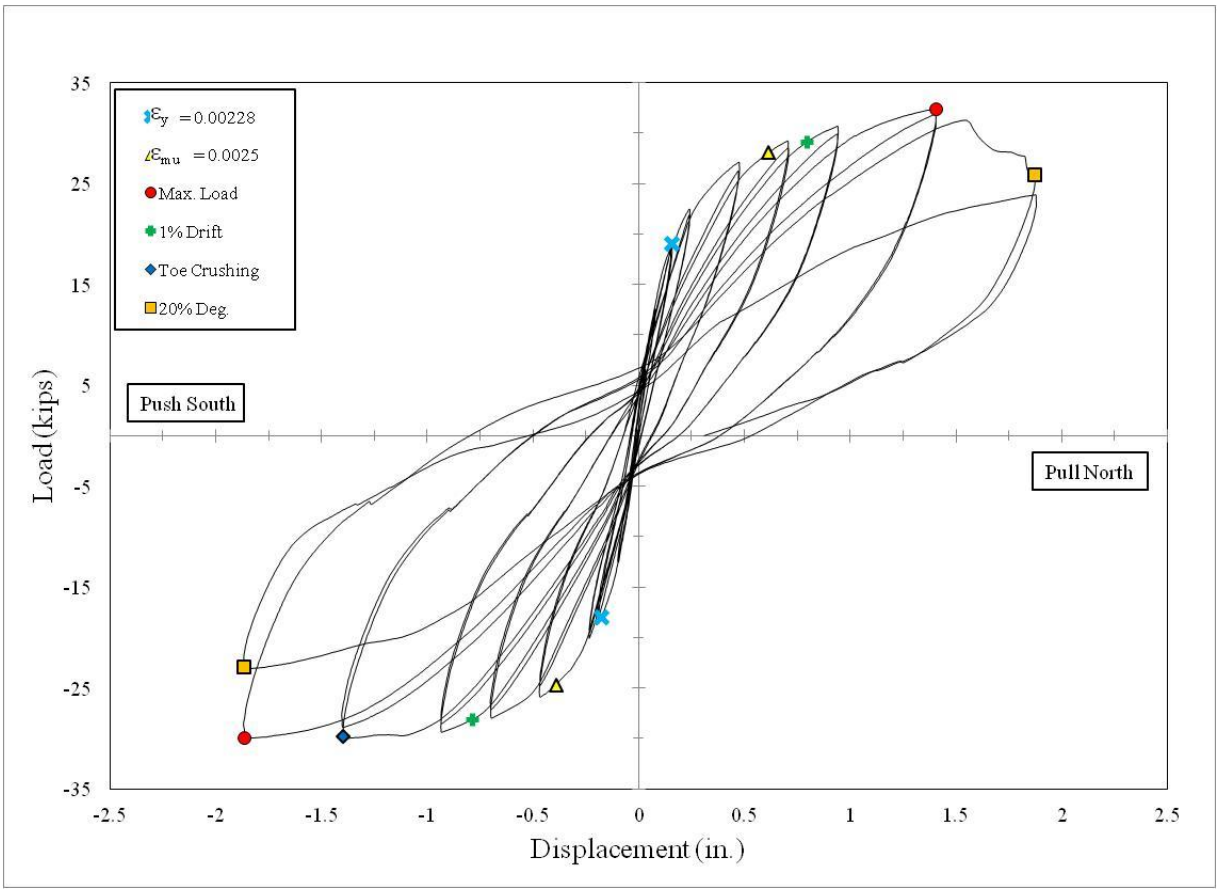

Figure 4.13 Wall C2: Load-Displacement Hysteresis Curves

Figure 4.14 Wall C2: South Toe (Left) and North Toe (Right) at Onset of Toe Damage

Displacement and Drift Components:

Load-displacement hysteresis curves showing the total lateral displacement and the three components of displacement are given in Figure 4.15. The average total drift and average drift contributions from flexure, sliding and shear deformations are presented in Table 4.8 at three important limit-states: critical masonry strain, peak lateral load and failure. Wall Specimen C2 was dominated by flexural deformations with small levels of shear and sliding deformations occurring near failure.

Table 4.8 Specimen C2: Components of Total Drift

Limit-State	**Total Drift (%)**	**Flexure (% Total)**	**Sliding (% Total)**	**Shear (% Total)**
ε_{mu}	0.6	95.2	1.1	3.8
Peak Load	2.1	92.1	1.5	6.4
Failure	2.4	92.2	1.9	5.9

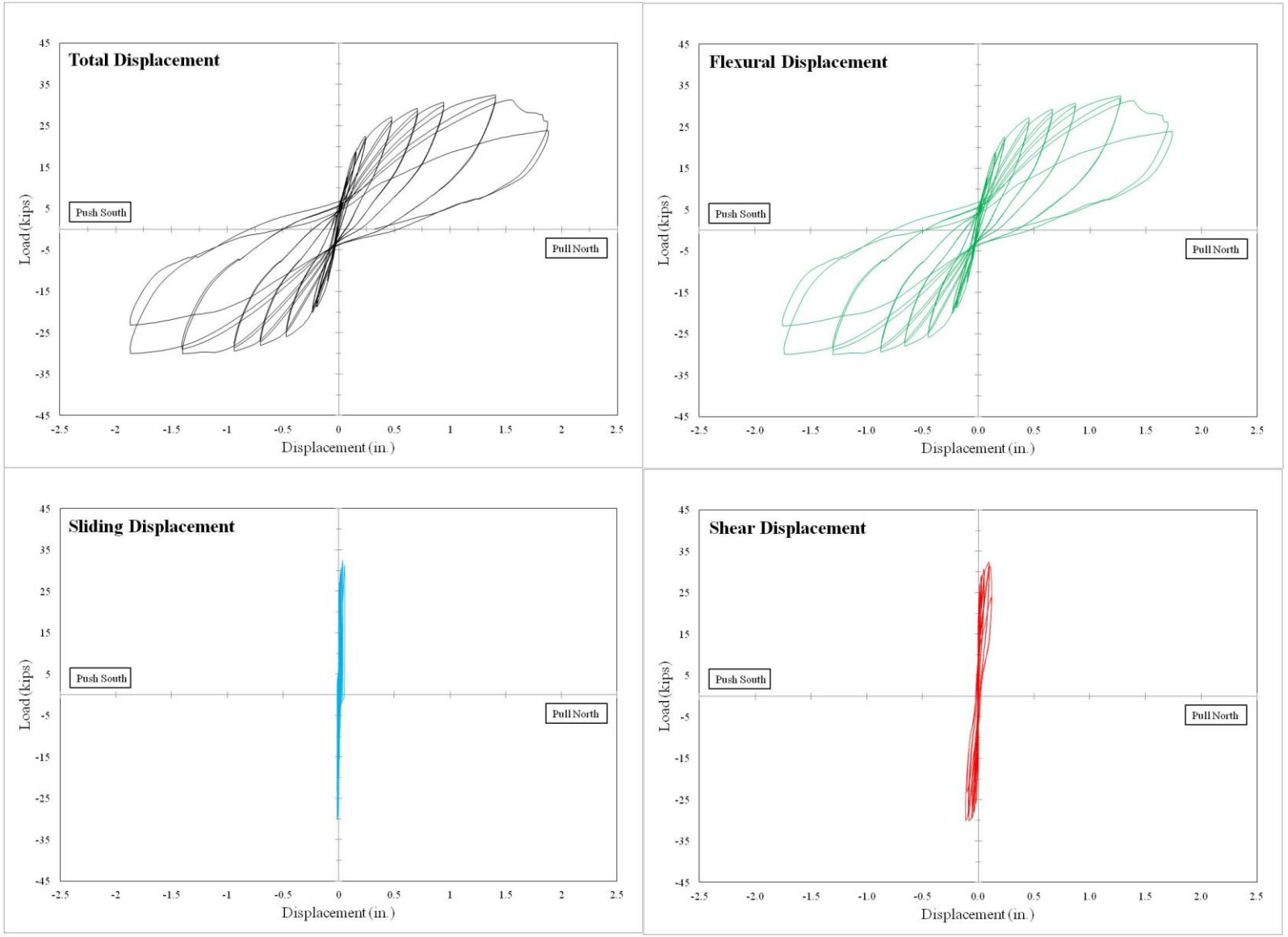

Figure 4.15 Wall C2: Total Lateral-Displacement and its Components

Wall Curvatures:

A plot of curvatures over the height of Wall Specimen C2 is given in Figure 4.16. Curvatures over the wall height were symmetric about the wall center line through 12ΔY. The ultimate curvature was defined at 20% load degradation of the maximum load attained for both loading directions.

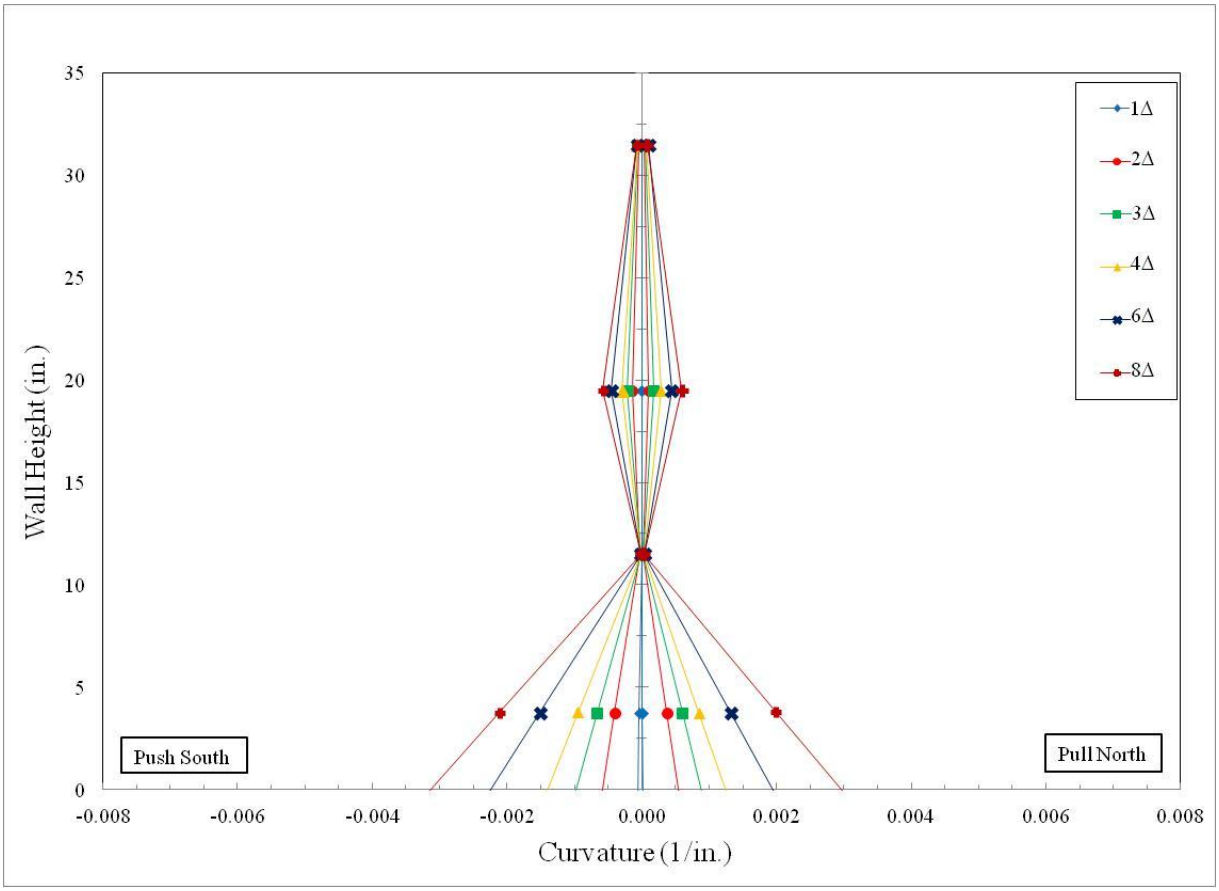

Figure 4.16 Wall C2: Curvature vs. Wall Height

Displacement and Curvature Ductility:

The displacement ductilities for the positive and negative loading directions along with the average value are presented in Table 4.9 for Wall Specimen C2. The total drift reached at 20% load degradation was 2.4%.

Table 4.9 Wall C2: Displacement Ductility

Direction of Load	Displacement					
	P'_y (kips)	Δ'_y (in.)	Δ_u (in.)	P_y (kips)	Δ_y (in.)	μ_Δ
Push South	-18.0	-0.18	-1.87	-28.3	-0.28	6.7
Pull North	19.1	0.16	1.87	29.1	0.24	7.8
Average	18.5	0.17	1.87	28.7	0.26	7.2

The curvature ductilities for the positive and negative loading directions along with the average value are presented in Table 4.10 for Wall Specimen C2.

Table 4.10 Wall C2: Curvature Ductility

Direction of Load	Curvature					
	M'_y (kip-in.)	ϕ'_y (in.$^{-1}$)	ϕ_u (in.$^{-1}$)	M_y (kip-in.)	ϕ_y (in.$^{-1}$)	μ_ϕ
Push South	-1426	-0.00015	-0.0023	-2170	-0.00022	10.2
Pull North	1511	0.00011	0.0020	2322	0.00017	11.9
Average	1468	0.00013	0.0021	2246	0.00019	11.1

Height of Plasticity and Equivalent Plastic Hinge Length:

The height of plasticity (L_p) and the equivalent plastic hinge length (l_p) for the positive and negative loading directions along with the average values are presented in Table 4.11 for Wall Specimen C2. The ratios of the average height of plasticity zone to the wall length and the average equivalent plastic hinge length to the wall length are also provided in the table.

Table 4.11 Wall C2: Height of Plasticity & Equivalent Plastic Hinge Length

Direction of Load	Height of Plasticity Zone (in.)	Plastic Hinge Length (in.)
Push South	28.3	10.5
Pull North	30.7	12.2
Average	29.5	11.4
L_p/L and l_p/L	74.4%	28.6%

Energy Dissipation:

The total energy dissipated in Wall Specimen C2 through the end of the displacement level in which failure occurred for the positive and negative loading directions was 271 kip-in.

Equivalent Hysteretic Damping:

The equivalent hysteretic damping for Wall Specimen C2 at approximately 0.6% and 1.5% drift was 10.6% and 12%, respectively.

4.4 Wall Specimen C3

Wall Specimen C3 had a height-to-length aspect ratio of 2.0, No. 7 vertical reinforcement spaced 16-in. on center with a splice length of 46 in. at the base of the wall, No. 4 horizontal reinforcement spaced 8-in. on center, and an axial load of 48 kips. The predicted maximum lateral load capacity of Wall Specimen C3 was 33 kips and 38.2 kips using the MSJC and XTRACT analysis methods, respectively. The horizontal reinforcement yielded in the first course but not in the fifth course. The extreme vertical reinforcement yielded in the footing of Wall Specimen C3.

Test Observations:

The preliminary test for Wall Specimen C3 produced a yield displacement (ΔY) of 0.44 in. The specimen was then loaded to displacements of ±1, 2, 3, 4 and 6 times the yield displacement for the primary test. During testing, the wall exhibited a mixture of flexure, shear and crushing behaviors. Separation of the mortar joints occurred at the base of the wall. Vertical splitting in the North toe appeared at $3\Delta Y$. Wide diagonal cracks that extended through the fourth course appeared at $6\Delta Y$. Buckling of the extreme vertical reinforcement in the South toe

was observed near test completion. Spalling in the North and South toes at test completion extended to the second and third courses, respectively. Damage was concentrated in the lower three courses of the wall and may be attributable to a complex dowel-action behavior associated with the large amount of spliced vertical reinforcement. The entire wall specimen and the North and South toe regions of the wall at test completion are shown in Figures 4.17 and 4.18, respectively. Test observations and their corresponding lateral displacements and loads are presented in Table 4.12.

Figure 4.17 Wall C3: Entire Wall at Test Completion

Figure 4.18 Wall C3: South Toe (Left) and North Toe (Right) at Test Completion

Table 4.12 Wall C3: Test Observations

Load (kips)	Disp. (in.)	Test Observation
30.41	0.35	1st Yield of extreme vertical reinforcement bar in north toe (pull)
-29.12	-0.36	1st Yield of extreme vertical reinforcement bar in south toe (push)
-31.80	-0.43	Critical masonry strain in south toe (push)
38.10	0.73	Critical masonry strain in north toe (pull)
-36.22	-0.79	1% Drift in push to south
38.65	0.80	1% Drift in pull to north
-34.95	-0.87	Maximum load resistance in push to south
-34.95	-0.87	Onset of toe crushing in south toe (push)*
38.72	0.89	Maximum load resistance in pull to north
38.36	1.32	Flexural cracking in south toe (pull)*
-25.83	-1.74	Flexural cracking in north toe (push)*
-25.83	-1.74	20% load degradation from maximum load resistance in push to south
27.27	1.97	20% load degradation from maximum load resistance in pull to north

*Visual Observation

Load Displacement:

The load-displacement hysteresis curves for the preliminary and primary tests for Wall Specimen C3 are presented in Figure 4.19. The six important limit-state events are marked on

the load-displacement curves and are presented in Table 4.12 along with the lateral displacement and load at the time of their occurrence. The initial yielding of the extreme tensile reinforcement (ε_y = 0.00228) occurred in the first cycle of 1ΔY in both loading directions. Critical masonry strain was reached in the first cycle of 1ΔY and 2ΔY in the push and pull directions, respectively. The specimen attained 1% drift and maximum lateral load in the first cycle of 2ΔY for both loading directions. The onset of toe damage in the South and North toe, presented in Figure 4.20, occurred in the first cycles of 2ΔY and 3ΔY, respectively. The specimen reached 20% load degradation in the second cycle of 4ΔY and the first cycle of 6ΔY in the push and pull directions, respectively. Wall Specimen C3 exhibited fairly symmetrical load-displacement relationships in the two loading directions. Throughout the entire test, the peak loads in the pull direction were slightly greater than in the push direction.

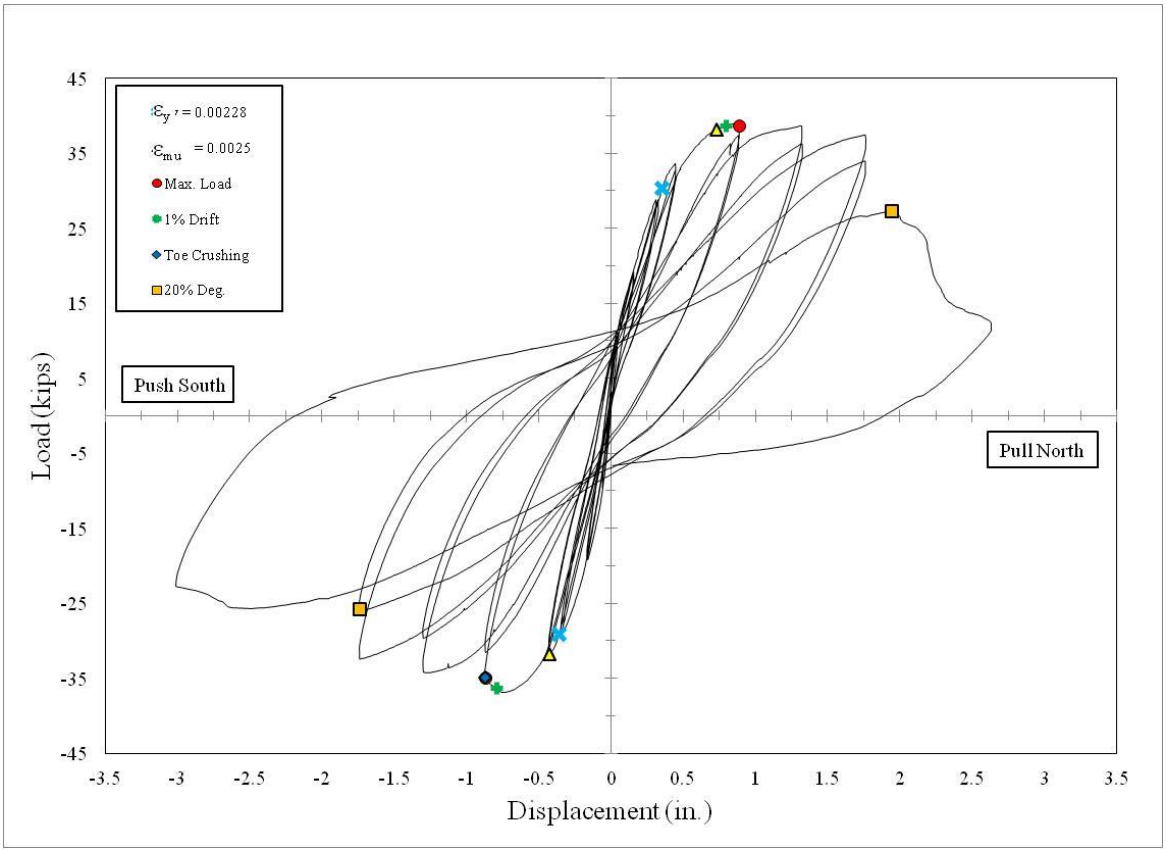

Figure 4.19 Wall C3: Load-Displacement Hysteresis Curves

Figure 4.20 Wall C3: South Toe (Left) and North Toe (Right) at Onset of Toe Damage

Displacement and Drift Components:

Load-displacement hysteresis curves showing the total lateral displacement and the three components of displacement are given in Figure 4.21. The average total drift and average drift contributions from flexure, sliding and shear deformations are presented in Table 4.13 at three important limit-states: critical masonry strain, peak lateral load and failure. It is difficult to distinguish the dominant displacement component at failure for Wall Specimen C3 due to the mixed flexural/shear wall behavior and the complex response caused by the dowel-action at the base of the wall.

Table 4.13 Wall C3: Components of Total Drift

Limit-State	Total Drift (%)	Flexure (% Total)	Sliding (% Total)	Shear (% Total)
ε_{mu}	0.7	95.1	2.3	2.5
Peak Load	1.1	94.4	1.9	3.7
Failure	2.3	94.0	2.4	3.6

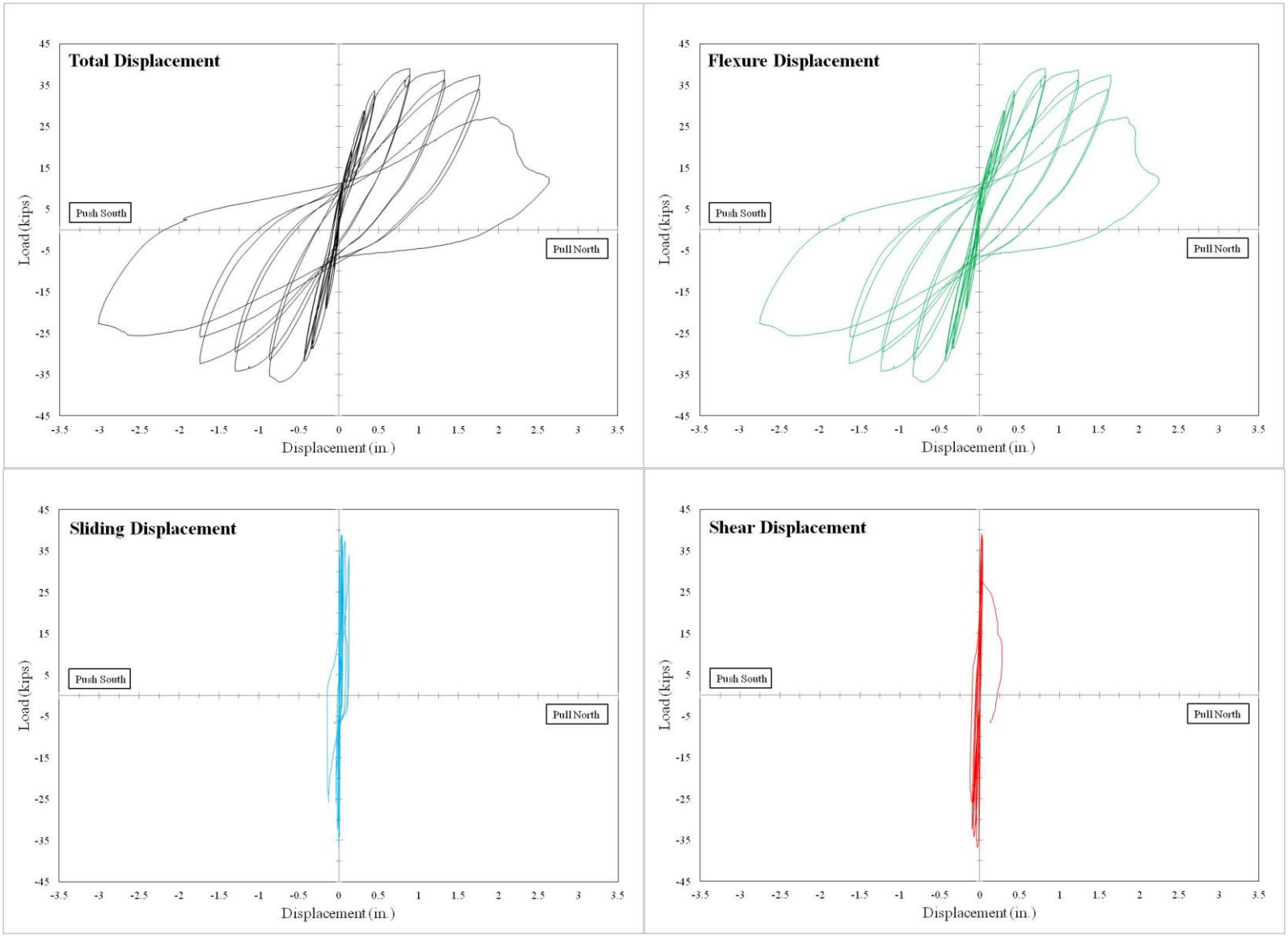

Figure 4.21 Wall C3: Total Lateral-Displacement and its Components

Wall Curvatures:

A plot of curvatures over the height of Wall Specimen C3 is given in Figure 4.22. Curvatures over the wall height were symmetric about the wall center line through 3ΔY. The ultimate curvature was defined at the first cycle of 2ΔY and 3ΔY, instead of at 20% load degradation of the maximum load attained, in the pull and push directions, respectively. This was because valid readings from the displacement potentiometers were no longer available at larger displacement levels. The displacement potentiometers on the South side of the wall at the first (approximately 4 in. above the footing) and third (approximately 20 in. above the footing) height levels were disconnected in the first cycle of 3ΔY and the second cycle of 4ΔY, respectively.

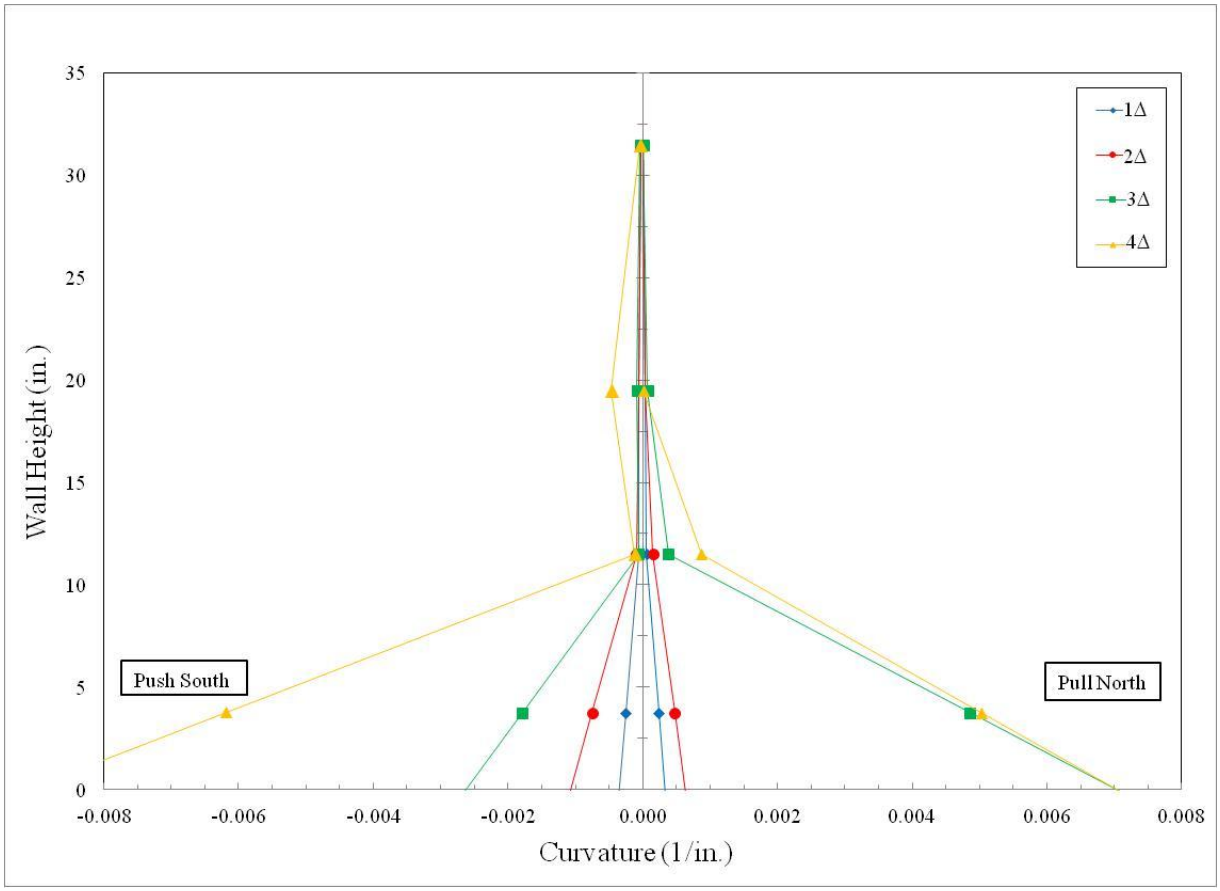

Figure 4.22 Wall C3: Curvature vs. Wall Height

Displacement and Curvature Ductility:

The displacement ductilities for the positive and negative loading directions along with the average value are presented in Table 4.14 for Wall Specimen C3. The total drift reached at 20% load degradation was 2.3%.

Table 4.14 Wall C3: Displacement Ductility

Direction of Load	**Displacement**					
	P'_y (kips)	Δ'_y (in.)	Δ_u (in.)	P_y (kips)	Δ_y (in.)	μ_Δ
Push South	-29.1	-0.36	-1.74	-34.5	-0.43	4.1
Pull North	30.4	0.35	1.94	37.6	0.44	4.5
Average	29.8	0.36	1.84	36.1	0.43	4.3

The curvature ductilities for the positive and negative loading directions along with the average value are presented in Table 4.15 for Wall Specimen C3. Damage in the wall towards the end of testing affected the displacement potentiometer readings, and thus the final values of curvatures determined for this wall were prior to 20% load degradation from the maximum load. As a result, the values for the ultimate curvature and the yield curvature in the elastoplastic approximation do not accurately reflect actual curvatures in the wall at failure.

Table 4.15 Wall C3: Curvature Ductility

Direction of Load	**Curvature**					
	M'_y (kip-in.)	ϕ'_y (in.$^{-1}$)	ϕ_u (in.$^{-1}$)	M_y (kip-in.)	ϕ_y (in.$^{-1}$)	μ_ϕ
Push South	-2308	-0.00020	-0.0018	-2764	-0.00024	7.6
Pull North	2410	0.00015	0.0005	2996	0.00019	2.6
Average	2359	0.00017	0.0011	2880	0.00021	5.1

Height of Plasticity and Equivalent Plastic Hinge Length:

The height of plasticity (L_p) and the equivalent plastic hinge length (l_p) for the positive and negative loading directions along with the average values are presented in Table 4.16 for

Wall Specimen C3. Because final curvatures were determined prior to failure in this wall, the calculated height of plasticity and equivalent plastic hinge length will be lower-bound estimates of the actual values. The ratios of the average height of plasticity zone to the wall length and the average equivalent plastic hinge length to the wall length are also provided in the table.

Table 4.16 Wall C3: Height of Plasticity & Equivalent Plastic Hinge Length

Direction of Load	Height of Plasticity Zone (in.)	Plastic Hinge Length (in.)
Push South	27.1	11.6
Pull North	31.0	NA
Average	29.1	11.6
L_p/L and l_p/L	73.3%	29.1%

Energy Dissipation:

The total energy dissipated in Wall Specimen C3 through the end of the displacement level in which failure occurred for the positive and negative loading directions was 396 kip-in.

Equivalent Hysteretic Damping:

The equivalent hysteretic damping for Wall Specimen C3 at approximately 0.6% and 1.5% drift was 6.1% and 14.5%, respectively.

4.5 Wall Specimen C4

Wall Specimen C4 had a height-to-length aspect ratio of 0.78, No. 7 vertical reinforcement spaced 16-in. on center with a splice length of 46 in. at the base of the wall, two No. 4 horizontal reinforcement spaced 8-in. on center, and an axial load of 86 kips. The predicted maximum lateral load capacity of Wall Specimen C4 was 144 kips and 157 kips using

the MSJC and XTRACT analysis methods, respectively. The horizontal reinforcement yielded in the first course but not in the fifth course. The extreme vertical reinforcement yielded in the footing of Wall Specimen C4.

Test Observations:

The preliminary test for Wall Specimen C4 produced a yield displacement (ΔY) of 0.34 in. The specimen was then loaded to displacements of ±1, 2 and 3 times the yield displacement for the primary test. During testing, the wall behavior was dominated by shear cracking that initiated at 2ΔY. Separation of the mortar joints started at the base of the wall and continued along the height of the wall. Vertical splitting in both toe regions appeared at 3ΔY. After peak load was attained, the wall experienced rapid strength degradation. During the last cycle of testing, the masonry face shells in the first through third courses completely fell away from the wall exposing the grout cores that had been crushed by the vertical reinforcement. The damage concentrated in the lower half of the wall may be attributable to a complex dowel-action behavior associated with the large amount of spliced vertical reinforcement. The entire wall specimen and the North and South toe regions of the wall at test completion are shown in Figures 4.23 and 4.24, respectively. Test observations and their corresponding lateral displacements and loads are presented in Table 4.17.

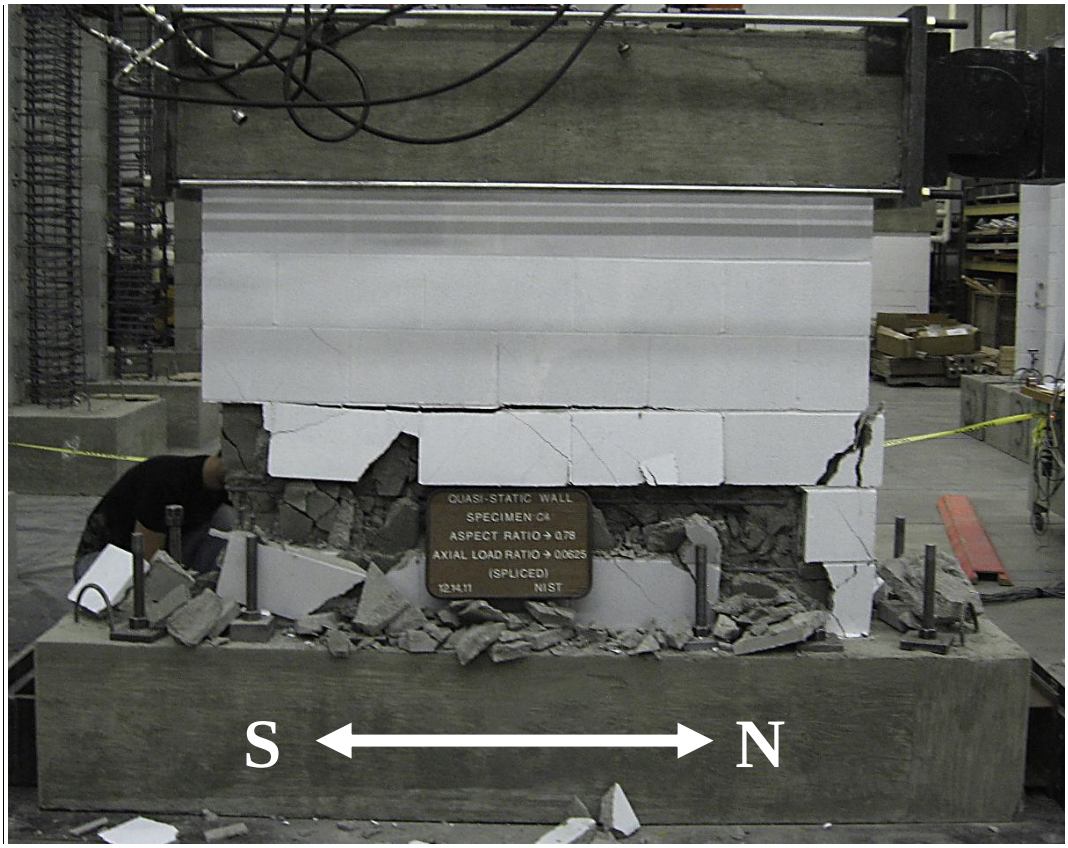

Figure 4.23 Wall C4: Entire Wall at Test Completion

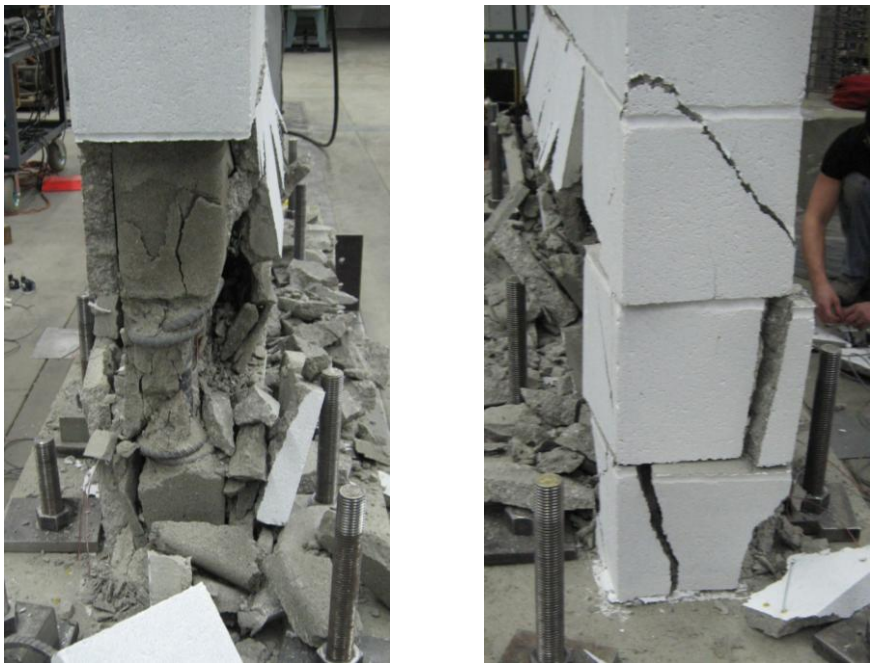

Figure 4.24 Wall C4: South Toe (Left) and North Toe (Right) at Test Completion

Table 4.17 Wall C4: Test Observations

Load (kips)	Disp. (in.)	Test Observation
-79.64	-0.09	1st Yield of extreme vertical reinforcement bar in south toe (push)
99.90	0.13	1st Yield of extreme vertical reinforcement bar in north toe (pull)
-123.11	-0.32	Critical masonry strain in south toe (push)
133.63	0.34	Critical masonry strain in north toe (pull)
132.69	0.35	Maximum load resistance in pull to north
-144.04	-0.56	1% Drift in push to south
134.34	0.56	1% Drift in pull to north
-143.94	-0.69	Maximum load resistance in push to south
-95.88	-0.69	20% load degradation from maximum load resistance in push to south
102.52	0.70	Flexural cracking in south toe (pull)*
102.52	0.70	20% load degradation from maximum load resistance in pull to north
129.87	0.72	Onset of toe crushing in north toe (pull)*
-49.38	-1.03	Flexural cracking in north toe (push)*

*Visual Observation

Load Displacement:

The load-displacement hysteresis curves for the preliminary and primary tests for Wall Specimen C4 are presented in Figure 4.25. The six important limit-state events are marked on the load-displacement curves and are presented in Table 4.17 along with the lateral displacement and load at the time of their occurrence. The initial yielding of the extreme tensile reinforcement (ε_y = 0.00228) occurred near the end of the preliminary test for both loading directions. Critical masonry strain was reached in the first cycle of 1ΔY for both loading directions. The maximum lateral load occurred in the first cycle of 1ΔY and 2ΔY in the pull and push directions, respectively. The specimen attained 1% drift in the first cycle of 2ΔY for both loading directions. The onset of toe damage in the North and South toes, presented in Figure 4.26, occurred in the first cycles of 2ΔY and 3ΔY, respectively. The specimen reached 20% load degradation in the second cycle of 2ΔY and the first cycle of 3ΔY in the pull and push directions, respectively. Wall Specimen C4 exhibited rapid strength degradation in the first cycle of 3ΔY.

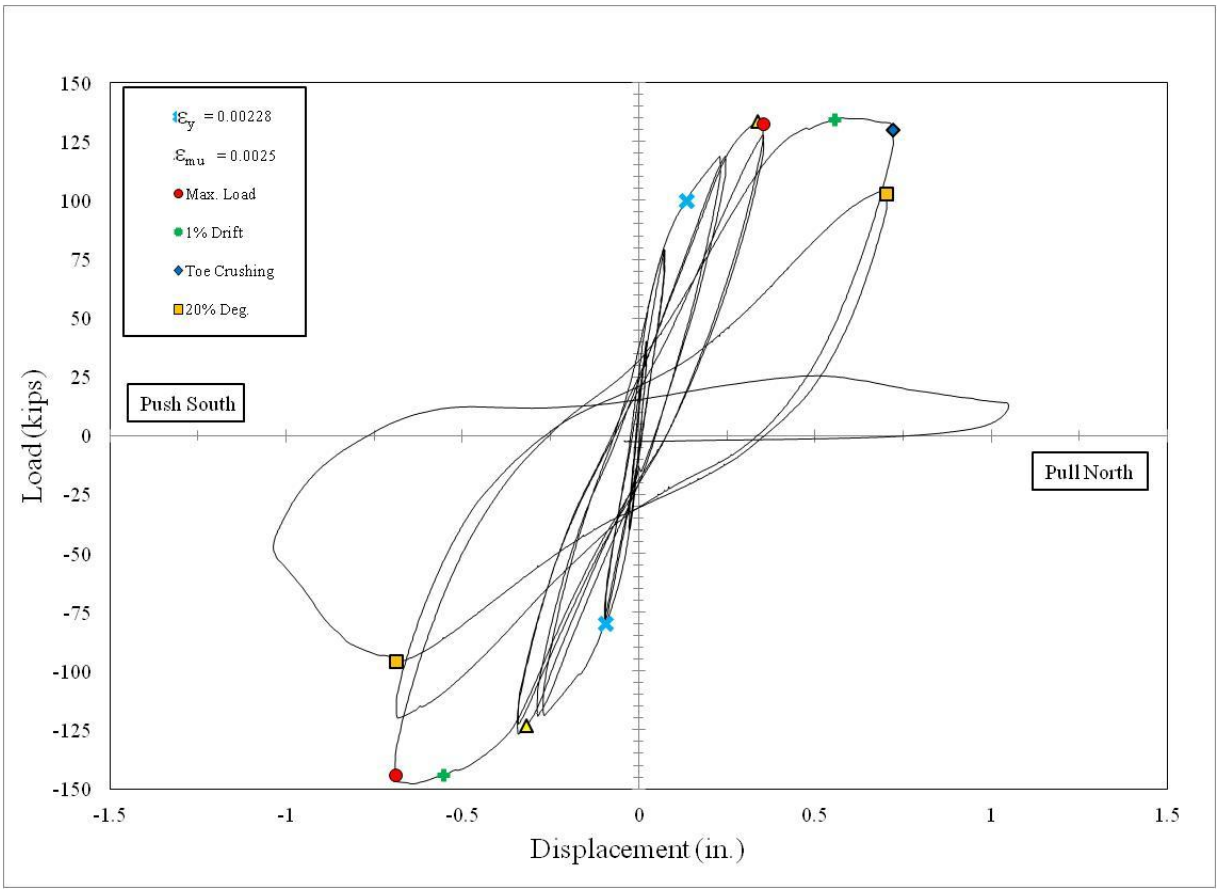

Figure 4.25 Wall C4: Load-Displacement Hysteresis Curves

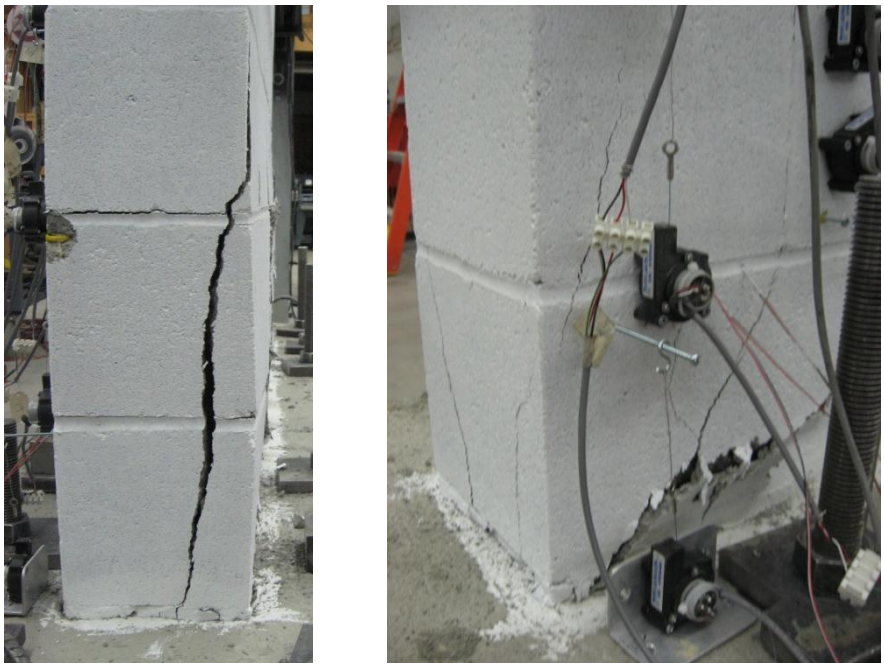

Figure 4.26 Wall C4: South Toe (Left) and North Toe (Right) at Onset of Toe Damage

Displacement and Drift Components:

Load-displacement hysteresis curves showing the total lateral displacement and the three components of displacement are given in Figure 4.27. The load-displacement hysteresis curves showing the flexural and shear components were discontinued after the second cycle at 1ΔY because valid readings from the displacement potentiometers were no longer available at larger displacement levels. The average total drift and average drift contributions from flexure, sliding and shear deformations are presented in Table 4.18 at three important limit-states: critical masonry strain, peak lateral load and failure. It is difficult to distinguish the dominant displacement component at failure for Wall Specimen C4 due to the complex response caused by the dowel-action at the base of the wall.

Table 4.18 Wall C4: Components of Total Drift

Limit-State	**Total Drift (%)**	**Flexure (% Total)**	**Sliding (% Total)**	**Shear (% Total)**
ε_{mu}	0.59	81.6	3.4	15.1
Peak Load	0.94	79.0	4.8	16.3
Instrumentation Failure	0.82	77.1	6.4	16.5
Failure	1.2	NA	3.0	NA

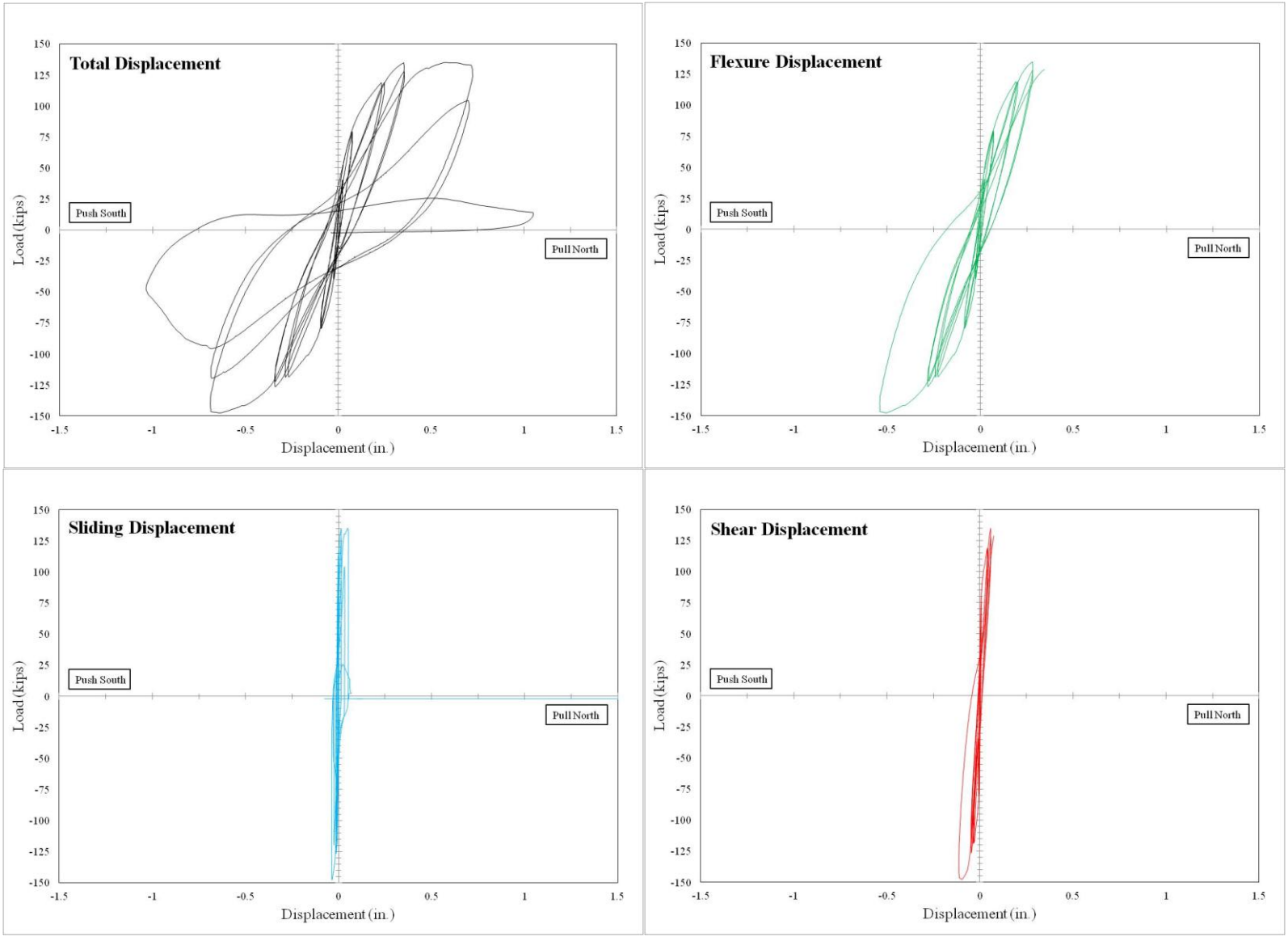

Figure 4.27 Wall C4: Total Lateral-Displacement and its Components

Wall Curvatures:

A plot of curvatures over the height of Wall Specimen C4 is given in Figure 4.28. Curvatures over the wall height were symmetric about the wall center line through 2ΔY. The ultimate curvature was defined at the first cycle of 2ΔY, instead of at 20% load degradation of the maximum load attained, in both loading directions. The curvatures at the first height level (approximately 4 in. above the footing) were smaller at 3ΔY than in the previous displacement levels. This might have been due to the dowel-action which crushed the grout around the vertical reinforcement resulting in less composite action between the reinforcement and the wall. This decreased movement in the first course of the wall which is seen in smaller curvatures. The curvatures at the second and third height levels (approximately 12in. and approximately 20in. above the footing) were significantly larger at 3ΔY than in the previous displacement levels. This might be due to the face shells separating from the grout cores which allowed for more movement of the wall shell.

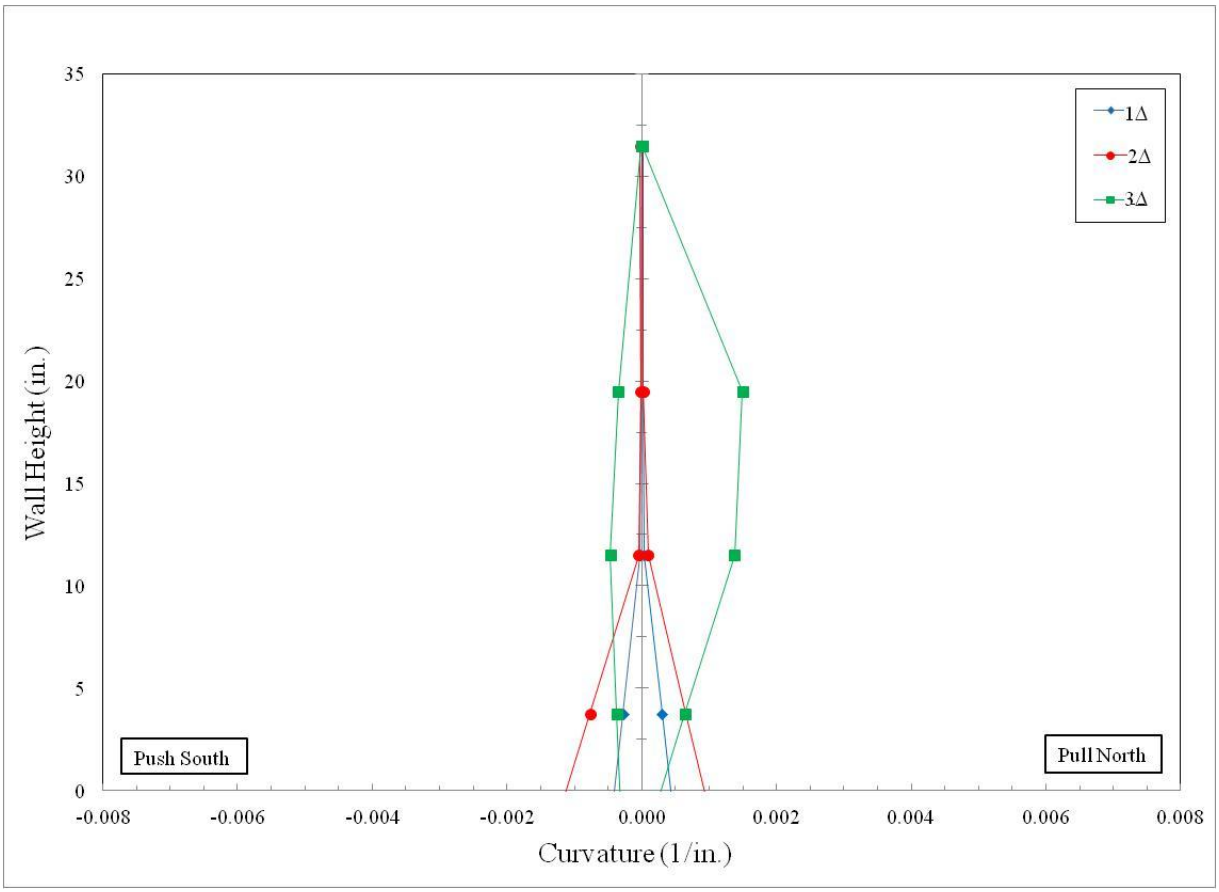

Figure 4.28 Wall C4: Curvature vs. Wall Height

Displacement and Curvature Ductility:

The displacement ductilities for the positive and negative loading directions along with the average value are presented in Table 4.19 for Wall Specimen C4. The total drift reached at 20% load degradation was 1.3%.

Table 4.19 Wall C4: Displacement Ductility

Direction of Load	**Displacement**					
	P'_y (kips)	Δ'_y (in.)	Δ_u (in.)	P_y (kips)	Δ_y (in.)	μ_Δ
Push South	-79.6	-0.09	-0.69	-125.9	-0.15	4.6
Pull North	99.9	0.13	0.72	126.7	0.17	4.2
Average	89.8	0.11	0.71	126.3	0.16	4.4

The curvature ductilities for the positive and negative loading directions along with the average value are presented in Table 4.20 for Wall Specimen C4. Damage in the wall towards the end of testing affected the displacement potentiometer readings, and thus the final values of curvatures determined for this wall were prior to 20% load degradation from the maximum load. As a result, the values for the ultimate curvature and the yield curvature in the elastoplastic approximation do not accurately reflect actual curvatures in the wall at failure.

Table 4.20 Wall C4: Curvature Ductility

Direction of Load	**Curvature**					
	M'_y (kip-in.)	ϕ'_y (in.$^{-1}$)	ϕ_u (in.$^{-1}$)	M_y (kip-in.)	ϕ_y (in.$^{-1}$)	μ_ϕ
Push South	-4430	-0.00004	-0.0008	-7142	-0.00007	10.7
Pull North	5557	0.00008	0.0007	7272	0.00011	6.1
Average	4993	0.00006	0.0007	7207	0.00009	8.4

Height of Plasticity and Equivalent Plastic Hinge Length:

The height of plasticity and the equivalent plastic hinge length for the positive and negative loading directions along with the average values are presented in Table 4.21 for Wall Specimen C4. Because final curvatures were determined prior to failure in this wall, the calculated height of plasticity and equivalent plastic hinge length will be lower-bound estimates of the actual values. The ratios of the average height of plasticity zone to the wall length and the average equivalent plastic hinge length to the wall length are also provided in the table.

Table 4.21 Wall C4: Height of Plasticity & Equivalent Plastic Hinge Length

Direction of Load	**Height of Plasticity Zone (in.)**	**Plastic Hinge Length (in.)**
Push South	23.3	16.3
Pull North	16.7	23.0
Average	20.0	19.7
L_p/L and l_p/L	27.9%	27.4%

Energy Dissipation:

The total energy dissipated in Wall Specimen C4 through the end of the displacement level in which failure occurred for the positive and negative loading directions was 397 kip-in.

Equivalent Hysteretic Damping:

The equivalent hysteretic damping for Wall Specimen C4 at approximately 0.6% and 1.5% drift was 10.3% and 18.4%, respectively.

4.6 Wall Specimen C5

Wall Specimen C5 had a height-to-length aspect ratio of 1.0, No. 7 vertical reinforcement spaced 16-in. on center with a splice length of 46 in. at the base of the wall, two No. 4 horizontal reinforcement spaced 8-in. on center, and an axial load of 86 kips. The predicted maximum lateral load capacity of Wall Specimen C5 was 112 kips and 122 kips using the MSJC and XTRACT analysis methods, respectively. The horizontal reinforcement did not yield at either location. The extreme vertical reinforcement yielded in the footing of Wall Specimen C5.

Test Observations:

The preliminary test for Wall Specimen C5 produced a yield displacement (ΔY) of 0.26 in. The specimen was then loaded to displacements of ±1, 2, 3, 4 and 6 times the yield displacement for the primary test. During testing, the wall behavior was dominated by shear cracking that initiated at $3\Delta Y$. Separation of the mortar joints occurred at the base of the wall and at the first course. Vertical splitting appeared in both toe regions early during the preliminary test. The wall experienced rapid strength degradation soon after the peak load was reached. During the last cycle of testing, the masonry face shells in the first and second courses

fell away from the wall completely exposing the grout cores that had been crushed by the vertical reinforcement. The damage concentrated in the lower two courses of the wall may be attributable to a complex dowel-action behavior associated with the large amount of spliced vertical reinforcement. The entire wall specimen and the North and South toe regions of the wall at test completion are shown in Figures 4.29 and 4.30, respectively. Test observations and their corresponding lateral displacements and loads are presented in Table 4.22.

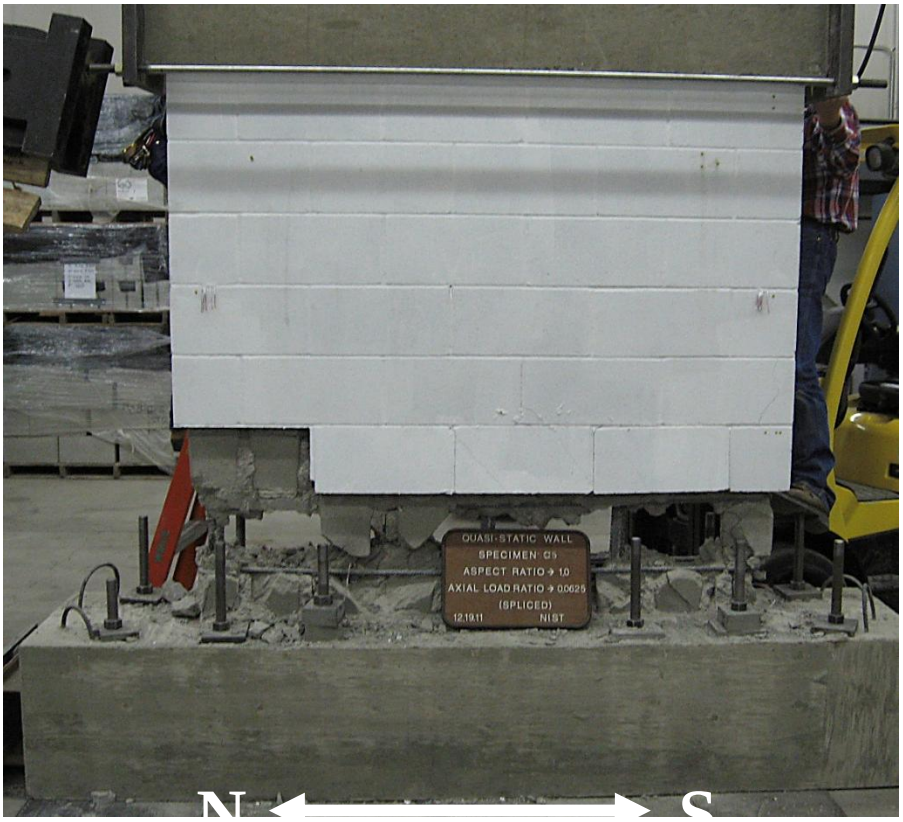

Figure 4.29 Wall C5: Entire Wall at Test Completion

Figure 4.30 Wall C5: South Toe (Left) and North Toe (Right) at Test Completion

Table 4.22 Wall C5: Test Observations

Load (kips)	Disp. (in.)	Test Observation
75.34	0.12	Critical masonry strain in north toe (pull)
-88.50	-0.16	Critical masonry strain in south toe (push)
-96.30	-0.21	1st Yield of extreme vertical reinforcement bar in south toe (push)
117.29	0.54	1st Yield of extreme vertical reinforcement bar in north toe (pull)
-122.82	-0.71	1% Drift in push to south
118.82	0.72	1% Drift in pull to north
-120.31	-0.78	Onset of toe crushing in south toe (push)*
-120.31	-0.78	Maximum load resistance in push to south
120.17	0.80	Flexural cracking in south toe (pull)*
120.17	0.80	Maximum load resistance in pull to north
-78.96	-1.04	20% load degradation from maximum load resistance in push to south
92.31	1.07	20% load degradation from maximum load resistance in pull to north

*Visual Observation

Load Displacement:

The load-displacement hysteresis curves for the preliminary and primary tests for Wall Specimen C5 are presented in Figure 4.31. The six important limit-state events are marked on the load-displacement curves and are presented in Table 4.22 along with the lateral displacement

and load at the time of their occurrence. Critical masonry strain was reached near the end of the preliminary test for both loading directions. The initial yielding of the extreme tensile reinforcement (ε_y = 0.00228) occurred in the first cycle of 1ΔY and 2ΔY in the push and pull directions, respectively. The specimen attained maximum lateral load and 1% drift in the first cycle of 3ΔY for both loading directions. The onset of toe damage in both toes, presented in Figure 4.32, also occurred at 3ΔY. The specimen reached 20% load degradation in the first and second cycle of 4ΔY in the pull and push directions, respectively. Wall Specimen C5 exhibited symmetrical load-displacement relationships in the two loading directions prior to reaching maximum load.

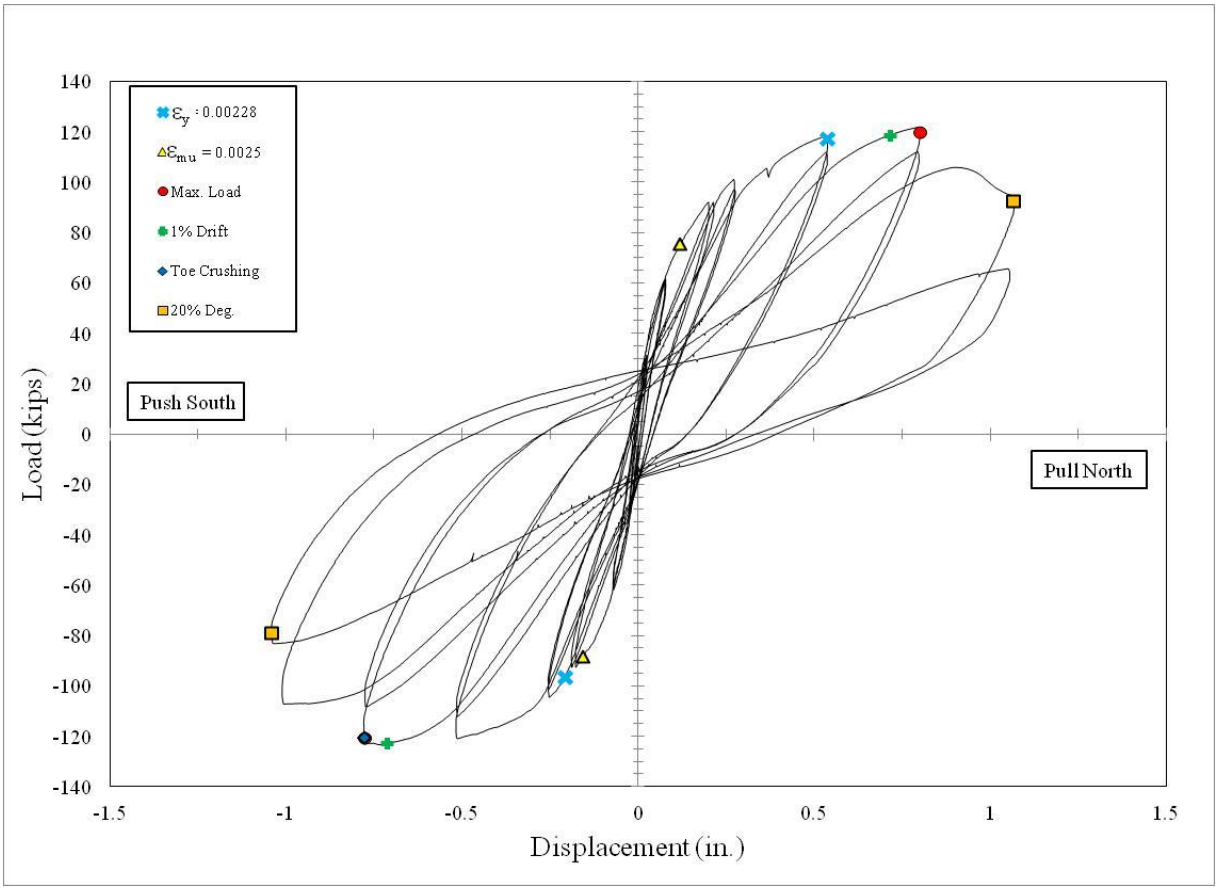

Figure 4.31 Wall C5: Load-Displacement Hysteresis Curves

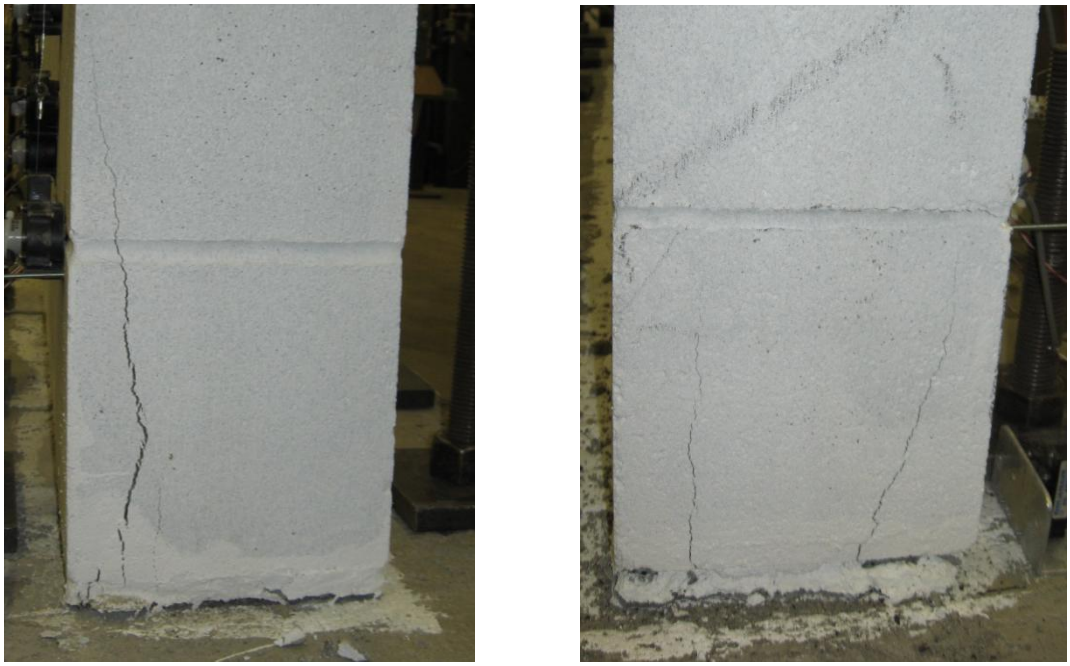

Figure 4.32 Wall C5: South Toe (Left) and North Toe (Right) at Onset of Toe Damage

Displacement and Drift Components:

Load-displacement hysteresis curves showing the total lateral displacement and the three components of displacement are given in Figure 4.33. The load-displacement hysteresis curves showing the flexural and shear components were discontinued after the first cycle of 4ΔY because valid readings from the displacement potentiometers where no longer available at larger displacement levels. The average total drift and average drift contributions from flexure, sliding and shear deformations are presented in Table 4.23 at three important limit-states: critical masonry strain, peak lateral load and failure. It is difficult to distinguish the dominant displacement component at failure for Wall Specimen C5 due to the complex response caused by the dowel-action at the base of the wall.

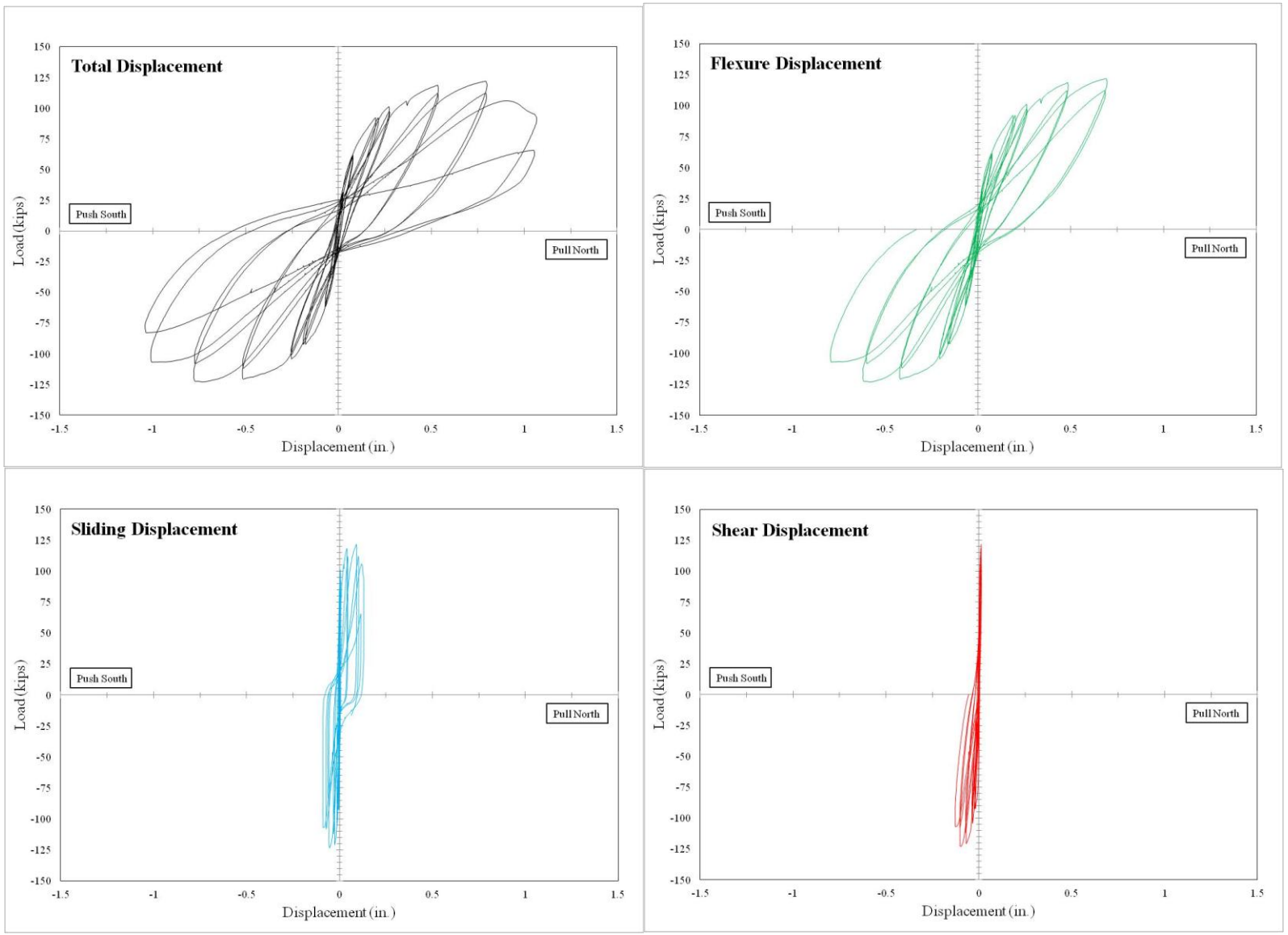

Figure 4.33 Wall C5: Total Lateral-Displacement and its Components

Table 4.23 Wall C5: Components of Total Drift

Limit-State	Total Drift (%)	Flexure (% Total)	Sliding (% Total)	Shear (% Total)
ε_{mu}	0.19	91.0	1.8	7.2
Peak Load	1.10	83.3	9.4	7.3
Instrumentation Failure	0.65	71.3	16.7	12.0
Failure	1.5	NA	9.1	NA

Wall Curvatures:

A plot of curvatures over the height of Wall Specimen C5 is given in Figure 4.34. Curvatures over the wall height were symmetric about the wall center line through 2ΔY. The ultimate curvature was defined at the second cycle of 3ΔY, instead of at 20% load degradation of the maximum load attained, in both loading directions. This was because valid readings from the displacement potentiometers were no longer available at larger displacement levels. The curvatures were approximately zero at the second, third and fourth height levels (approximately 12 in., 20 in. and 32 in. above the footing, respectively).

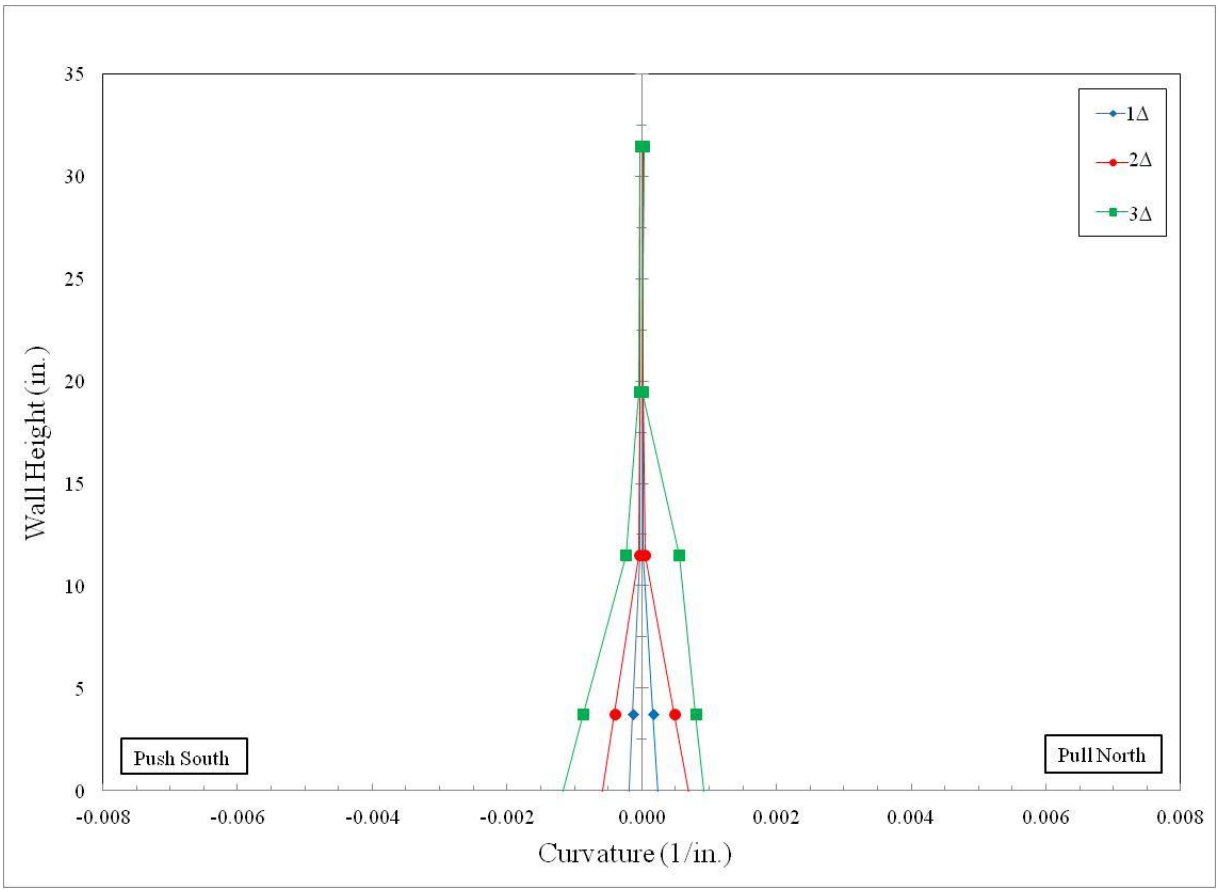

Figure 4.34 Wall C5: Curvature vs. Wall Height

Displacement and Curvature Ductility:

The displacement ductilities for the positive and negative loading directions along with the average value are presented in Table 4.24 for Wall Specimen C5. The total drift reached at 20% load degradation was 1.5%.

Table 4.24 Wall C5: Displacement Ductility

Direction of Load	**Displacement**					
	P'_y (kips)	Δ'_y (in.)	Δ_u (in.)	P_y (kips)	Δ_y (in.)	μ_Δ
Push South	-96.3	-0.21	-1.04	-118.5	-0.26	4.1
Pull North	117.3	0.54	1.07	148.0	0.68	1.6
Average	106.8	0.37	1.05	133.3	0.47	2.8

The curvature ductilities for the positive and negative loading directions along with the average value are presented in Table 4.25 for Wall Specimen C5. Damage in the wall towards the end of testing affected the displacement potentiometer readings, and thus the final values of curvatures determined for this wall were prior to 20% load degradation from the maximum load. As a result, the values for the ultimate curvature and the yield curvature in the elastoplastic approximation do not accurately reflect actual curvatures in the wall at failure. When calculating the curvature ductility factor in the pull direction ϕ'_y was used because ϕ_y could not be calculated from the elastoplastic approximation.

Table 4.25 Wall C5: Curvature Ductility

Direction of Load	**Curvature**					
	M'_y (kip-in.)	ϕ'_y (in.$^{-1}$)	ϕ_u (in.$^{-1}$)	M_y (kip-in.)	ϕ_y (in.$^{-1}$)	μ_ϕ
Push South	-6897	-0.00010	-0.0009	-8378	-0.00013	6.8
Pull North	8401	0.00049	0.0008	13490	0.00078	1.6
Average	7649	0.00030	0.0008	10934	0.00045	4.2

Height of Plasticity and Equivalent Plastic Hinge Length:

The height of plasticity and the equivalent plastic hinge length for the positive and negative loading directions along with the average values are presented in Table 4.26 for Wall Specimen C5. Because final curvatures were determined prior to failure in this wall, the calculated height of plasticity and equivalent plastic hinge length will be lower-bound estimates of the actual values. When calculating the plastic hinge length in the pull direction ϕ'_y was used because ϕ_y could not be calculated from the elastoplastic approximation. The ratios of the average height of plasticity zone to the wall length and the average equivalent plastic hinge length to the wall length are also provided in the table.

Table 4.26 Wall C5: Height of Plasticity & Equivalent Plastic Hinge Length

Direction of Load	Height of Plasticity Zone (in.)	Plastic Hinge Length (in.)
Push South	19.1	16.8
Pull North	12.5	29.6
Average	15.8	23.3
L_p/L and l_p/L	22.1%	32.4%

Energy Dissipation:

The total energy dissipated in Wall Specimen C5 through the end of the displacement level in which failure occurred for the positive and negative loading directions was 489 kip-in.

Equivalent Hysteretic Damping:

The equivalent hysteretic damping for Wall Specimen C5 at approximately 0.6% and 1.5% drift was 13.8% and 17.5%, respectively.

4.7 Wall Specimen C6

Wall Specimen C6 had a height-to-length aspect ratio of 2.0, No. 6 vertical reinforcement spaced 8-in. on center with no splice at the base of the wall, No. 4 horizontal reinforcement spaced 16-in. on center, and zero axial load. The predicted maximum lateral load capacity of Wall Specimen C6 was 38 kips and 43.9 kips using the MSJC and XTRACT analysis methods, respectively. The horizontal reinforcement yielded in both courses. The extreme vertical reinforcement yielded in the footing of Wall Specimen C6.

Test Observations:

The preliminary test for Wall Specimen C6 produced a yield displacement (ΔY) of 0.69 in. The specimen was then loaded to displacements of ±1, 2, 3, 4 and 6 times the yield displacement for the primary test. During testing, the wall behavior was dominated by flexural cracking that initiated at 2ΔY. Shear cracks propagated and widened throughout the lower half of the wall at increased displacement levels. Separation of the mortar joints started at the base of the wall and continued along the height of the wall. Vertical splitting in the South toe appeared at 3ΔY. Buckling of the extreme vertical reinforcement in both toes was observed near test completion. Spalling in both toes at test completion extended to the third course. The entire wall specimen and the North and South toe regions of the wall at test completion are shown in Figures 4.35 and 4.36, respectively. Test observations and their corresponding lateral displacements and loads are presented in Table 4.27.

Table 4.27 Wall C6: Test Observations

Load (kips)	Disp. (in.)	Test Observation
-26.71	-0.35	1st Yield of extreme vertical reinforcement bar in south toe (push)
28.46	0.39	1st Yield of extreme vertical reinforcement bar in north toe (pull)
-38.12	-0.68	Critical masonry strain in south toe (push)
-43.59	-1.11	1% Drift in push to south
42.15	1.11	1% Drift in pull to north
43.90	1.26	Critical masonry strain in north toe (pull)
-43.91	-1.38	Flexural cracking in north toe (push)*
-43.91	-1.38	Onset of toe crushing in south toe (push)*
42.74	1.40	Flexural cracking in south toe (pull)*
-44.80	-2.07	Maximum load resistance in push to south
43.23	2.09	Maximum load resistance in pull to north
43.23	2.09	Onset of toe crushing in north toe (pull)*
-33.16	-2.76	20% load degradation from maximum load resistance in push to south
35.38	2.77	20% load degradation from maximum load resistance in pull to north

*Visual Observation

Figure 4.35 Wall C6: Entire Wall at Test Completion

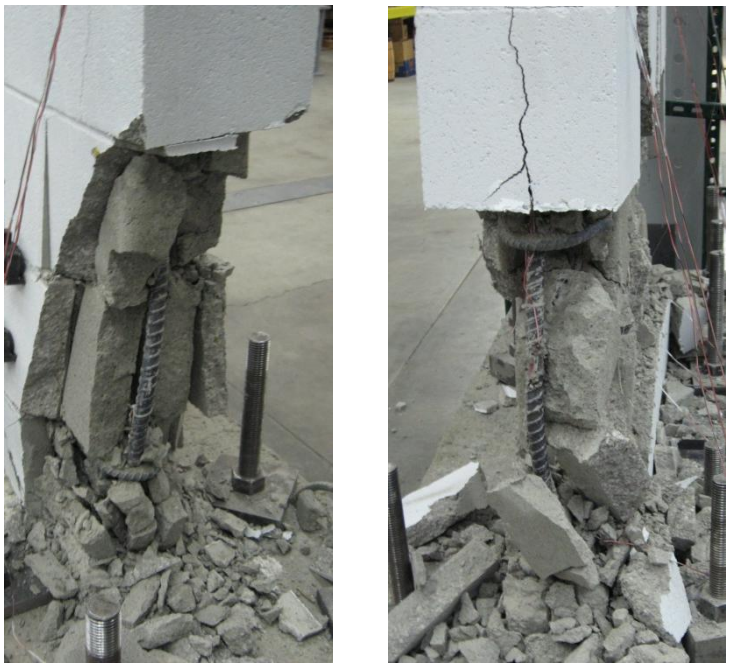

Figure 4.36 Wall C6: South Toe (Left) and North Toe (Right) at Test Completion

Load Displacement:

The load-displacement hysteresis curves for the preliminary and primary tests for Wall Specimen C6 are presented in Figure 4.37. The six important limit-state events are marked on the load-displacement curves and are presented in Table 4.27 along with the lateral displacement and load at the time of their occurrence. The initial yielding of the extreme tensile reinforcement (ε_y = 0.00233) occurred near the end of the preliminary test for both loading directions. Critical masonry strain was reached in the first cycle of 1ΔY and 2ΔY in the push and pull directions, respectively. The specimen attained 1% drift in the first cycle of 2ΔY for both loading directions. The onset of toe crushing occurred in the first cycle of 2ΔY and 3ΔY in the South and North toe, respectively. The onset of toe damage in both toe regions is presented in Figure 4.38. The maximum lateral load was reached in the first cycle of 3ΔY for both loading directions. The specimen reached 20% load degradation in the second cycle of 4ΔY and the first cycle of 6ΔY in the push and pull directions, respectively. Wall Specimen C6 exhibited symmetrical load-displacement relationships in the two loading directions throughout the entire test. Rapid strength degradation and abrupt failure occurred in the first cycle of 6ΔY which caused the test to stop prior to reaching the predetermined displacement at that level.

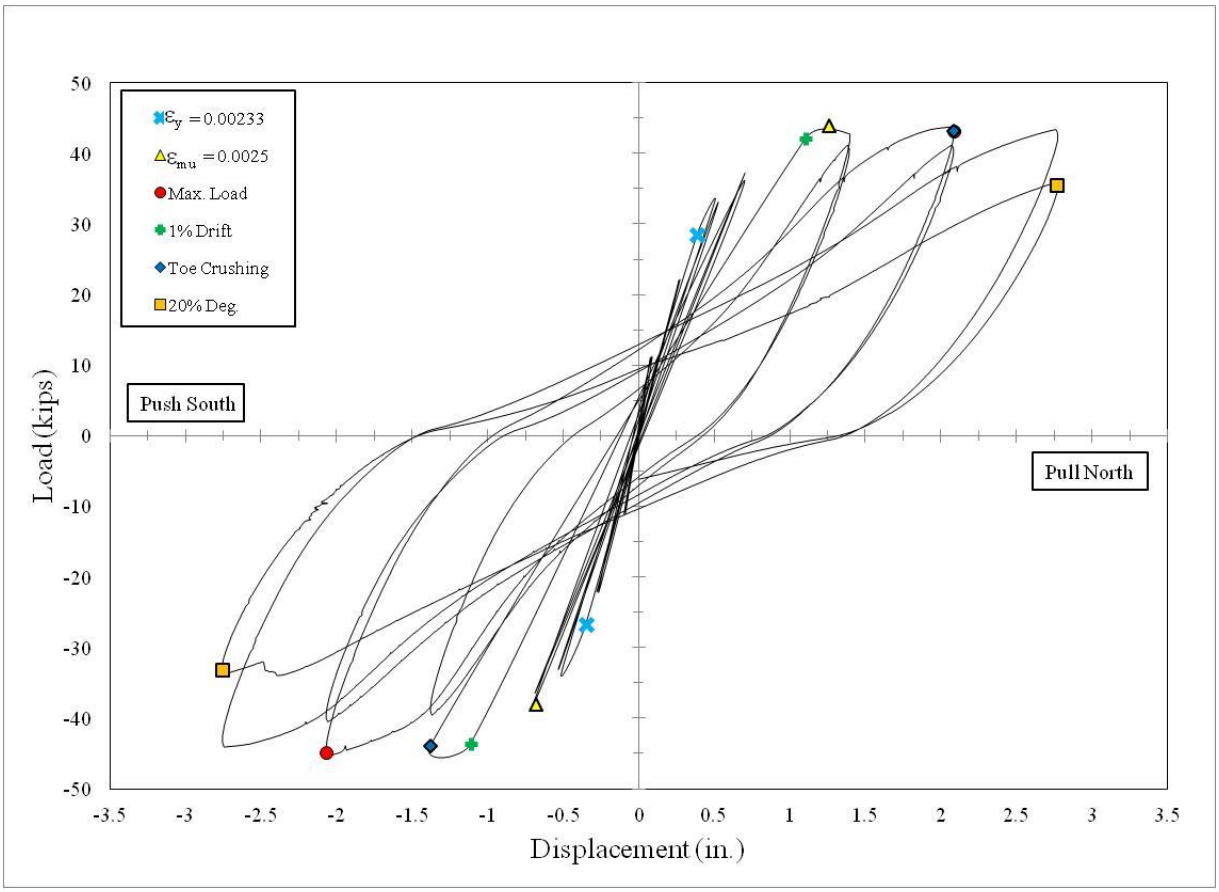

Figure 4.37 Wall C6: Load-Displacement Hysteresis Curves

Figure 4.38 Wall C6: South Toe (Left) and North Toe (Right) at Onset of Toe Damage

Displacement and Drift Components:

Load-displacement hysteresis curves showing the total lateral displacement and the three components of displacement are given in Figure 4.39. The load-displacement hysteresis curves showing the flexural and shear components were unavailable due to invalid readings from the displacement potentiometers. The average total drift and average drift contributions from flexure, sliding and shear deformations are presented in Table 4.28 at three important limit-states: critical masonry strain, peak lateral load and failure.

Table 4.28 Wall C6: Components of Total Drift

Limit-State	Total Drift (%)	Flexure (% Total)	Sliding (% Total)	Shear (% Total)
ε_{mu}	0.9	NA	1.0	NA
Peak Load	1.9	NA	2.1	NA
Failure	2.5	NA	3.1	NA

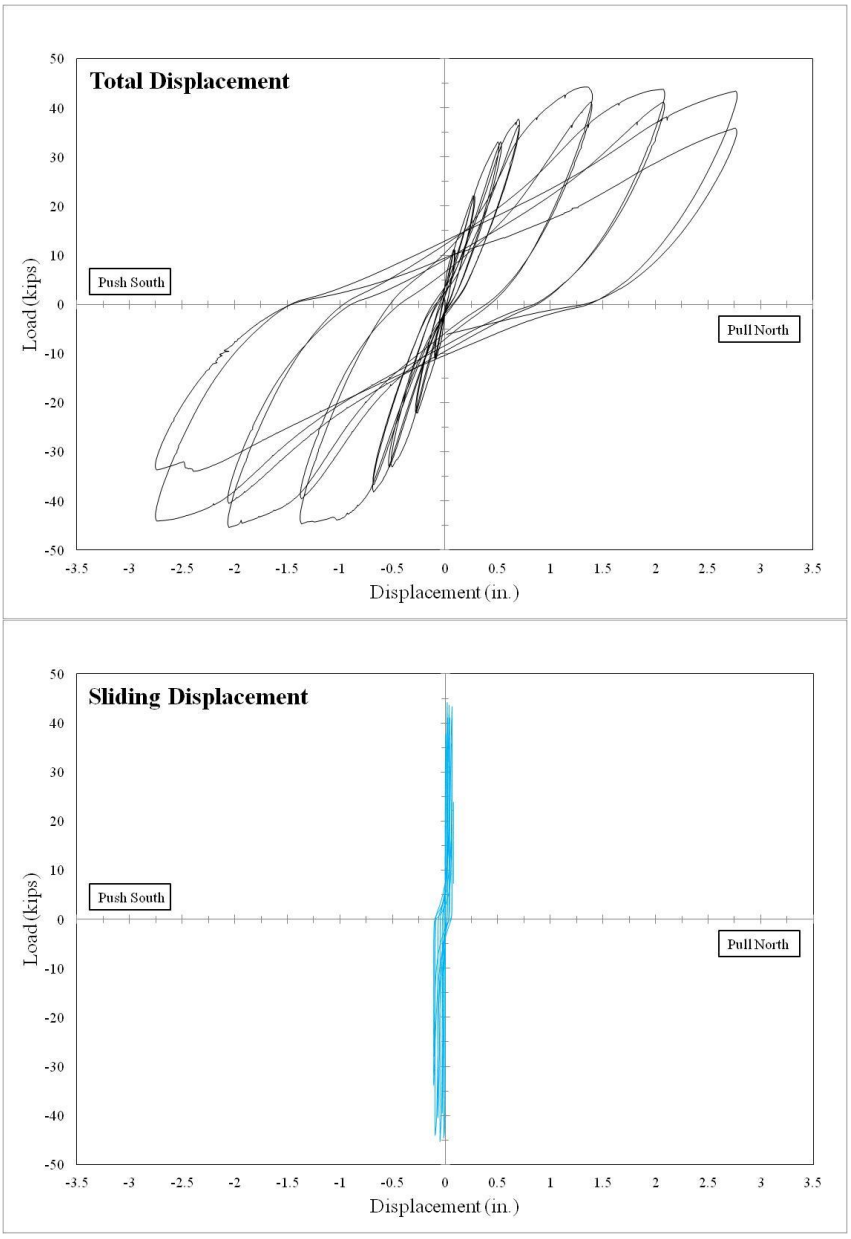

Figure 4.39 Wall C6: Total Lateral Displacement and its Components

Wall Curvatures:

A plot of curvatures over the height of Wall Specimen C6 is given in Figure 4.40. Curvatures over the wall height were symmetric about the wall center line through 4ΔY. The ultimate curvature was defined at the first cycle of 3ΔY 4ΔY, instead of at 20% load degradation

of the maximum load attained, in the push and pull directions, respectively. This was because valid readings from the displacement potentiometers where no longer available at larger displacement levels.

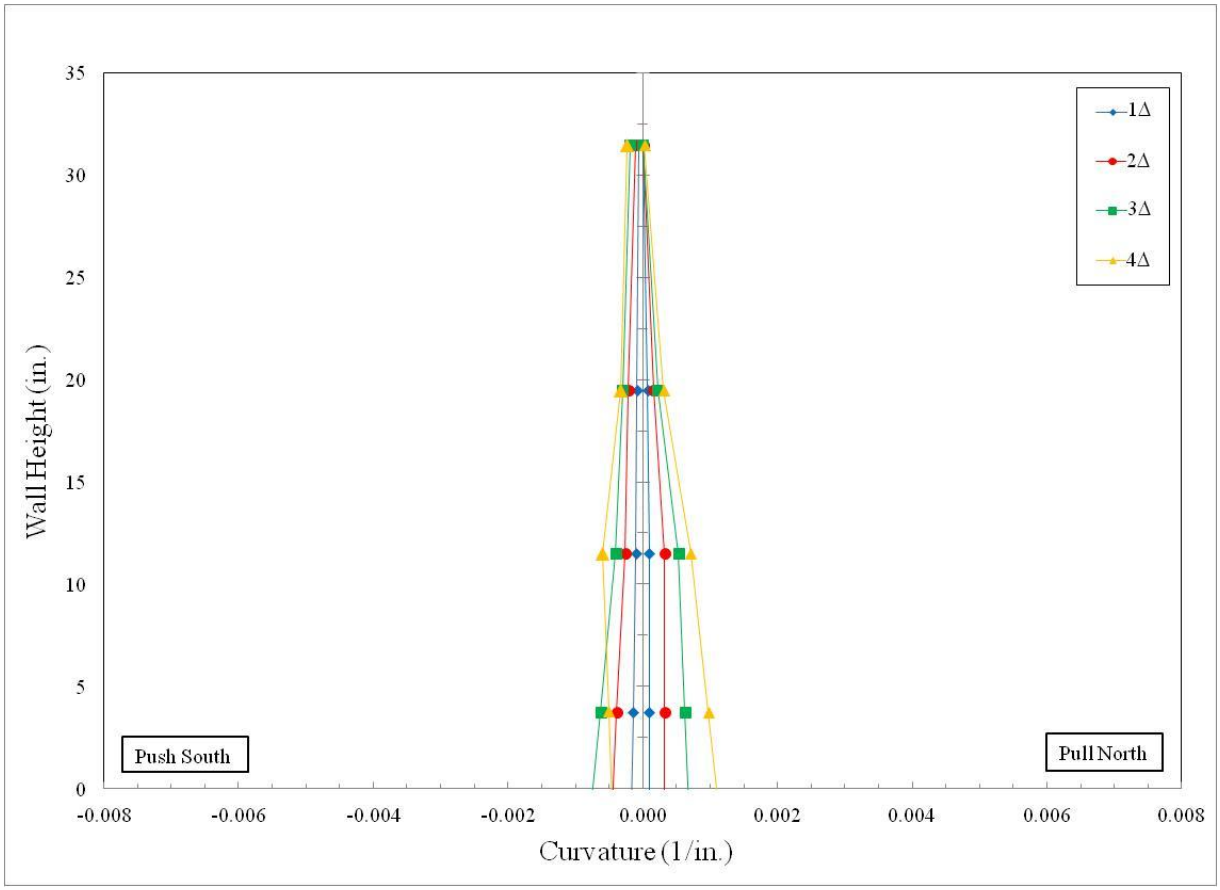

Figure 4.40 Wall C6: Curvature vs. Wall Height

Displacement and Curvature Ductility:

The displacement ductility for the positive and negative loading directions along with the average value are presented in Table 4.29 for Wall Specimen C6. The total drift reached at 20% load degradation was 2.5%.

Table 4.29 Wall C6: Displacement Ductility

Direction of Load	Displacement					
	P'_y (kips)	Δ'_y (in.)	Δ_u (in.)	P_y (kips)	Δ_y (in.)	μ_Δ
Push South	-26.7	-0.35	-2.76	-41.1	-0.54	5.1
Pull North	28.5	0.39	2.77	40.6	0.55	5.0
Average	27.6	0.37	2.76	40.8	0.55	5.1

The curvature ductilities for the positive and negative loading directions along with the average value are presented in Table 4.30 for Wall Specimen C6. Damage in the wall towards the end of testing affected the displacement potentiometer readings, and thus the final values of curvatures determined for this wall were prior to 20% load degradation from the maximum load. As a result, the values for the ultimate curvature and the yield curvature in the elastoplastic approximation do not accurately reflect actual curvatures in the wall at failure.

Table 4.30 Wall C6: Curvature Ductility

Direction of Load	Curvature					
	M'_y (kip-in.)	ϕ'_y (in.$^{-1}$)	ϕ_u (in.$^{-1}$)	M_y (kip-in.)	ϕ_y (in.$^{-1}$)	μ_ϕ
Push South	-2971	-0.00003	-0.0006	-4618	-0.00005	12.3
Pull North	3166	0.00006	0.0010	4706	0.00008	11.7
Average	3068	0.00004	0.0008	4662	0.00007	12.0

Height of Plasticity and Equivalent Plastic Hinge Length:

The height of plasticity and the equivalent plastic hinge length for the positive and negative loading directions along with the average values are presented in Table 4.31 for Wall Specimen C6. Because final curvatures were determined prior to failure in this wall, the calculated height of plasticity and equivalent plastic hinge length will be lower-bound estimates of the actual values. The height of the plasticity zone in the push direction could not be calculated because valid readings from the displacement potentiometers were no longer available

at larger displacement levels. The ratios of the average height of plasticity zone to the wall length and the average equivalent plastic hinge length to the wall length are also provided in the table.

Table 4.31 Wall C6: Height of Plasticity & Equivalent Plastic Hinge Length

Direction of Load	Height of Plasticity Zone (in.)	Plastic Hinge Length (in.)
Push South	NA	42.8
Pull North	30.1	25.4
Average	30.1	34.1
L_p/L and l_p/L	54.0%	61.2%

Energy Dissipation:

The total energy dissipated in Wall Specimen C6 through the end of the displacement level in which failure occurred for the positive and negative loading directions was 525 kip-in.

Equivalent Hysteretic Damping:

The equivalent hysteretic damping for Wall Specimen C6 at approximately 0.6% and 1.5% drift was 6.8% and 15.1%, respectively.

4.8 Wall Specimen C7

Wall Specimen C7 had a height-to-length aspect ratio of 2.0, four No. 6 vertical reinforcement bars located in the two outermost cells (jamb reinforcement) and one No. 4 vertical reinforcement bar located at mid-length, two No. 3 horizontal reinforcement bars spaced 8-in. on center, and zero axial load. The vertical reinforcement did not contain lap splices. The predicted maximum lateral load capacity of Wall Specimen C7 was 46 kips and 55.5 kips using the MSJC and XTRACT analysis methods, respectively. The horizontal reinforcement yielded

in the first course but not in the fifth course. The extreme vertical reinforcement yielded in the footing of Wall Specimen C7.

Test Observations:

The preliminary test for Wall Specimen C7 produced a yield displacement (ΔY) of 0.78 in. The specimen was then loaded to displacements of ±1, 2, 3, 4 and 6 times the yield displacement for the primary test. During testing, the wall displayed a mixture of flexure and shear cracks that initiated at 2ΔY. They continued to open and propagate at increased displacement levels. Separation of the mortar joints started at the base of the wall and continued along the height of the wall. Vertical splitting in both toes appeared at 3ΔY. Buckling of the extreme vertical reinforcement in both toes was observed near test completion. Spalling in both toes at test completion extended to the third course. The entire wall specimen and the North and South toe regions of the wall at test completion are shown in Figures 4.41 and 4.42, respectively. Test observations and their corresponding lateral displacements and loads are presented in Table 4.32.

Table 4.32 Wall C7: Test Observations

Load (kips)	Disp. (in.)	Test Observation
-13.16	-0.13	1st Yield of extreme vertical reinforcement bar in south toe (push)
-31.20	-0.38	Critical masonry strain in south toe (push)
44.68	0.65	1st Yield of extreme vertical reinforcement bar in north toe (pull)
-54.02	-1.11	1% Drift in push to south
52.79	1.11	1% Drift in pull to north
-57.76	-1.55	Flexural cracking in north toe (push)*
57.61	1.57	Flexural cracking in south toe (pull)*
58.96	2.12	Critical masonry strain in north toe (pull)
-58.01	-2.34	Maximum load resistance in push to south
60.48	2.35	Maximum load resistance in pull to north
-33.26	-3.12	20% load degradation from maximum load resistance in push to south
37.52	3.13	20% load degradation from maximum load resistance in pull to north

*Visual Observation

Figure 4.41 Wall C7: Entire Wall at Test Completion

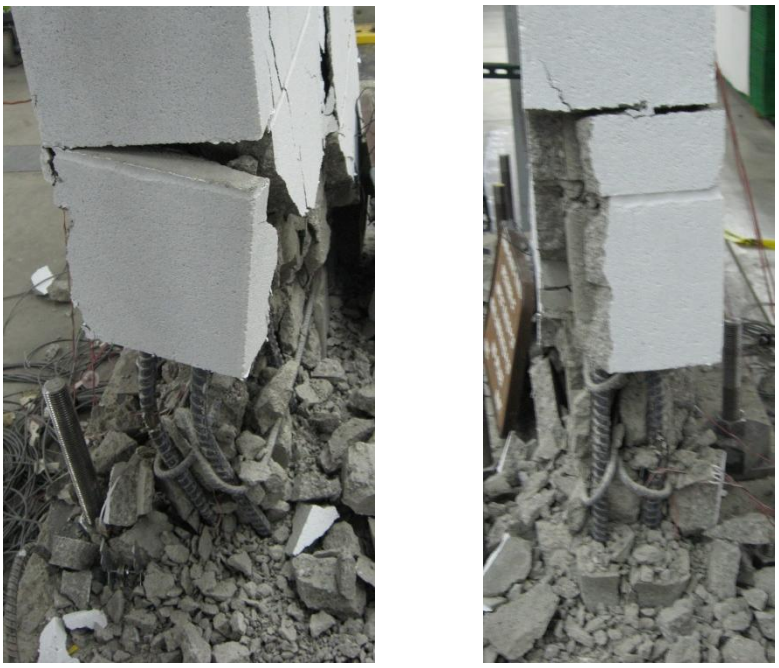

Figure 4.42 Wall C7: South Toe (Left) and North Toe (Right) at Test Completion

Load Displacement:

The load-displacement hysteresis curves for the preliminary and primary tests for Wall Specimen C7 are presented in Figure 4.43. The six important limit-state events are marked on the load-displacement curves and are presented in Table 4.32 along with the lateral displacement and load at the time of their occurrence. The initial yielding of the extreme tensile reinforcement ($\varepsilon_y = 0.00233$) occurred near the beginning of the preliminary test and in the first cycle of 1ΔY in the push and pull directions, respectively. Critical masonry strain was reached near the end of the preliminary test in the push direction. The specimen attained 1% drift in the first cycle of 2ΔY for both loading directions. Maximum lateral load in both directions and critical masonry strain in the pull direction occurred in the first cycle of 3ΔY. The onset of toe damage in both toe regions, presented in Figure 4.44, occurred at 3ΔY. The specimen reached 20% load degradation in the second cycle of 4ΔY for both loading directions. Wall Specimen C7 exhibited symmetrical load-displacement relationships in the two loading directions prior to reaching maximum load. Strength decreased faster in the push direction than in the pull direction after maximum load was attained. The test was stopped prior to reaching the predetermined displacement at 6ΔY due to abrupt failure of the wall. The 'jumps' in the load-displacement hysteresis curves were caused by minor slip in the actuator-to-column connection. This slip had a negligible effect on the testing of the wall.

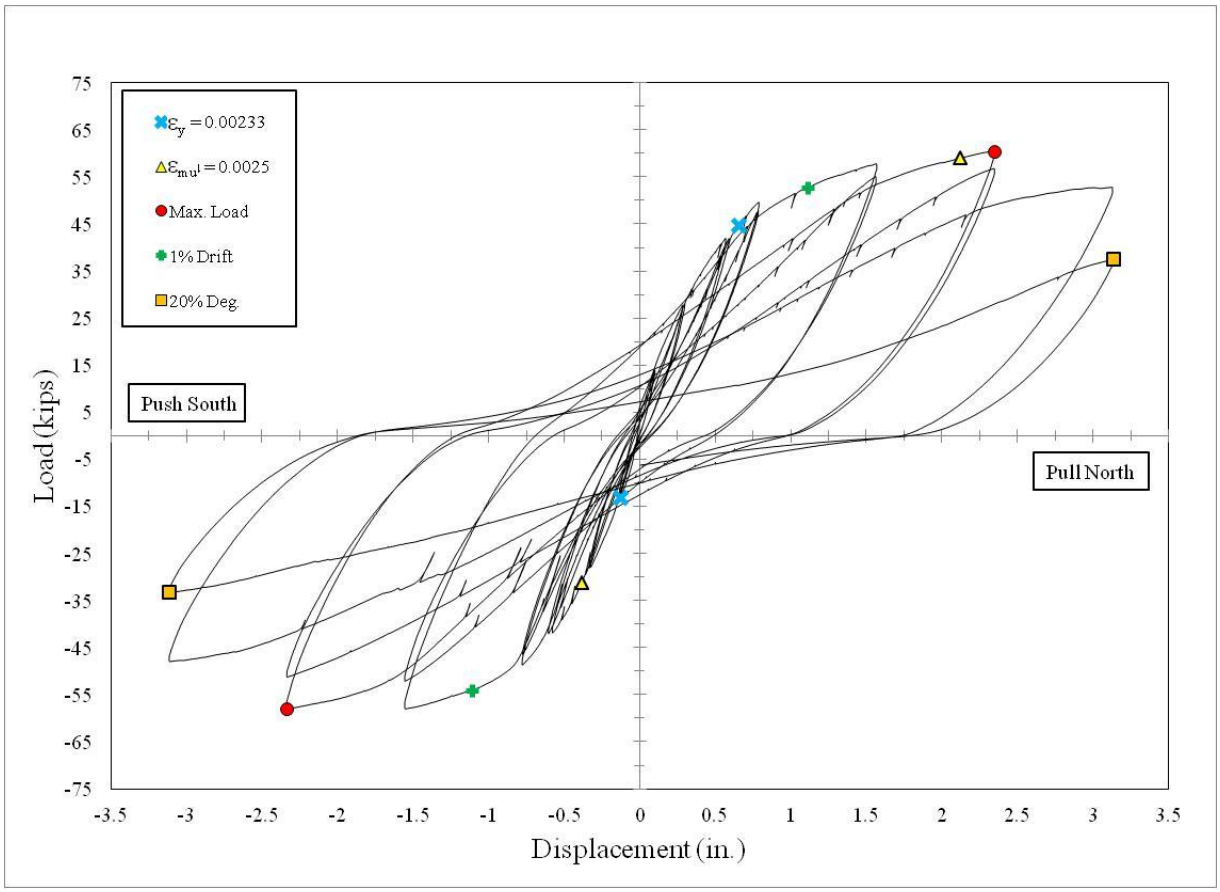

Figure 4.43 Wall C7: Load-Displacement Hysteresis Curves

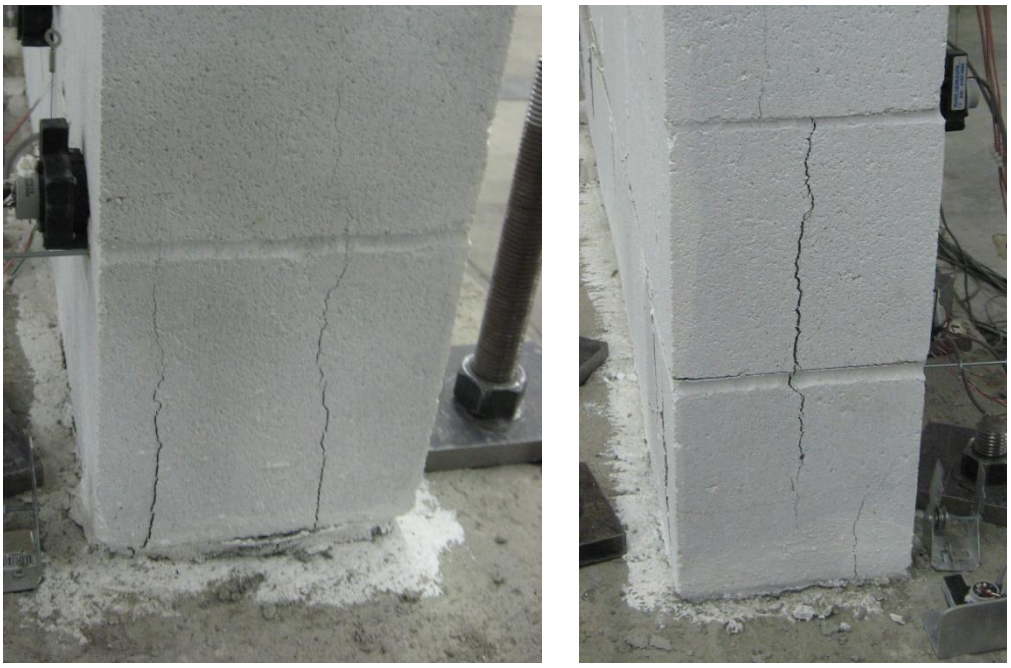

4.44 Wall C7: South Toe (Left) and North Toe (Right) at Onset of Toe Damage

Displacement and Drift Components:

Load-displacement hysteresis curves showing the total lateral displacement and the three components of displacement are given in Figure 4.45. The load-displacement hysteresis curves showing the flexural and shear components were unavailable due to invalid readings from the displacement potentiometers. The average total drift and average drift contributions from flexure, sliding and shear deformations are presented in Table 4.33 at three important limit-states: critical masonry strain, peak lateral load and failure.

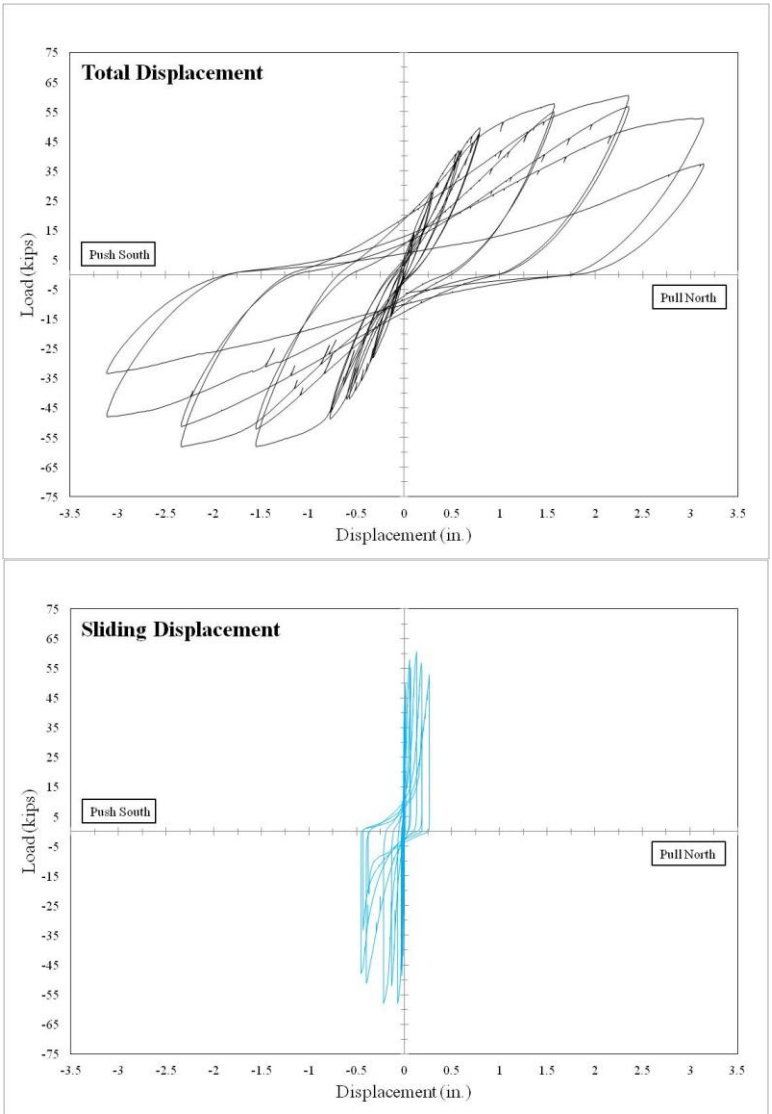

Figure 4.45 Wall C7: Total Lateral Displacement and its Components

Table 4.33 Wall C7: Components of Total Drift

Limit-State	Total Drift (%)	Flexure (% Total)	Sliding (% Total)	Shear (% Total)
ε_{mu}	1.1	NA	5.2	NA
Peak Load	2.1	NA	7.4	NA
Failure	2.8	NA	9.8	NA

Wall Curvatures:

A plot of curvatures over the height of Wall Specimen C7 is given in Figure 4.46. Curvatures over the wall height were symmetric about the wall center line through 3ΔY. The ultimate curvature was defined at the first cycle of 3ΔY, instead of at 20% load degradation of the maximum load attained, for both loading directions. This was because valid readings from the displacement potentiometers where no longer available at larger displacement levels.

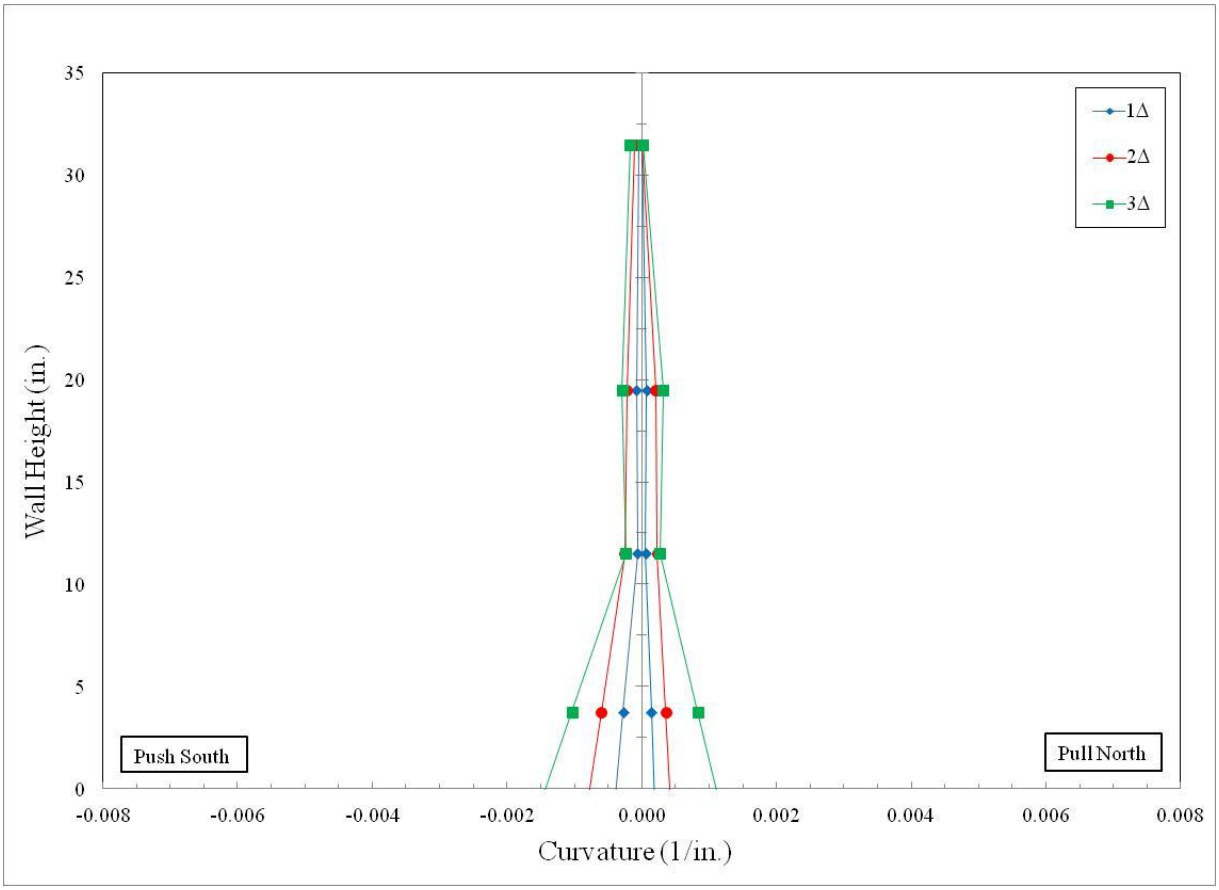

Figure 4.46 Wall C7: Curvature vs. Wall Height

Displacement and Curvature Ductility:

The displacement ductilities for the positive and negative loading directions along with the average value are presented in Table 4.34 for Wall Specimen C7. The total drift reached at 20% load degradation was 2.8%.

Table 4.34 Wall C7: Displacement Ductility

Direction of Load	**Displacement**					
	P'_y (kips)	Δ'_y (in.)	Δ_u (in.)	P_y (kips)	Δ_y (in.)	μ_Δ
Push South	-13.2	-0.13	-3.12	-52.8	-0.53	5.9
Pull North	44.7	0.65	3.13	57.8	0.84	3.7
Average	28.9	0.39	3.13	55.3	0.69	4.8

The curvature ductilities for the positive and negative loading directions along with the average value, is presented in Table 4.35 for Wall Specimen C7. Damage in the wall towards the end of testing affected the displacement potentiometer readings, and thus the final values of curvatures determined for this wall were prior to 20% load degradation from the maximum load. As a result, the values for the ultimate curvature and the yield curvature in the elastoplastic approximation do not accurately reflect actual curvatures in the wall at failure.

Table 4.35 Wall C7: Curvature Ductility

Direction of Load	**Curvature**					
	M'_y (kip-in.)	ϕ'_y (in.$^{-1}$)	ϕ_u (in.$^{-1}$)	M_y (kip-in.)	ϕ_y (in.$^{-1}$)	μ_ϕ
Push South	-1464	-0.00001	-0.0010	-5715	-0.00004	26.2
Pull North	4970	0.00008	0.0008	6373	0.00010	8.5
Average	3217	0.00004	0.0009	6044	0.00007	17.4

Height of Plasticity and Equivalent Plastic Hinge Length:

The height of plasticity and the equivalent plastic hinge length for the positive and negative loading directions along with the average values are presented in Table 4.36 for Wall

Specimen C7. Because final curvatures were determined prior to failure in this wall, the calculated height of plasticity and equivalent plastic hinge length will be lower-bound estimates of the actual values. The height of the plasticity zone in the push direction could not be calculated because valid readings from the displacement potentiometers were no longer available at larger displacement levels. The ratios of the average height of plasticity zone to the wall length and the average equivalent plastic hinge length to the wall length are also provided in the table.

Table 4.36 Wall C7: Height of Plasticity & Equivalent Plastic Hinge Length

Direction of Load	**Height of Plasticity Zone (in.)**	**Plastic Hinge Length (in.)**
Push South	NA	26.5
Pull North	29.3	33.0
Average	29.3	29.7
L_p/L and l_p/L	52.6%	53.4%

Energy Dissipation:

The total energy dissipated in Wall Specimen C7 through the end of the displacement level in which failure occurred for the positive and negative loading directions was 764 kip-in.

Equivalent Hysteretic Damping:

The equivalent hysteretic damping for Wall Specimen C7 at approximately 0.6% and 1.5% drift was 6.2% and 15.9%, respectively.

4.9 Wall Specimen C8

Wall Specimen C8 had a height-to-length aspect ratio of 2.0, four No. 6 vertical reinforcement bars located in the two outermost cells (jamb reinforcement) and one No. 4 vertical reinforcement bar located at mid-length, two No. 3 horizontal reinforcement bars spaced 8-in. on center, and an axial load of 67 kips. The vertical reinforcement did not contain lap splices. The predicted maximum lateral load capacity of Wall Specimen C8 was 59 kips and 64.4 kips using the MSJC and XTRACT analysis methods, respectively. The horizontal reinforcement yielded in the first course but not in the fifth course. The extreme vertical reinforcement yielded in the footing of Wall Specimen C8.

Test Observations:

The preliminary test for Wall Specimen C8 produced a yield displacement (ΔY) of 0.54 in. The specimen was then loaded to displacements of ±1, 2, 3, 4 and 6 times the yield displacement for the primary test. During testing, the wall displayed a mixture of flexure and shear cracks that initiated at $2\Delta Y$. They continued to open and propagate at increased displacement levels. Separation of the mortar joints started at the base of the wall and continued along the height of the wall. Vertical splitting in the North and South toe appeared at $2\Delta Y$ and $3\Delta Y$, respectively. Buckling of the extreme vertical reinforcement in both toes was observed near test completion. Spalling in both toes at test completion extended to the second course. The entire wall specimen and the North and South toe regions of the wall at test completion are shown in Figures 4.47 and 4.48, respectively. Test observations and their corresponding lateral displacements and loads are presented in Table 4.37.

Figure 4.47 Wall C8: Entire Wall at Test Completion

Figure 4.48 Wall C8: South Toe (Left) and North Toe (Right) at Test Completion

Table 4.37 Wall C8: Test Observations

Load (kips)	Disp. (in.)	Test Observation
46.73	0.38	1st Yield of extreme vertical reinforcement bar in north toe (pull)
-52.59	-0.46	1st Yield of extreme vertical reinforcement bar in south toe (push)
-55.06	-0.54	Critical masonry strain in south toe (push)
64.00	0.85	Critical masonry strain in north toe (pull)
-68.48	-1.08	Flexural cracking in north toe (push)*
64.93	1.09	Flexural cracking in south toe (pull)*
-65.32	-1.11	1% Drift in push to south
61.61	1.11	1% Drift in pull to north
-71.22	-2.16	Maximum load resistance in push to south
69.63	2.18	Maximum load resistance in pull to north
55.71	2.82	20% load degradation from maximum load resistance in pull to north
-58.21	-3.25	20% load degradation from maximum load resistance in push to south

*Visual Observation

Load Displacement:

The load-displacement hysteresis curves for the preliminary and primary tests for Wall Specimen C8 are presented in Figure 4.49. The six important limit-state events are marked on the load-displacement curves and are presented in Table 4.37 along with the lateral displacement and load at the time of their occurrence. The initial yielding of the extreme tensile reinforcement ($\varepsilon_y = 0.00233$) occurred near the end of the preliminary test and in the first cycle of 1ΔY in the pull and push directions, respectively. Critical masonry strain was reached in the second cycle of 1ΔY and the first cycle of 2ΔY in the push and pull directions, respectively. The onset of toe damage, presented in Figure 4.50 occurred in the first cycle of 2ΔY for both toe regions. The specimen attained 1% drift in the first cycle of 3ΔY for both loading directions. Maximum lateral load occurred in the first cycle of 4ΔY for both loading directions. The specimen reached 20% load degradation in the first and second cycle of 6ΔY in the pull and push directions, respectively. Toe crushing did not appear in either toe. Wall Specimen C8 exhibited symmetrical load-displacement relationships in the two loading directions with a gradual

reduction in strength following maximum load. The test was stopped prior to reaching the predetermined displacement at 6ΔY due to abrupt failure of the wall.

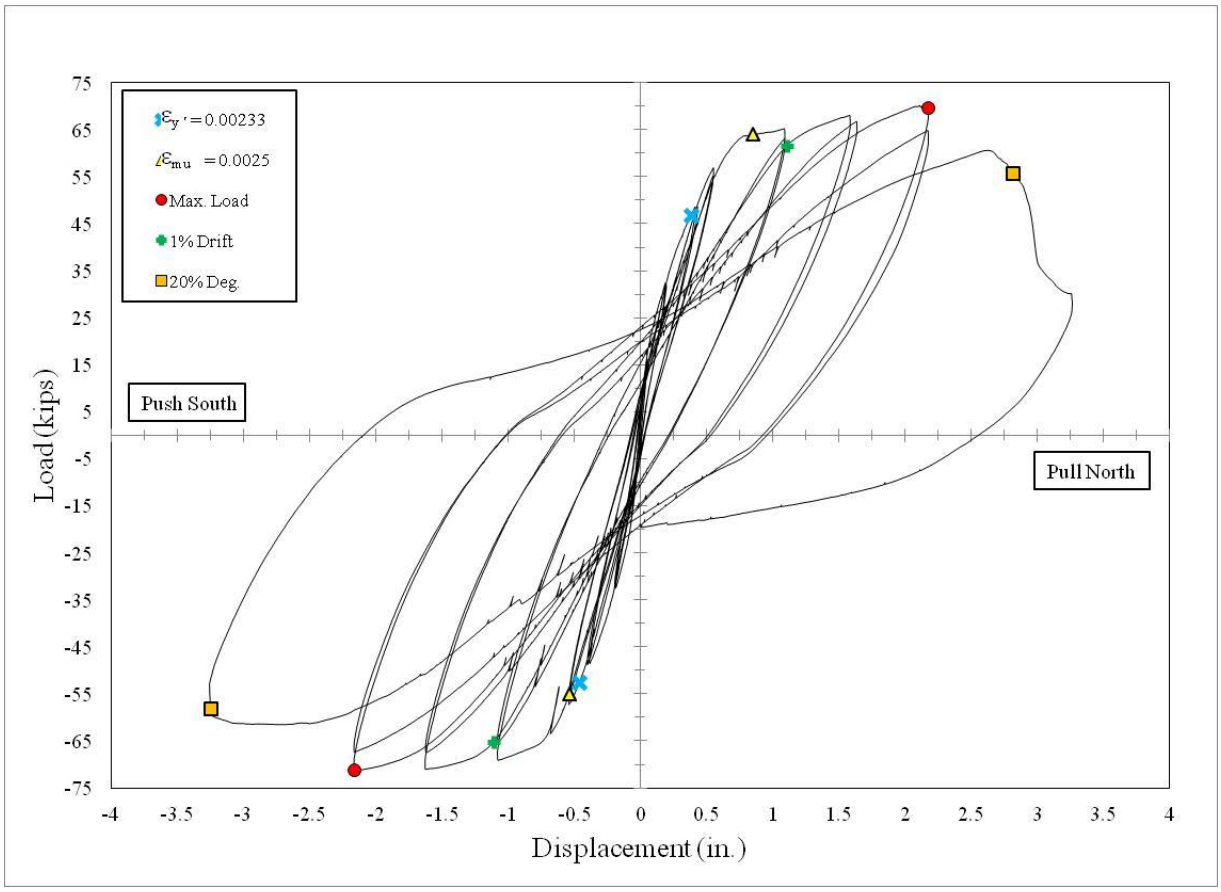

Figure 4.49 Wall C8: Load-Displacement Hysteresis Curves

Figure 4.50 Wall C8: South Toe (Left) and North Toe (Right) at Onset of Toe Damage

Displacement and Drift Components:

Load-displacement hysteresis curves showing the total lateral displacement and the three components of displacement are given in Figure 4.51. The load-displacement hysteresis curves showing the flexural and shear components were discontinued before the first cycle of 6ΔY in the pull direction due to invalid readings from the displacement potentiometers. The average total drift and average drift contributions from flexure, sliding and shear deformations are presented in Table 4.38 at three important limit-states: critical masonry strain, peak lateral load and failure. Wall Specimen C8 was dominated by flexural deformations with small levels of shear and sliding deformations occurring near failure.

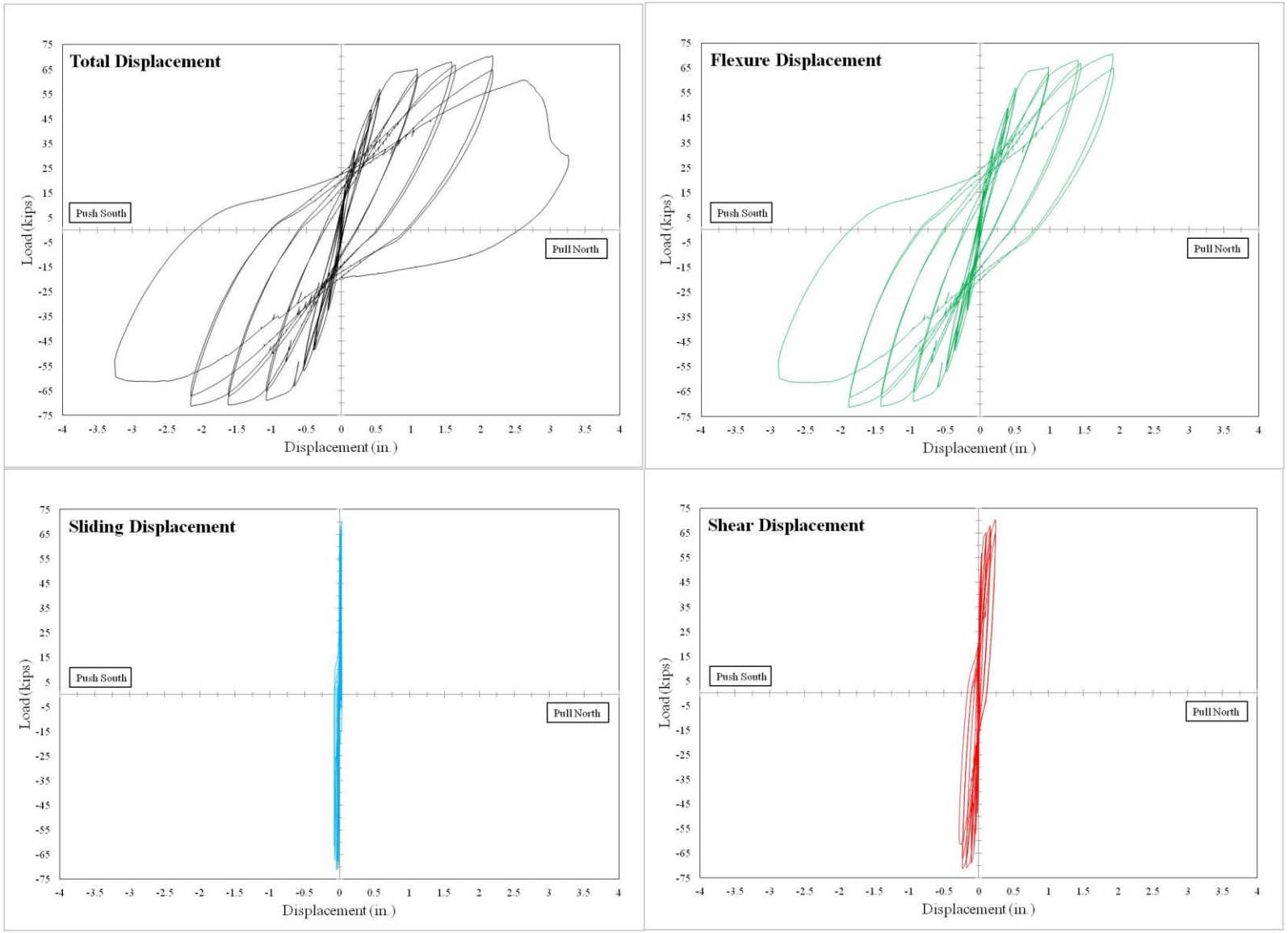

Figure 4.51 Wall C8: Total Lateral-Displacement and its Components

Table 4.38 Wall C8: Components of Total Drift

Limit-State	Total Drift (%)	Flexure (% Total)	Sliding (% Total)	Shear (% Total)
ε_{mu}	0.62	89.9	0.9	9.2
Peak Load	2.0	87.3	1.7	11.0
Instrumentation Failure	2.3	92.6	0.4	7.0
Failure	2.7	NA	1.1	NA

Wall Curvatures:

A plot of curvatures over the height of Wall Specimen C8 is given in Figure 4.52. Curvatures over the wall height were symmetric about the wall center line through 3ΔY. The ultimate curvature was defined at the first cycle of 3ΔY and 4ΔY, instead of at 20% load degradation of the maximum load attained, in the push and pull directions, respectively. This was because valid readings from the displacement potentiometers where no longer available at larger displacement levels.

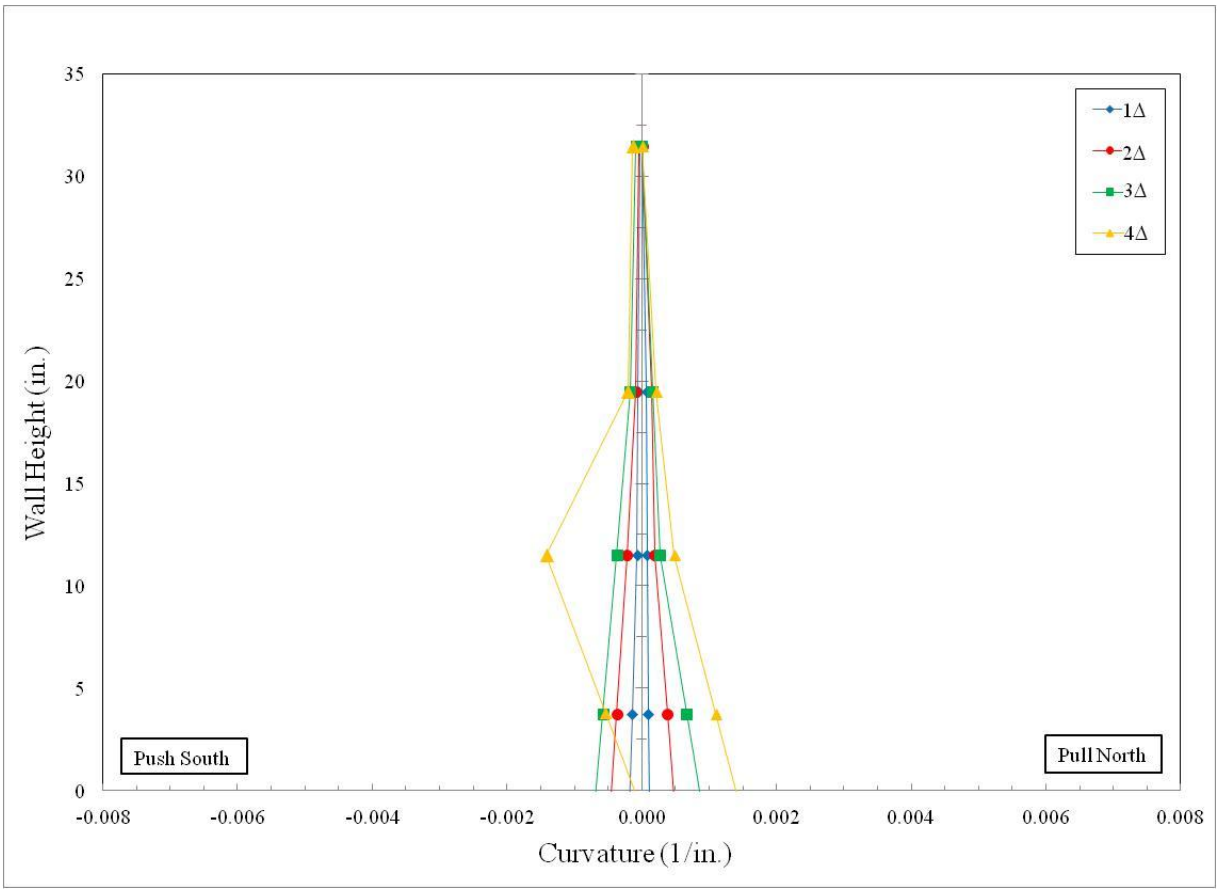

Figure 4.52 Wall C8: Curvature vs. Wall Height

Displacement and Curvature Ductility:

The displacement ductilities for the positive and negative loading directions along with the average value are presented in Table 4.39 for Wall Specimen C8. The total drift reached at 20% load degradation was 2.7%.

Table 4.39 Wall C8: Displacement Ductility

Direction of Load	**Displacement**					
	P'_y (kips)	Δ'_y (in.)	Δ_u (in.)	P_y (kips)	Δ_y (in.)	μ_Δ
Push South	-52.6	-0.46	-3.25	-67.9	-0.59	5.5
Pull North	46.7	0.38	2.82	65.1	0.53	5.3
Average	49.7	0.42	3.03	66.5	0.56	5.4

The curvature ductilities for the positive and negative loading directions along with the average value are presented in Table 4.40 for Wall Specimen C8. Damage in the wall towards the end of testing affected the displacement potentiometer readings, and thus the final values of curvatures determined for this wall were prior to 20% load degradation from the maximum load. As a result, the values for the ultimate curvature and the yield curvature in the elastoplastic approximation do not accurately reflect actual curvatures in the wall at failure.

Table 4.40 Wall C8: Curvature Ductility

Direction of Load	**Curvature**					
	M'_y (kip-in.)	ϕ'_y (in.$^{-1}$)	ϕ_u (in.$^{-1}$)	M_y (kip-in.)	ϕ_y (in.$^{-1}$)	μ_ϕ
Push South	-5851	-0.00012	-0.0006	-7880	-0.00017	3.5
Pull North	5199	0.00008	0.0008	7216	0.00011	7.5
Average	5525	0.00010	0.0007	7548	0.00014	5.5

Height of Plasticity and Equivalent Plastic Hinge Length:

The height of plasticity and the equivalent plastic hinge length for the positive and negative loading directions along with the average values are presented in Table 4.41 for Wall Specimen C8. Because final curvatures were determined prior to failure in this wall, the calculated height of plasticity and equivalent plastic hinge length will be lower-bound estimates of the actual values. The height of the plasticity zone in the push direction could not be calculated because valid readings from the displacement potentiometers were no longer available at larger displacement levels. The ratios of the average height of plasticity zone to the wall length and the average equivalent plastic hinge length to the wall length are also provided in the table.

Table 4.41 Wall C8: Height of Plasticity & Equivalent Plastic Hinge Length

Direction of Load	Height of Plasticity Zone (in.)	Plastic Hinge Length (in.)
Push South	NA	NA
Pull North	29.4	23.3
Average	29.4	23.3
L_p/L and l_p/L	52.8%	41.8%

Energy Dissipation:

The total energy dissipated in Wall Specimen C8 through the end of the displacement level in which failure occurred for the positive and negative loading directions was 981 kip-in.

Equivalent Hysteretic Damping:

The equivalent hysteretic damping for Wall Specimen C8 at approximately 0.6% and 1.5% drift was 6.1% and 14.8%, respectively.

4.10 Summary

Test results for eight concrete masonry shear walls were presented in this chapter. Photos of each wall at the end of testing and at the onset of toe damage were provided. Plots of the load-displacement hysteresis curves and the curvature along the height of each wall were also included. Test observations, displacement and drift components, displacement and curvature ductilities, height of plasticities and equivalent plastic hinge lengths were tabulated for each wall. The energy dissipation capacity and equivalent hysteretic damping were also provided for each wall.

CHAPTER 5:

ANALYSIS OF TEST RESULTS

5.1 Introduction

The effects of four different wall parameters (height-to-length aspect ratio, axial compressive stress, reinforcement ratio, and jamb reinforcement vs. distributed reinforcement) on the behavior of the eight reinforced concrete masonry shear walls discussed previously are presented in this chapter. Wall performance was evaluated based on a comparison of the failure modes, predicted vs. actual load capacity, drift capacity, displacement ductility, height of plasticity, equivalent plastic hinge length, amount of energy dissipation, and value of equivalent hysteretic damping. The wall test results in this study were also compared to results obtained by Sherman (2011) and by other researchers to gain a better understanding of how the parameters influence wall behavior.

5.2 Failure Modes

The different failure modes observed during testing are evaluated in this section. Table 5.1 lists the parameters associated with each wall. Visual observations of the walls during testing were compared for the different wall parameters and performance criteria.

Table 5.1 Evaluation of Failure Modes

Wall	Aspect Ratio	P/ (f'_mA_g)	Vertical Reinf.	Dominant Failure Mode
C1	2.0	0	#4 @ 8 in.	Flexure
C2	2.0	0.0625	#4 @ 8 in.	Flexure
C3	2.0	0.0625	#7 @ 16 in.	Flexure/Shear/Crushing
C4	0.78	0.0625	#7 @ 16 in.	Flexure/Shear/Crushing
C5	1	0.0625	#7 @ 16 in.	Flexure/Shear/Crushing
C6	2.0	0	#6 @ 8 in.	Flexure
C7	2.0	0	8 #6, 1 #4	Flexure
C8	2.0	0.0625	8 #6, 1 #4	Flexure

Walls C1, C2 and C6 through C8 were classified as having a primarily flexural failure mode. Figures 5.1 through 5.3 show a typical progression of damage for a wall failing in flexure. Visual observations of these walls include the development of flexural cracks and eventual crushing, splitting and face shell spalling in the toe regions. All of the walls failing in flexure had a height-to-length aspect ratio of 2.0. Different magnitudes of axial compressive stress and vertical reinforcement ratios were present in these walls. Walls failing in a primarily flexural mode also had both evenly distributed vertical reinforcement and jamb reinforcement.

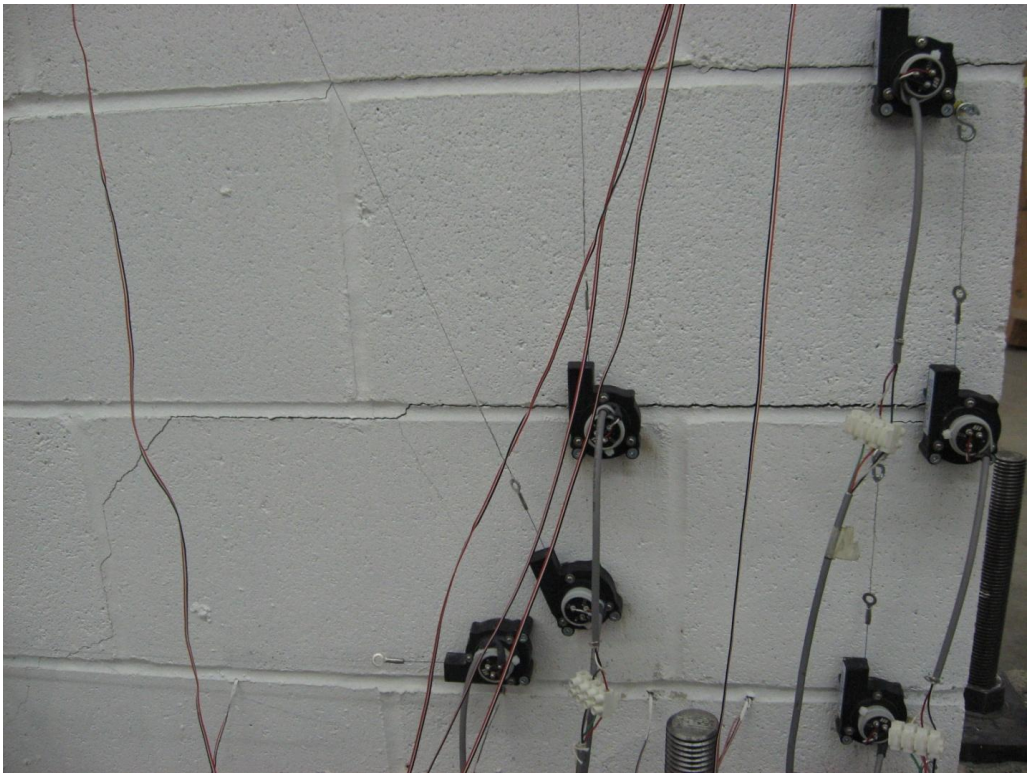

Figure 5.1 Wall C2: Development of Flexural Cracks

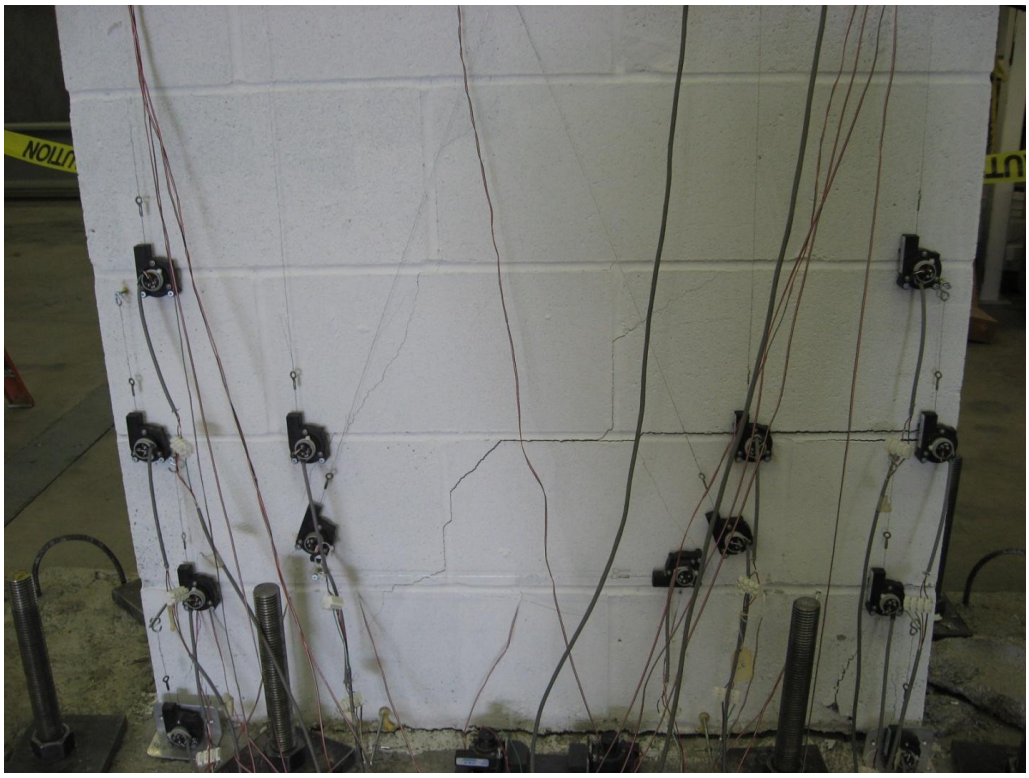

Figure 5.2 Wall C2: Further Development of Flexural Cracks Along with Some Shear Cracks

Figure 5.3 Wall C2: Toe Damage Typical of Flexural Failure

Walls C3, C4 and C5 were classified as having a complex flexure/shear/crushing failure mode. Figures 5.4 through 5.9 show the progression of cracking and crushing for this mode of failure in Walls C3 and C4. Visual observations of these walls include the propagation and widening of flexural and shear cracks, followed by crushing and spalling of the masonry face shells in the lower courses and eventual crushing of the grout cores. Significant amounts of sliding were also observed between the second and third courses in Wall C4 (see Figure 5.8). The walls failing in this mode encompassed height-to-length aspect ratios of 0.78, 1.0 and 2.0, an axial compressive stress of 158 psi, and a vertical reinforcement ratio of 0.0055. These walls also had a lap splice length of 46 in. at the base of the wall which effectively doubled the vertical reinforcement ratio to 0.011 at this location. This contributed to the complex dowel-action behavior that was observed in these three walls at failure.

Figure 5.4 Wall C3: Development of Flexural, Shear and Splitting Cracks

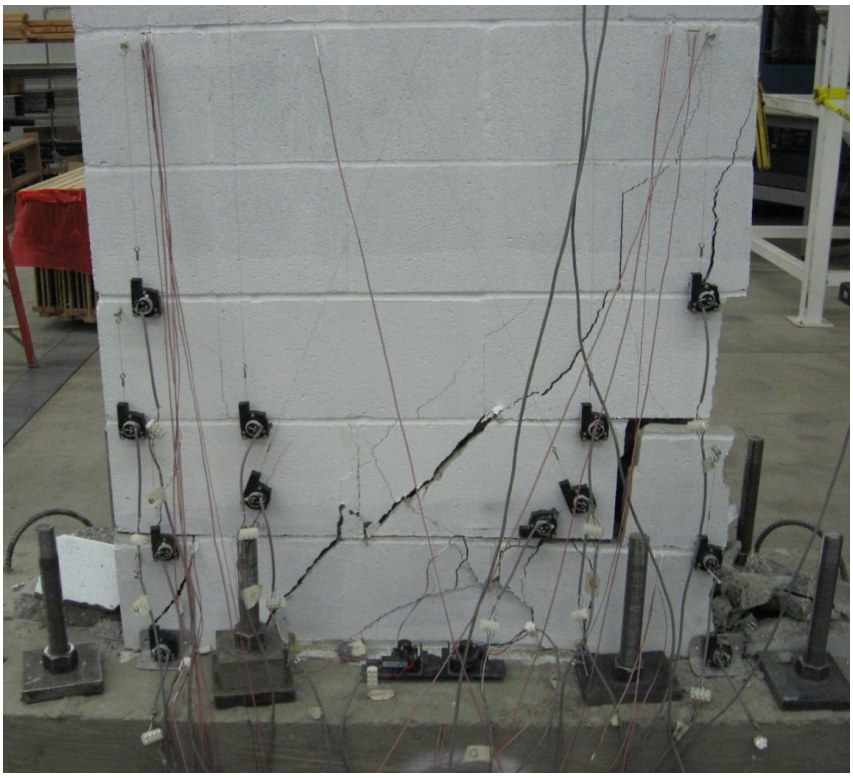

Figure 5.5 Wall C3: Opening of Shear Cracks

Figure 5.6 Wall C3: Crushing and Spalling of Face Shells

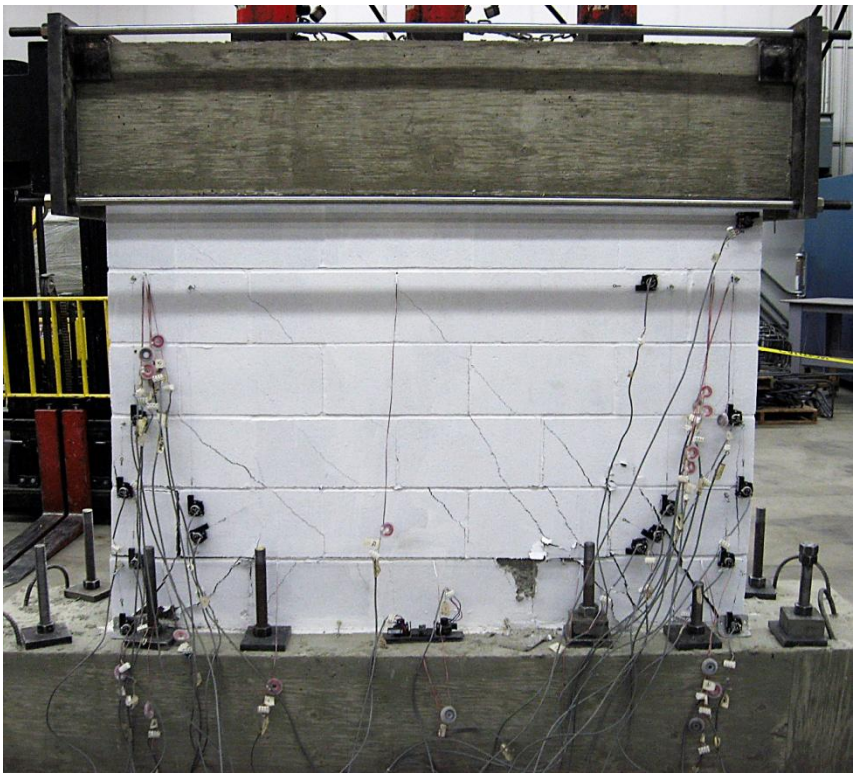

Figure 5.7 Wall C4: Propagation of Shear Cracks

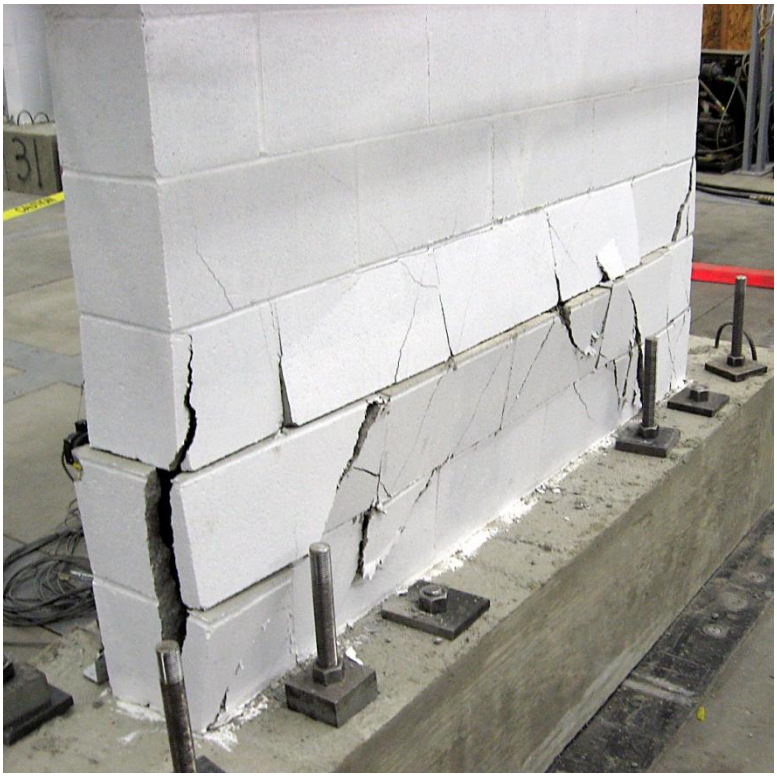

Figure 5.8 Wall 4: Crushing of Face Shells

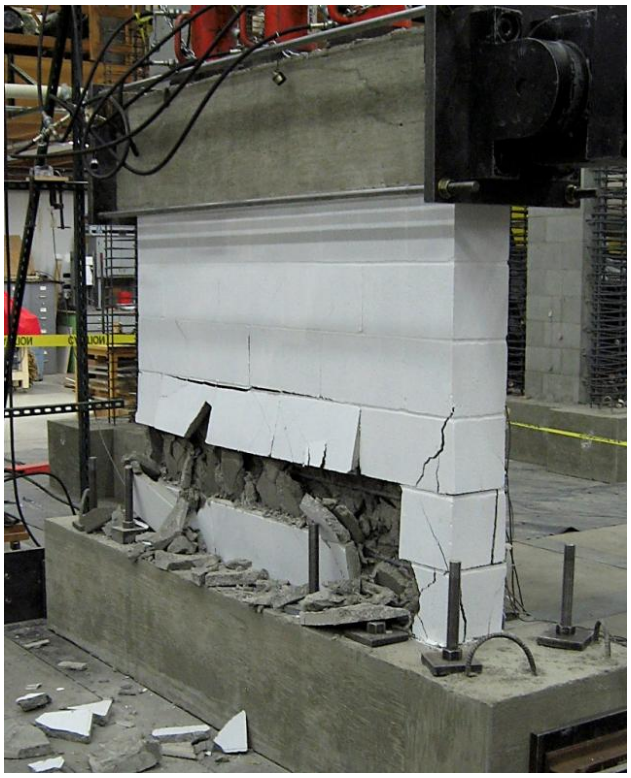

Figure 5.9 Wall C4: Spalling of Face Shells

The flexure-dominated walls had displacement ductilities ranging between 5.0 and 7.0. The walls with the complex flexure/shear/crushing failure mode had displacement ductilities of approximately 4. The ratio of the height of plasticity to wall length was above 50% for all of the walls with flexural behavior and below 30% for the walls with a complex failure mode, except for Wall C3 which had a ratio of 73%. There was no apparent trend in the ratio of equivalent plastic hinge length to wall length for walls failing in flexure. For walls with the complex failure mode, the ratio of equivalent plastic hinge length to wall length was approximately 30%. The walls with a flexure-dominated failure that had similar reinforcement ratios to the walls with a mixed failure mode dissipated considerably more energy.

5.3 Wall Capacity

Predicted peak loads determined based on the 2011 MSJC Code provisions and the software program XTRACT along with the average experimental peak load are presented in Table 5.2 for each wall specimen. The ratios of experimental peak load to predicted peak load are also presented.

Table 5.2 Comparison of Expected and Experimental Wall Capacities

Wall	Aspect Ratio	$P/(f'_m A_g)$	Vertical Reinf.	Predicted Peak Load (kips)		Average Experimental Peak Load (kips)	V_{exp}/V_{MSJC}	V_{exp}/V_{XTRACT}
				2011 MSJC[a]	XTRACT			
C1	2.0	0	#4 @ 8 in.	13.0	16.5	17.7	1.36	1.07
C2	2.0	0.0625	#4 @ 8 in.	23.0	24.6	31.2	1.36	1.27
C3	2.0	0.0625	#7 @ 16 in.	33.0	38.2	36.8	1.12	0.96
C4	0.78	0.0625	#7 @ 16 in.	144.0	157.0	138.3	0.96	0.88
C5	1.0	0.0625	#7 @ 16 in.	112.0	122.1	120.2	1.07	0.98
C6	2.0	0	#6 @ 8 in.	38.0	43.9	44.0	1.16	1.00
C7	2.0	0	8 #6, 1 #4	46.0	55.5	59.2	1.29	1.07
C8	2.0	0.0625	8 #6, 1 #4	59.0	64.4	70.4	1.19	1.09

[a]Compression reinforcement was considered in strength calculations

The experimental peak loads ranged from 7% to 36% more than the peak loads predicted using the 2011 MSJC for seven of the walls, and they were more conservative for walls with height-to-length aspect ratios of 2.0. The MSJC Code slightly over-predicted the peak load capacity of Wall C4. XTRACT over-predicted the load capacity for walls with large-diameter (No. 7) vertical reinforcement: C3, C4 and C5. This was most likely because these walls experienced a complex failure mechanism caused by dowel-action which is not accounted for in the XTRACT analysis. For the remaining walls, the experimental peak loads ranged from 7% to 27% more than the peak loads predicted using XTRACT. Sherman (2011) reported experimental peak loads from his test that were about 23% and 10% more than the peak loads predicted using the 2008 MSJC Code and XTRACT, respectively. The peak load capacities predicted using

XTRACT were less conservative than those predicted using the MSJC Code. This is because XTRACT accounts for strain hardening of the vertical reinforcement in its analysis and the MSJC Code does not.

5.4 Drift

The average total drift for each wall is presented in Table 5.3 at three limit-states: critical masonry strain (ε_{mu} = 0.0025), peak load, and failure defined as 20% load degradation from the maximum load attained. The average total drift at critical masonry strain ranged from 0.2% to 1.1%. At peak load, walls with height-to-length aspect ratios of 0.78 and 1.0 had drifts of approximately 1.5%, and walls with height-to-length aspect ratios of 2.0 had drifts of approximately 2%. The average total drift at failure ranged from 1.3% to 2.8%. Sherman (2011) reported values for average total drift at failure that ranged from 0.9% to 2.8% for walls with similar parameters. Correlations between the total drift at failure and the design parameters are discussed in Section 5.9.

Table 5.3 Total Wall Drift at Three Limit-States

Wall	Aspect Ratio	P/ (f'_mA_g)	Vertical Reinf.	Total Drift (%)			Peak/ ε_{mu}	Failure/ ε_{mu}
				ε_{mu}	Peak Load	Failure		
C1	2.0	0	#4 @ 8 in.	0.2	2.2	2.4	11.0	12.5
C2	2.0	0.0625	#4 @ 8 in.	0.6	2.1	2.4	3.5	4.0
C3	2.0	0.0625	#7 @ 16 in.	0.7	1.1	2.3	1.6	3.3
C4	0.78	0.0625	#7 @ 16 in.	0.6	0.9	1.3	1.6	2.2
C5	1.0	0.0625	#7 @ 16 in.	0.2	1.1	1.5	5.5	7.5
C6	2.0	0	#6 @ 8 in.	0.9	1.9	2.5	2.2	2.9
C7	2.0	0	8 #6, 1 #4	1.1	2.1	2.8	1.9	2.5
C8	2.0	0.0625	8 #6, 1 #4	0.6	2	2.7	3.3	4.5

The MSJC defines failure as the point when the masonry reaches a critical compressive strain of 0.0025. Only two walls, C6 and C7, reached approximately 1% drift at the critical

masonry strain. The ratios of drift at peak load and at failure to drift at this critical masonry strain value are also provided in Table 5.2. These ratios show the magnitude of the differences between the displacements that can be attained at the peak load and at the experimentally-determined failure of 20% load degradation relative to the code-defined point of failure when the critical masonry strain is reached. Values of drift at the peak load ranged from 1.6 to 11 times greater than those at the critical masonry strain, while values of drift at the experimentally-determined failure point were 2.2 to 12.5 times greater than those at the critical masonry strain. These results show that substantially larger drift capacities than those specified in the MSJC are attainable at actual wall failure.

The average total drift and average drift contributions from sliding, shear and flexural deformations are provided in Table 5.4 for each wall at 20% load degradation from the maximum load attained. The average drift contributions ranged from 0.4% to 16.7% for sliding, 2.3% to 12% for shear, and 71.3% to 94.0% for flexure. Walls with height-to-length aspect ratios of 0.78 and 1.0 had significantly more drift contributions from sliding and shear than walls with height-to-length aspect ratios of 2.0. Walls with height-to-length aspect ratios of 2.0 all had flexural drift contributions that were above 91%. Sherman (2011) reported similar findings from testing his walls.

Table 5.4 Components of Total Drift at 20% Load Degradation

Wall	Aspect Ratio	P/ (f'_mA_g)	Vertical Reinf.	20% Load Degradation			
				Total Drift (%)	Sliding (% Total)	Shear (% Total)	Flexure (% Total)
C1	2.0	0	#4 @ 8 in.	2.4	6.0	2.7	91.3
C2	2.0	0.0625	#4 @ 8 in.	2.4	1.9	5.9	92.2
C3	2.0	0.0625	#7 @ 16 in.	2.3	2.4	3.6	94.0
C4*	0.78	0.0625	#7 @ 16 in.	0.8	16.5	6.4	77.1
C5*	1.0	0.0625	#7 @ 16 in.	0.7	16.7	12	71.3
C6	2.0	0	#6 @ 8 in.	2.5	3.1	NA	NA
C7	2.0	0	8 #6, 1 #4	2.8	9.8	NA	NA
C8*	2.0	0.0625	8 #6, 1 #4	2.3	0.4	7	92.6

*Values for the components of drift taken at instrumentation failure

5.5 Displacement Ductility

The average yield and ultimate displacements along with the displacement ductility factor for each wall are presented in Table 5.5. For walls C1, C2 and C3 (nominal height of 80 in.) the average yield displacement ranged from 0.26 in. to 0.43 in. and the average ultimate displacement was approximately 1.86 in. for all three walls. For walls with the same height, Sherman (2011) reported average yield displacements that ranged from 0.25 in. to 0.41 in. and average ultimate displacements that ranged from 1.23 in. to 2.2 in. Walls with height-to-length aspect ratios of 0.78 and 1.0 had considerably smaller yield and ultimate displacement values. Correlations between average yield and ultimate displacements and the displacement ductility factor and the design parameters are discussed in Section 5.9.

Table 5.5 Average Yield & Ultimate Displacement and Displacement Ductility

Wall	Aspect Ratio	P/ (f'_mA_g)	Vertical Reinf.	Yield Displacement, ΔY (in.)	Ultimate Displacement, Δ_u (in.)	Displacement Ductility, μ_Δ
C1	2.0	0	#4 @ 8 in.	0.29	1.88	6.6
C2	2.0	0.0625	#4 @ 8 in.	0.26	1.87	7.2
C3	2.0	0.0625	#7 @ 16 in.	0.43	1.84	4.3
C4	0.78	0.0625	#7 @ 16 in.	0.16	0.71	4.4
C5	1.0	0.0625	#7 @ 16 in.	0.47	1.05	2.8
C6	2.0	0	#6 @ 8 in.	0.55	2.76	5.1
C7	2.0	0	8 #6, 1 #4	0.69	3.13	4.8
C8	2.0	0.0625	8 #6, 1 #4	0.56	3.03	5.4

5.6 Height of Plasticity and Plastic Hinge Length

The average height of plasticity and equivalent plastic hinge length along with those values divided by the wall length are presented in Table 5.6 for each wall specimen. The calculated height of plasticity and equivalent plastic hinge length for Walls C3 through C8 are lower-bound estimates of the actual values because final curvatures were determined prior to failure in these walls due to damage towards the end of testing that affected instrumentation readings. The ratio of height of plasticity to wall length ranged from 22% to 74%, and the ratio of equivalent plastic hinge length to wall length ranged from 23% to 61%. Sherman (2011) reported ratios of height of plasticity to wall length that ranged from 16% to 75% and ratios of equivalent plastic hinge length to wall length that ranged from 15% to 64%. Correlations between the height of plasticity and the equivalent plastic hinge length and the design parameters are discussed in Section 5.9.

Table 5.6 Ratios of Height of Plasticity and Plastic Hinge Length over Wall Length

Wall	Aspect Ratio	P/ (f'_mA_g)	Vertical Reinf.	Height of Plasticity, L_p (in.)	Plastic Hinge Length, l_p (in.)	L_p/L (%)	l_p/L (%)
C1	2.0	0	#4 @ 8 in.	18.9	8.9	48	23
C2	2.0	0.0625	#4 @ 8 in.	29.5	11.4	74	29
C3*	2.0	0.0625	#7 @ 16 in.	29.1	11.6	73	29
C4*	0.78	0.0625	#7 @ 16 in.	20.0	19.7	28	27
C5*	1.0	0.0625	#7 @ 16 in.	15.8	23.3	22	32
C6*	2.0	0	#6 @ 8 in.	30.1	34.1	54	61
C7*	2.0	0	8 #6, 1 #4	29.3	29.7	53	53
C8*	2.0	0.0625	8 #6, 1 #4	29.4	23.3	53	42

*Height of plasticity and plastic hinge length values are lower-bound estimates

5.7 Energy Dissipation

The total energy dissipated by each wall specimen is presented in Table 5.7. Wall C1 dissipated the least amount of energy at 168 kip-in., and Wall C8 dissipated the most amount of energy at 981 kip-in. Sherman (2011) reported values for total energy dissipation that ranged from 110 kip-in. to 529 kip-in. Walls in this study contained substantially more vertical reinforcement than walls tested by Sherman (2011), resulting in larger peak load capacities and noticeably greater energy dissipation capacities for walls with similar dimensions. Correlations between the total energy dissipation and the design parameters are discussed in Section 5.9.

Table 5.7 Total Energy Dissipation

Wall	Aspect Ratio	P/ (f'_mA_g)	Vertical Reinf.	Total Energy Dissipation (kip-in)
C1	2.0	0	#4 @ 8 in.	168
C2	2.0	0.0625	#4 @ 8 in.	271
C3	2.0	0.0625	#7 @ 16 in.	396
C4	0.78	0.0625	#7 @ 16 in.	397
C5	1.0	0.0625	#7 @ 16 in.	489
C6	2.0	0	#6 @ 8 in.	525
C7	2.0	0	8 #6, 1 #4	764
C8	2.0	0.0625	8 #6, 1 #4	981

5.8 Equivalent Hysteretic Damping

The equivalent hysteretic damping for each wall specimen is presented in Table 5.8. The displacement levels were chosen to be as close to 0.6% and 1.5% drift as possible. The drift for the first displacement level ranged from 0.5% to 0.7%, and the drift for the second displacement level ranged from 1.2% to 1.6%. The average equivalent hysteretic damping at approximately 0.6% and 1.5% drift were 8% and 16%, respectively. Correlations between the equivalent hysteretic damping and the design parameters are discussed in Section 5.9.

Table 5.8 Equivalent Hysteretic Damping

Wall	Aspect Ratio	P/ (f'_mA_g)	Vertical Reinf.	Drift (%)	Damping (%)
C1	2.0	0	#4 @ 8 in.	0.5	6.5
				1.5	17.1
C2	2.0	0.0625	#4 @ 8 in.	0.6	10.6
				1.2	12
C3	2.0	0.0625	#7 @ 16 in.	0.6	6.1
				1.6	14.5
C4	0.78	0.0625	#7 @ 16 in.	0.6	10.3
				1.3	18.4
C5	1.0	0.0625	#7 @ 16 in.	0.7	13.8
				1.4	17.5
C6	2.0	0	#6 @ 8 in.	0.6	6.8
				1.3	15.1
C7	2.0	0	8 #6, 1 #4	0.7	6.2
				1.4	15.9
C8	2.0	0.0625	8 #6, 1 #4	0.5	6.1
				1.5	14.8

5.9 Effects of Design Parameters on Wall Behavior

The test results for walls C1 through C8 of this study were compared to each other and to the test results from Sherman (2011). Sherman's walls are identified as walls 1A, 1B, 2A, 2B and 3 through 6. General results and conclusions from previous studies by other researchers are

also discussed. The different parameters and their effects on wall behavior are presented in Sections 5.9.1 through 5.9.4.

5.9.1 Aspect Ratio

The effects of height-to-length aspect ratio on wall performance are evaluated in this section. Table 5.9 contains the parameters associated with each group of comparable walls.

Table 5.9 Evaluation of Aspect Ratio

Wall		Reinforcement Ratio	Axial Compressive Stress (psi)	Aspect Ratio
Group1	C3	0.0055	158	2.0
	C5			1.0
	C4			0.78
Group 2	C1	0.0033	0	2.0
	3			1.0
	5			0.78
Group 3	C2	0.0033	158	2.0
	4			1.0
	6			0.78

The load-displacement envelope curves for the considered walls are given in Figure 5.10. In each group, the initial stiffness of the walls increased as the aspect ratio decreased. The peak load capacity also increased as the aspect ratio decreased for each group of walls. Walls with aspect ratios of 0.78 and 1.0 experienced more rapid strength degradation than did walls with an aspect ratio of 2.0. For all but one wall, the displacement at failure increased as the aspect ratio increased.

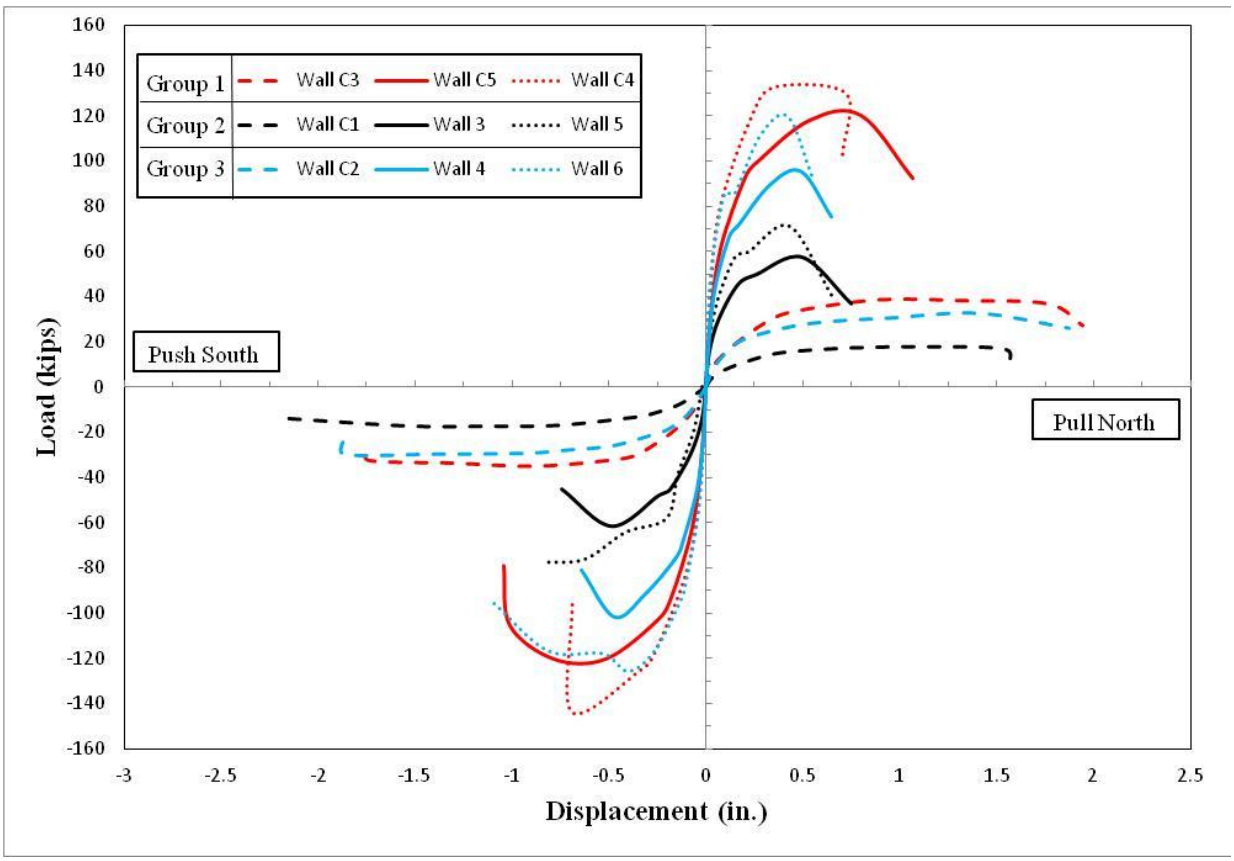

Figure 5.10 Load-Displacement Envelopes for Aspect Ratio Comparison

Test results from all of the wall groups showed that walls with an aspect ratio of 2.0 had a larger total drift at failure than walls with an aspect ratio of 0.78 and 1.0 (Table 5.3). Studies by Ibrahim and Suter (1999) and Eikanas (2003) also found that as the wall aspect ratio increased, the drift increased. The average total drift contributions from sliding and shear tended to increase as the aspect ratio decreased (Table 5.4); this was similar to findings by Sherman (2011). For Wall Groups 2 and 3, the average yield displacement was larger in walls with an aspect ratio of 2.0 than in walls with an aspect ratio of 0.78 and 1.0 (Table 5.5). Results did not show a relationship between the displacement ductility and the aspect ratio (Table 5.5). Ibrahim and Suter (1993) and Sherman (2011) reported that as the wall aspect ratio decreased, the displacement ductility decreased. In general, walls with aspect ratios of 2.0 had much larger

ratios of average height of plasticity to wall length than walls with aspect ratios of 0.78 and 1.0 (Table 5.6). Results from all three groups of walls did not show a strong relationship between the ratio of average equivalent plastic hinge length to wall length and the aspect ratio (Table 5.6); this was consistent with results from Sherman (2011). Wall Group 3 showed the greatest difference between the ratios of equivalent plastic hinge length to aspect ratio (the wall with an aspect ratio of 2.0 had the highest ratio in the group). The total amount of energy dissipated was not associated with the aspect ratio in any wall group (Table 5.7). In Wall Group 1, walls with aspect ratios of 0.78 and 1.0 had larger hysteretic damping values than the wall with an aspect ratio of 2.0 (Table 5.8).

5.9.2 Axial Compressive Stress

The effects that axial compressive stress had on wall performance are evaluated in this section. Table 5.10 contains the parameters associated with this group of comparable walls.

Table 5.10 Evaluation of Axial Compressive Stress

Wall		**Reinforcement Ratio**	**Aspect Ratio**	**Axial Compressive Stress (psi)**
Group 1	C1	0.0033	2.0	0
	C2			158
	2B			313
Group 2	C7	0.0087	2.0	0
	C8			158

The load-displacement envelope curves for the considered walls are given in Figure 5.11. The initial stiffness of the walls increased as the axial compressive stress increased. The peak load capacity also increased as the axial compressive stress increased; this was consistent with

results from Voon and Ingham (2006). For all but one wall, the displacement at failure increased as the axial compressive stress decreased.

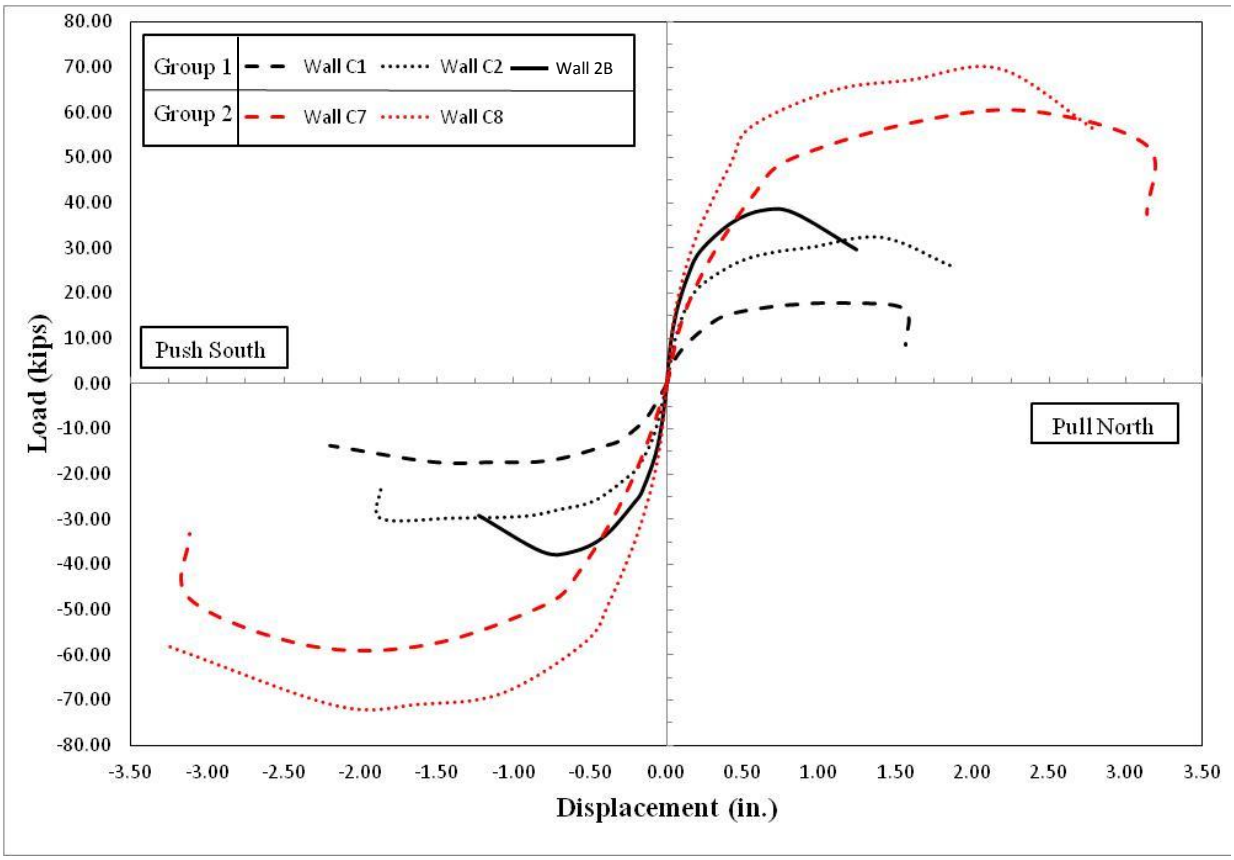

Figure 5.11 Load-Displacement Envelopes for Axial Compressive Stress Comparison

The average total drift at failure remained the same for the walls, in their respective groups, with axial compressive stresses of 0 psi and 158 psi, but it decreased in Wall Group 1 when the axial compressive stress increased to 313 psi (Table 5.3). Ibrahim and Suter (1999) also reported that drift decreased as the axial compressive stress increased. The flexural drift contribution at failure was approximately 93% for all magnitudes of axial compressive stress (Table 5.4). The average total drift contributions from sliding and shear were fairly small in all of the walls. Shedid et al. (2008) found that the yield displacement tended to increase as the axial compressive stress increased. However, the average yield displacement was the same for

all of the walls in their respective groups in this study (Table 5.5). The displacement ductility values were the same for the walls, in their respective groups, for axial compressive stresses of 0 psi and 158 psi, but it decreased in Wall Group 1 when the axial compressive stress increased to 313 psi (Table 5.5). Shedid et al. (2008) also found that the displacement ductility slightly decreased with increased magnitudes of axial compressive stress however the results from Ibrahim and Suter (1999) did not support this trend. In Wall Group 1, there appeared to be no correlation between the axial compressive stress and the ratio of average height of plasticity to wall length (Table 5.6). In Wall Group 2, the ratio of average height of plasticity to wall length was the same for both magnitudes of axial compressive stress. The ratio of average equivalent plastic hinge length to wall length was the same for all the walls in Group 1, and it decreased as the axial compressive stress increased in Wall Group 2 (Table 5.6). The total amount of energy dissipated was similar for each wall in Group 1, and it increased as the axial compressive stress increased in Wall Group 2 (Table 5.7). In Wall Group 2, the hysteretic damping values were very similar for both magnitudes of axial compressive stress (Table 5.8).

5.9.3 Vertical Reinforcement Ratio

The effects of vertical reinforcement ratio on wall performance are evaluated in this section. Table 5.11 contains the parameters associated with each group of comparable walls.

Table 5.11 Evaluation of Reinforcement Ratio

Wall		Aspect Ratio	Axial Compressive Stress (psi)	Reinforcement Ratio
Group 1	C2	2.0	158	0.0033
	C3			0.0059
	1B			0.0072
Group 2	C1	2.0	0	0.0033
	C6			0.0072
Group 3	4	1.0	158	0.0033
	C5			0.0055
Group 4	6	0.78	158	0.0033
	C4			0.0055

The load-displacement envelope curves for the considered walls are given in Figure 5.12. In each group of walls, the initial stiffness of the walls increased as the vertical reinforcement ratio increased. The peak load capacity also increased as the vertical reinforcement ratio increased for each group of walls. In Wall Groups 2, 3 and 4, the displacement at failure increased as the vertical reinforcement ratio increased. The test results from Wall Group 1 did not exhibit any consistent trends between the displacement at failure and the vertical reinforcement ratio in either loading direction.

The effects of vertical reinforcement ratio on the average total drift at failure show that in general, drift remained the same as the reinforcement ratio changed, although for walls with an aspect ratio of 1.0 it appeared to increase as the reinforcement ratio increased (Table 5.3). Ibrahim and Suter (1999) also found that drift increased as the reinforcement ratio increased; however, Shedid et al. (2008) and Eikanas (2003) reported that drift decreased as the reinforcement ratio increased. There was not a strong relationship between the three drift components at failure and the amount of vertical reinforcement for all of the wall groups (Table 5.4). Results from Wall Groups 2, 3 and 4 showed that the yield displacement increased when

the vertical reinforcement ratio increased (Table 5.5); this was supported by findings from Shedid et al. (2008). Test results from Wall Groups 2, 3 and 4 exhibited a decrease in displacement ductility as the vertical reinforcement ratio increased (Table 5.5); this trend corresponded to results from Shedid et al. (2008) and Sherman (2011). The ratio of average height of plasticity to wall length and the ratio of average equivalent plastic hinge length to wall length both increased as the vertical reinforcement ratio increased in Wall Groups 2, 3 and 4 (Table 5.6). The opposite trend was observed by Sherman (2011). The ratio of average equivalent plastic hinge length to wall length was the same for all three walls in Group 1. There was not a consistent trend in the test results between the total amount of energy dissipated and the vertical reinforcement ratio (Table 5.7).

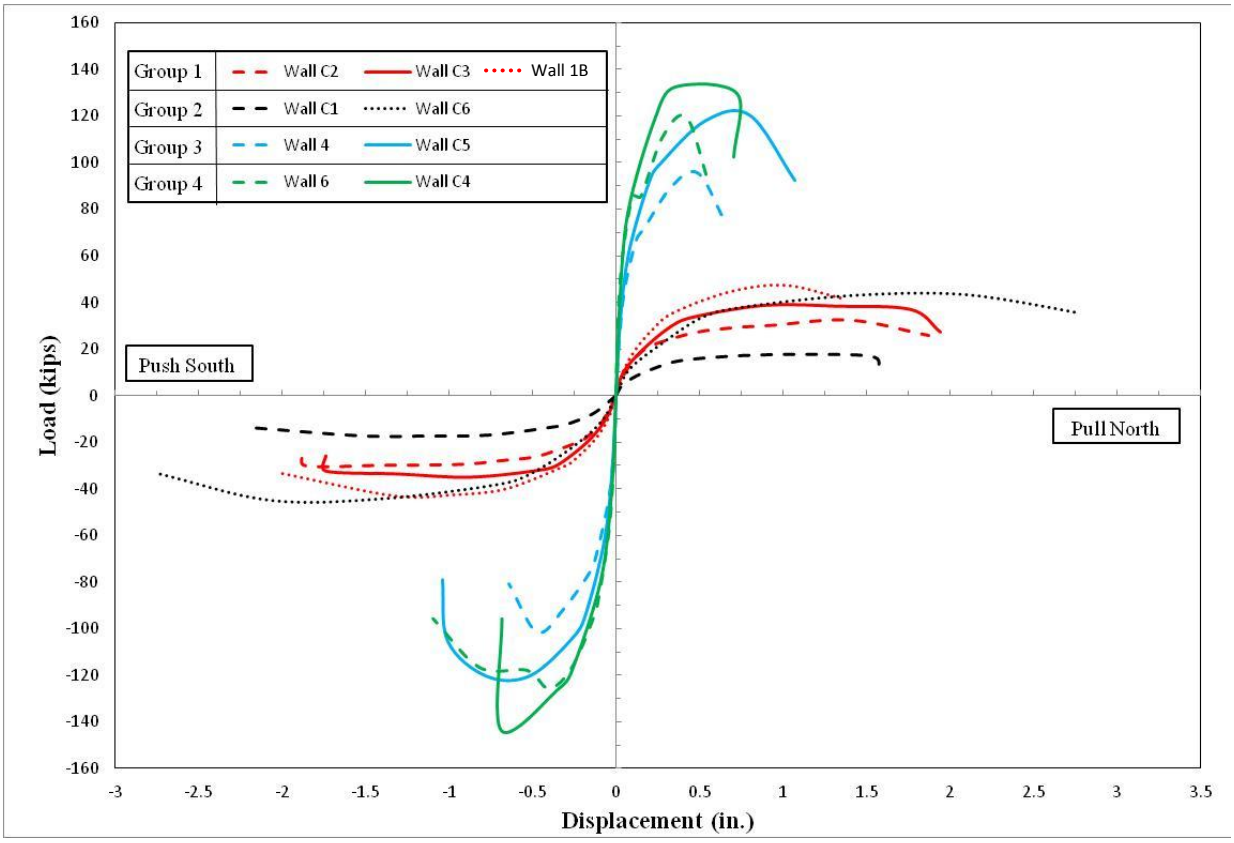

Figure 5.12 Load-Displacement Envelopes for Reinforcement Ratio Comparison

5.9.4 Jamb Reinforcement

The effects of jamb reinforcement compared to distributed reinforcement on wall performance are evaluated in this section. Table 5.12 contains the parameters associated with this group of comparable walls. Wall C6 had approximately the same ratio of vertical reinforcement as Walls C7, but the reinforcement was evenly distributed instead of concentrated in the two end cells.

Table 5.12 Evaluation of Jamb Reinforcement

Wall	Reinforcement Ratio	Aspect Ratio	Axial Compressive Stress (psi)
C6	0.0072	2.0	0
C7	0.0087		0

Figures 5.13 through 5.16 compare the progression of failure between Walls C6 and C7. At the first cycle of 3ΔY, Wall C6 had predominantly flexural cracks while Wall C7 displayed a mixture of flexural and shear cracks. At the first cycle of 6ΔY, it was observed that Wall C6 had developed shear cracks, considerable face shell spalling in the toe regions had occurred, and the extreme tensile reinforcement had buckled. In the same displacement cycle, Wall C7 had significantly more face shell spalling that extended beyond the toe regions towards the centerline of the wall.

Figure 5.13 Wall C6 Progression of Failure (3ΔY Cycle 1)

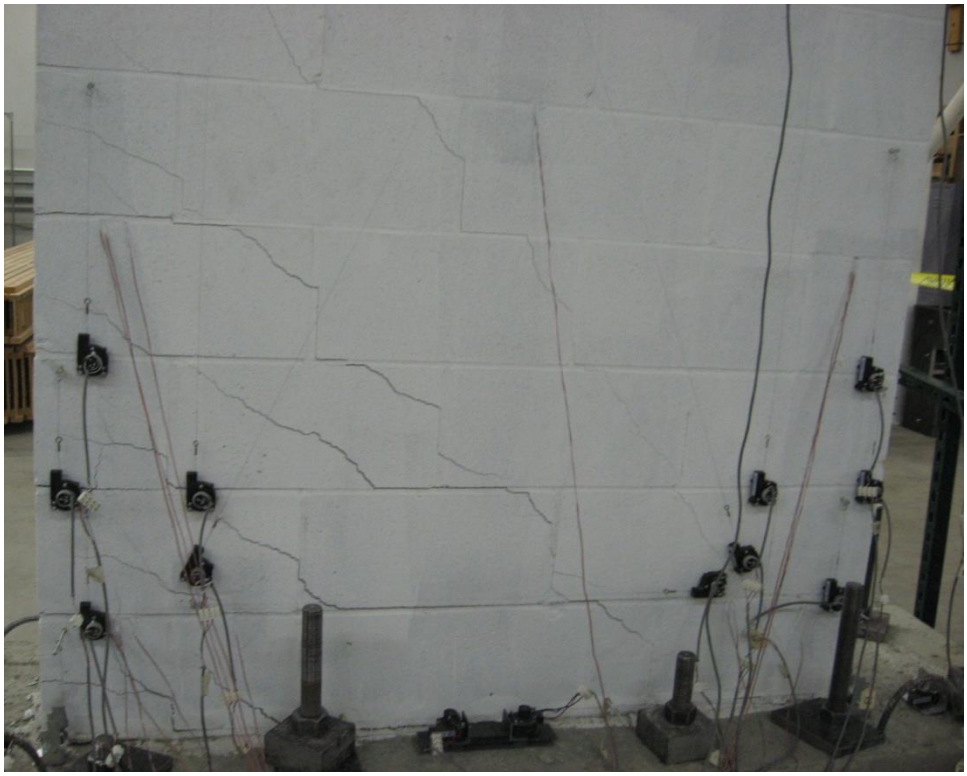

Figure 5.14 Wall C7: Progression of Failure (3ΔY Cycle 1)

Figure 5.15 Wall C6: Progression of Failure (6ΔY Cycle 1)

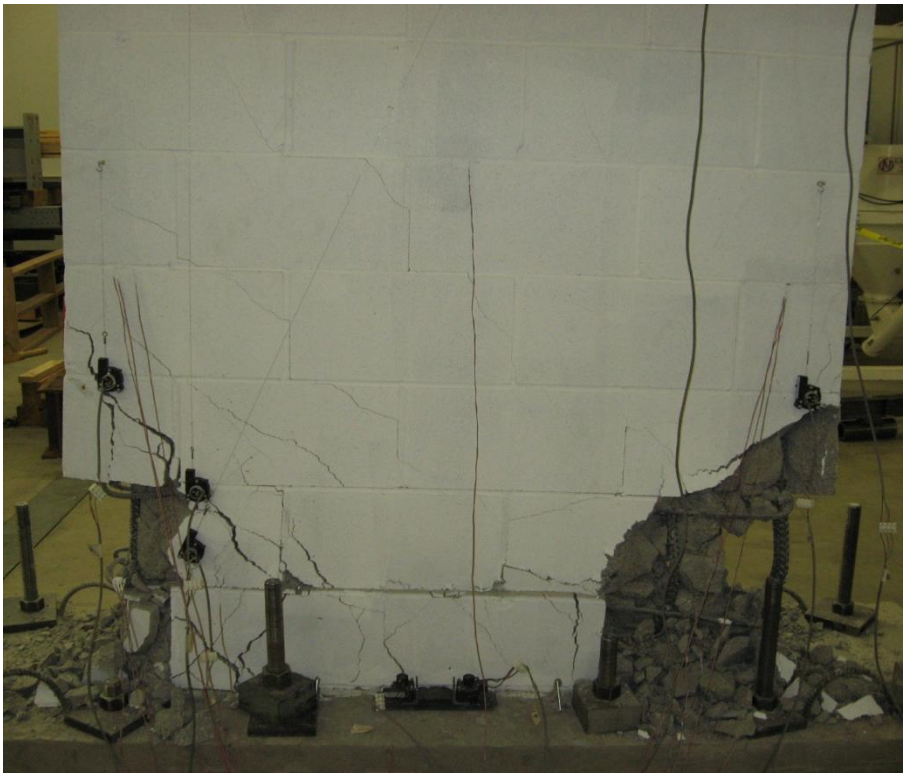

Figure 5.16 Wall C7: Progression of Failure (6ΔY Cycle 1)

The load-displacement envelope curves for the considered walls are given in Figure 5.17. The initial stiffness and peak load capacity of Wall C7 was greater than Wall C6. This difference may be attributed to the slightly larger amount of vertical reinforcement and to the concentrated reinforcement in the end cells which increased the moment of inertia for Wall C7. Both walls exhibited similar patterns of strength degradation and levels of displacement at failure.

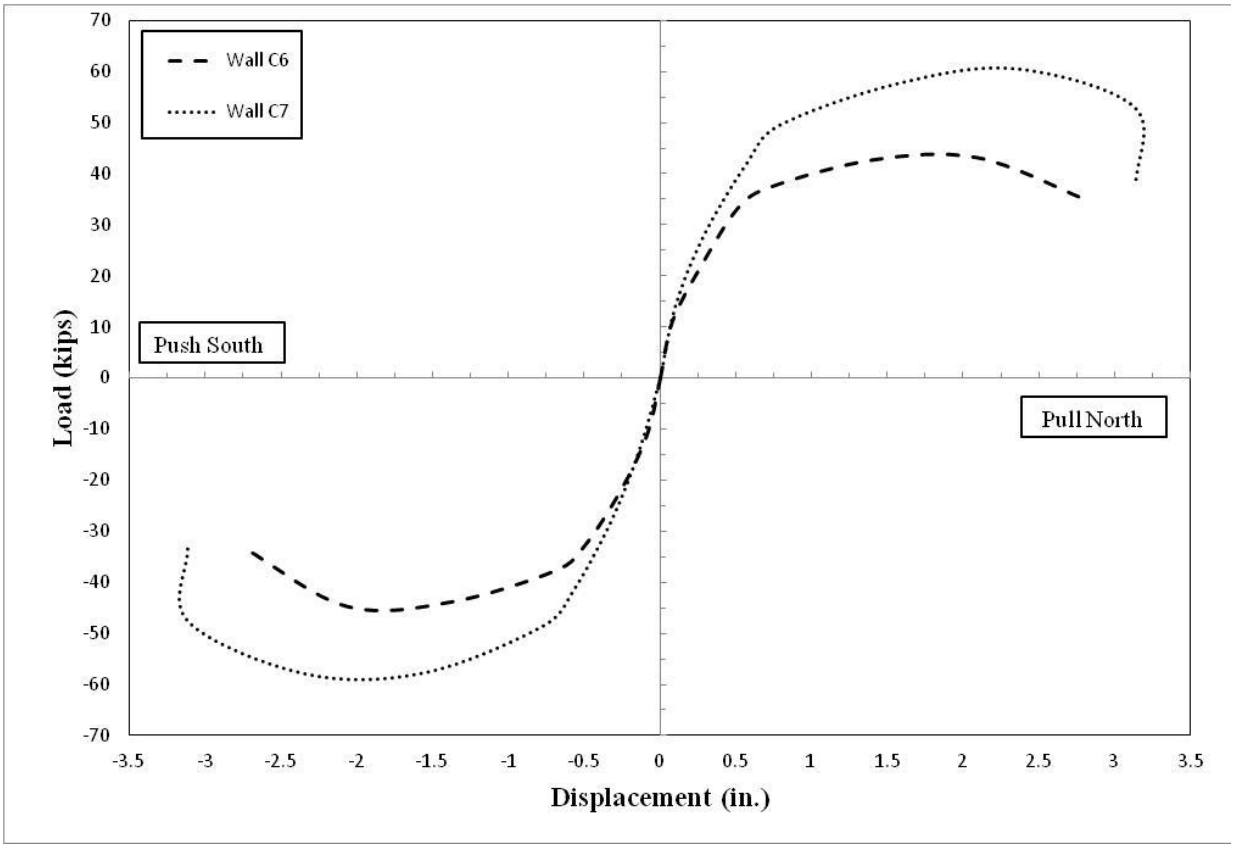

Figure 5.17 Load-Displacement Envelopes for Jamb Reinforcement Comparison

The average total drift at failure was fairly similar for both walls (Table 5.3). A comparison of the components of drift at failure was unable to be made because displacement potentiometers were removed prior to failure as a result of wall damage. The yield displacement increased slightly while the displacement ductility value was the same between Walls C6 and C7 (Table 5.5). These results indicated that the ductility of the wall with jamb reinforcement was

comparable to the wall with evenly distributed reinforcement. The ratio of average height of plasticity to wall length was the same for both walls (Table 5.6). The ratio of average equivalent plastic hinge length to wall length decreased between Walls C6 and C7 (Table 5.6). Wall C7 dissipated approximately 50% more energy than the Wall C6 (Table 5.7). This difference was attributable, at least in part, to the slightly larger amount of vertical reinforcement in Wall C7. In Wall C6, the load capacity remained fairly constant as displacements increased, while in Wall C7, the load capacity increased as displacements increased, which resulted in larger hysteresis curves. This may be a result of the location of the vertical reinforcement and how it affects the extent of yielding of the vertical reinforcement throughout the cross-section of the wall. The hysteretic damping values were very similar for both walls (Table 5.8).

5.10 Summary and Conclusions.

This chapter evaluated the effects that the height-to-length aspect ratio, axial compressive stress, reinforcement ratio and jamb reinforcement have on the behavior of reinforced concrete masonry shear walls under in-plane cyclic loading. Wall performance was evaluated based on a comparison of predicted vs. actual load capacity, drift capacity, displacement ductility, height of plasticity, equivalent plastic hinge length, amount of energy dissipated, and value of equivalent hysteretic damping.

The peak load capacities for walls C3, C4 and C5, which had large-diameter vertical reinforcement (No. 7), were over-predicted by 2% to 12% using the XTRACT program. This was most likely because the XTRACT analysis does not account for the complex failure mode that these walls exhibited. The predicted peak load capacities using XTRACT were

approximately 10% less conservative than those predicted using the MSJC Code because XTRACT accounts for strain hardening of the vertical reinforcement.

Walls exhibited either a typical flexure failure mode or a complex flexure/shear/crushing failure mode. Walls exhibiting flexural behavior had larger plastic hinge zones and dissipated more energy than walls with the complex failure mode. As the height-to-length aspect ratio increased, larger drifts and higher displacement ductilities were obtained. In general, as the vertical reinforcement ratio increased, the displacement ductility decreased. Walls with large-diameter vertical reinforcement and lap splices at the base of the wall, which effectively doubled the area of reinforcement at this location, exhibited a mixed failure mode associated with a complex dowel-action behavior. The magnitude of applied axial load did not appear to have a significant impact on any of the wall performance criteria.

Wall performance was very similar for the wall with jamb reinforcement and the wall with evenly distributed reinforcement. The displacement ductilities were similar for the wall with jamb reinforcement and the comparable wall with evenly distributed reinforcement, but the wall with jamb reinforcement dissipated more energy. Due to the limited number of comparable specimens, additional testing is recommended to confirm this conclusion.

CHAPTER 6:

SUMMARY, CONCLUSIONS AND FUTURE RESEARCH

6.1 SUMMARY

This study was funded by the National Institute of Standards and Technology (NIST). It was conducted as part of a joint effort between researchers at the University of California at San Diego, the University of Texas at Austin and Washington State University. The objective of the overall project is to develop improved performance-based design methodologies and provisions for reinforced concrete masonry shear walls under seismic loading. The primary objective of the research reported in this thesis was to investigate the behavior of reinforced concrete masonry shear walls subjected to in-plane lateral loading while varying the wall aspect ratio, level of applied axial stress, and reinforcement ratio. The secondary objective was to examine the effects of concentrated reinforcement at the ends of the walls (jambs) compared with evenly distributed reinforcement on shear wall performance.

Eight, fully grouted, concrete masonry shear walls were designed according to the requirements of the 2011 MSJC Code. The walls had three different height-to-length aspect ratios (0.78, 1.0 and 2.0), two different magnitudes of axial compressive stress (0 and 158 psi), and two different vertical reinforcement ratios (0.0033 and 0.0072). Two of the walls contained jamb reinforcement. The walls were constructed at the Composite Materials and Engineering Center at Washington State University by professional masons.

The walls were tested by applying a prescribed cyclic, in-plane lateral displacement sequence. Strain gages, displacement potentiometers, a load cell and a dial gauge were used to monitor and acquire data while the wall specimens were tested. Measurements from these instruments were used to plot load-displacement hysteresis curves. The area underneath the

hysteresis curves was used to determine the amount of energy dissipated and equivalent hysteretic damping in each wall. Three displacement components, sliding, shear and flexure, were either directly measured or calculated from data obtained from several displacement potentiometers. Curvatures over the wall height were also plotted and used to calculate the height of plasticity and curvature ductility. The displacement ductilities and equivalent plastic hinge lengths were also calculated from the acquired data. Visual observations were also made during testing and used to describe wall behavior at each displacement level.

Test results were analyzed to evaluate the effects that the height-to-length aspect ratio, axial compressive stress and reinforcement ratio have on wall performance. Wall performance was evaluated based on the peak load capacity, drift, displacement ductility, height of plasticity, equivalent plastic hinge length and energy dissipation. The effects of jamb reinforcement compared to distributed reinforcement on wall behavior were also assessed. The wall test results in this study were compared to the wall test results from Sherman (2011) and to general results and conclusions from other studies in order to better understand the effects of key parameters on the performance of masonry shear walls.

6.2 CONCLUSIONS

The eight walls in this study exhibited two different types of failure modes: flexural and a complex flexure/shear/crushing. The walls where flexure was the primary mode of failure had displacement ductilities between 5.0 and 7.0, while walls with the complex mixed failure mode had displacement ductilities of approximately 4.0. The ratio of the height of plasticity to wall length was greater in the walls exhibiting flexural failure behavior. There was no apparent trend in the ratio of equivalent plastic hinge length to wall length that was distinguished by the failure

modes. The walls with a flexure-dominated failure mode that had similar reinforcement ratios to the walls with a mixed failure mode dissipated considerably more energy.

The predicted peak load capacities were obtained using criteria given in the 2011 MSJC Code and from the analysis program XTRACT. The experimental peak loads ranged from 7% to 36% more than the peak loads predicted using the 2011 MSJC for seven of the walls. The experimental peak loads ranged from 7% to 27% more than the peak loads predicted using XTRACT for five of the walls. The predicted peak load capacities from the MSJC Code were approximately 10% more conservative than those using the XTRACT analysis because the XTRACT analysis accounts for strain hardening of the vertical reinforcement. The MSJC Code over-predicted the peak load capacity (i.e., was not conservative) of Wall C4 by 4%. XTRACT also over-predicted the peak load capacity by 2% to 12% for the walls with large-diameter vertical reinforcement (No. 7). This was most likely due to the complex dowel-action associated with the failure mode for these walls.

Effects of Aspect Ratios: Walls with lower aspect ratios exhibited greater initial stiffness and had a larger peak load capacity than walls with larger aspect ratios. In general, the yield displacement of the elastoplastic approximation was larger in walls with an aspect ratio of 2.0 than in walls with aspect ratios of 0.78 and 1.0. The ultimate displacement increased as the aspect ratio increased. Walls with lower aspect ratios had larger contributions from sliding and shear deformations. There was no apparent relationship between the aspect ratio and height of plastic hinging. Changes in aspect ratio did not have an effect on the ductility of the walls. All of the walls had relatively large displacement ductility values.

Effects of Axial Compressive Stress: As the axial compressive stress was increased, the initial stiffness and peak load capacity of the walls also increased. Wall behavior changed when

the magnitude of axial compressive stress was large, but it remained relatively constant with various smaller magnitudes of axial compressive stress. The yield displacement of the elastoplastic approximation remained constant while the ultimate displacement slightly decreased as the magnitude of axial compressive stress increased. These findings corresponded to a decrease in the displacement ductility for walls with a larger axial compressive stress. For walls with a height-to-length aspect ratio of 2.0, the flexural deformation contribution exceeded 90% for all magnitudes of axial compressive stress. This was most likely due to the fact that the walls which had an aspect ratio of 2.0 were seen to exhibit primarily flexural behavior. No consistent trends were observed relating axial compressive stress with plastic hinging or energy dissipation. Walls with lower magnitudes of axial compressive stress behaved similarly and there was only an observed difference in behavior when the magnitude of axial compressive stress was increased significantly

Effects of Reinforcement Ratios: As the vertical reinforcement ratio increased, the initial stiffness and peak load capacity of the walls also increased. In general, as the vertical reinforcement ratio increased, the yield displacement also increased and the displacement ductility decreased. The total drift at failure remained fairly constant as the amount of vertical reinforcement changed. In general, the ratios of average height of plasticity to wall length and average equivalent plastic hinge length to wall length increased with larger vertical reinforcement ratios. There was no apparent relationship between the vertical reinforcement ratio and the amount of energy dissipated. Using large-diameter vertical reinforcement bars with lap splices at the base of the wall should be avoided because of their propensity towards abrupt failure as seen in the wall specimens in this project.

Effects of Jamb Reinforcement: Wall performance was very similar for walls with jamb reinforcement and evenly distributed reinforcement. There was a decrease in the average equivalent plastic hinge length for the wall with jamb reinforcement. The wall with jamb reinforcement dissipated more energy than the wall with evenly distributed reinforcement. This result may be attributed to the slight difference in the vertical reinforcement ratio, the size of the hysteresis loops, and the location of the vertical reinforcement within the cross-section of the wall.

6.3 FUTURE RESEARCH

The conclusions drawn in this study are limited by the relatively small number of specimens that were tested. It is recommended that additional wall tests comparing the effects of height-to-length aspect ratio, axial compressive stress and reinforcement ratio on wall performance be conducted to obtain a larger sample size and more conclusive results. Research is currently in progress that will compare the performance of the walls with jamb reinforcement in this study with walls containing confined boundary elements. Test results from this study will contribute to efforts within the overall research project to develop new performance-based design methodologies and provisions for reinforced concrete masonry shear walls.

REFERENCES

ASTM Standard C140. (2011). "Standard Test Methods for Sampling and Testing Concrete Masonry Units and Related Units," ASTM International, West Conshohocken, PA, 2011, DOI: 10.1520/C0140-11, www.astm.org.

ASTM Standard C476. (2010). "Standard Specification for Grout for Masonry," ASTM International, West Conshohocken, PA, 2010, DOI: 10.1520/C0476-10, www.astm.org.

ASTM Standard C780. (2011). "Standard Test Method for Preconstruction and Construction Evaluation of Mortars for Plain and Reinforced Unit Masonry," ASTM International, West Conshohocken, PA, 2011, DOI: 10.1520/C0780-11, www.astm.org.

ASTM Standard C1019. (2011). "Standard Test Method for Sampling and Testing Grout," ASTM International, West Conshohocken, PA, 2011, DOI: 10.1520/C1019-11, www.astm.org.

ASTM Standard C1314. (2011). "Standard Test Method for Compressive Strength of Masonry Prisms," ASTM International, West Conshohocken, PA, 2011, DOI: 10.1520/C1314-11, www.astm.org.

Canadian Standards Association (CSA). (2004). "Design of Masonry Structures." *CSA S304.1-04*, Mississauga, Ont., Canada.

Eikanas, I.K. (2003). "Behavior of Concrete Masonry Shear Walls with Varying Aspect Ratio and Flexural Reinforcement." M.S. Thesis, Department of Civil and Environmental Engineering, Washington State University, Pullman, WA.

Ibrahim, K.S. and Suter, G.T. (1999). "Ductility of Concrete Masonry Shear Walls Subjected to Cyclic Loading." *Proceedings of the 8th North American Masonry Conference*, The Masonry Society, University of Texas, Austin, TX.

International Code Council, Inc. (ICC). (2000). 2000 International Building Code (IBC). Falls Church, VA.

Masonry Standards Joint Committee (MSJC). (2005). Building Code Requirements for Masonry Structures." *TMS 402/ACI 530/ASCE 5*, American Concrete Institute, Detroit, MI., American Society of Civil Engineers, New York, and The Masonry Society, Boulder, CO.

Masonry Standards Joint Committee (MSJC). (2011). Building Code Requirements for Masonry Structures." *TMS 402/ACI 530/ASCE 5*, American Concrete Institute, Farmington Hills, MI., American Society of Civil Engineers, Reston, VA and The Masonry Society, Boulder, CO.

Massone, L.M. and Wallace, J.W. (2004). "Load-Deformation Responses of Slender Reinforced Concrete Walls." *ACI Structural Journal*, 101(1), 103-113.

National Earthquake Hazards Reduction Program (NEHRP). (1997). "Recommended Provisions for Seismic Regulations for New Buildings and Other Structures. Part 1: Provisions." *Building Seismic Safety Council*, Washington, D.C.

Priestley, M.J.N. (2000). "Performance based seismic design." *Proceedings 12th World Conference Earthquake Engineering*, Auckland, New Zealand.

Priestley, M.J.N., Calvi, G.M. and Kowalsky, M.J. (2007). Displacement-Based Seismic Design of Structures. Pavia, Italy: IUSS Press.

Shedid, M.T., Drysdale, R.G. and El-Dakhakhni, W.W. (2008). "Behavior of Fully Grouted Reinforced Concrete Masonry Shear Walls Failing in Flexure: Experimental Results." *Journal of Structural Engineering*, 134(11), 1754-1767.

Sherman, J.D. (2011). "Effects of Key Parameters on the Performance of Concrete Masonry Shear Walls Under In-Plane Loading." M.S. Thesis, Department of Civil and Environmental Engineering, Washington State University, Pullman, WA.

Shing, P.B., Noland, J.L., Klamerus, E. and Spaeh, H. (1989). "Inelastic Behavior of Concrete Masonry Shear Walls." *Journal of Structural Engineering*, 115(9), 2204-2225.

Snook, M. (2005). "Effects of Confinement Reinforcement on the Performance of Masonry Shear Walls." M.S. Thesis, Department of Civil and Environmental Engineering, Washington State University, Pullman, WA.

Voon, K.C. and Ingham, J.M. (2006). "Experimental In-Plain Shear Strength Investigation of Reinforced Concrete Masonry Walls." *Journal of Structural Engineering*, 132(3), 400-408.

APPENDIX A

NOTATION

α = distance from the top of the wall to the center of the rotation; assumed to be 0.67

Δ_{shear} = average shear displacement

Δ_C = measured compressive displacements (in.)

Δ_m = maximum displacement at the target displacement level (in.)

Δ_T = measured tensile displacements (in.)

Δ_u = ultimate displacement at 20% load degradation (in.)

ΔY = yield displacement from preliminary test used in testing protocol (in.)

Δ_y = yield displacement of elastoplastic approximation (in.)

Δ'_y = yield displacement at first yield of tensile reinforcement (in.)

Δ_1 = displacement at data point 1 (in.)

Δ_2 = displacement at data point 2 (in.)

ε_{mu} = critical masonry yield strain

ε_y = tensile reinforcement yield strain

ϕ = curvature at a given cross-section (1/in.)

ϕ_u = ultimate curvature at 20% load degradation (1/in.)

ϕ_y = yield curvature of elastoplastic approximation (1/in.)

ϕ'_y = yield curvature at first yield of tensile reinforcement (1/in.)

μ_Δ = displacement ductility

μ_ϕ = curvature ductility

A_h = area within first cycle of the target displacement level (kip-in.)

D_1 = diagonal length 1 of the deformed displacement potentiometers forming an X across the wall specimen

D_2 = diagonal length 2 of the deformed displacement potentiometers forming an X across the wall specimen

d_{gage} = in-plane distance between gages (in.)

E = energy between data points (kip-in.)

F_m = maximum force at the target displacement level (kip)

H = nominal height of wall specimen (in.)

h = height of diagonal pattern (in.)

L = nominal length of wall specimen (in.)

L_p = height of the plasticity zone (in.)

L_1 = load at data point 1 (kip)

L_2 = load at data point 2 (kip)

l = length of diagonal pattern (in.)

l_{gage} = applicable gage length (in.)

l_p = equivalent plastic hinge length (in.)

M_y = yield moment of elastoplastic approximation (kip-in.)

M'_y = yield moment at first yield of tensile reinforcement (kip-in.)

P_y = yield force of elastoplastic approximation (kips)

P'_y = yield force at first yield of tensile reinforcement (kips)

V_1 = vertical displacement 1 at the top of the wall specimen (in.)

V_2 = vertical displacement 2 at the top of the wall specimen (in.)